

1. Report No. FHWA/TX-13/0-6744-1		2. Government Accession No.		3. Recipient's Catalog No.	
4. Title and Subtitle HMA SHEAR RESISTANCE, PERMANENT DEFORMATION, AND RUTTING TESTS FOR TEXAS MIXES: YEAR-1 REPORT				5. Report Date Published: April 2014	
				6. Performing Organization Code	
7. Author(s) Lubinda F. Walubita, Sang Ick Lee, Jun Zhang, Abu NM Faruk, Stan Nguyen, and Tom Scullion				8. Performing Organization Report No. Report 0-6744-1	
9. Performing Organization Name and Address Texas A&M Transportation Institute College Station, Texas 77843-3135				10. Work Unit No. (TRAIS)	
				11. Contract or Grant No. Project 0-6744	
12. Sponsoring Agency Name and Address Texas Department of Transportation Research and Technology Implementation Office 125 E. 11 <sup>th</sup> Street Austin, Texas 78701-2483				13. Type of Report and Period Covered Technical Report: September 2012–August 2013	
				14. Sponsoring Agency Code	
15. Supplementary Notes Project performed in cooperation with the Texas Department of Transportation and the Federal Highway Administration. Project Title: New HMA Shear Resistance and Rutting Test for Texas Mixes URL: <a href="http://tti.tamu.edu/documents/0-6744-1.pdf">http://tti.tamu.edu/documents/0-6744-1.pdf</a>					
16. Abstract <p>Traditionally run at one test temperature (122°F), the Hamburg Wheel Tracking Test (HWTT) has a proven history of identifying hot-mix asphalt (HMA) mixes that are moisture susceptible and/or prone to rutting. However, with the record summer temperatures of the recent years, several shear and rutting failures have occurred with HMA mixes that had passed the HWTT in the laboratory; mostly in high shear locations, in particular with slow moving (accelerating/decelerating) traffic at controlled intersections, stop-go sections, in areas of elevated temperatures, heavy/high traffic loading, and/or where lower PG asphalt-binder grades have been used.</p> <p>As a supplement to the HWTT, this two-year study is being undertaken to develop a simpler and less time consuming shear resistance and permanent deformation (PD)/rutting test that is also cost-effective, repeatable, and produces superior results in terms of correlation with field rutting performance. In particular, such a test should have the potential to discriminate HMA mixes for application in high shear stress areas (i.e., intersections) as well as being an indicator of the critical temperatures at which a given HMA mix, with a given PG asphalt-binder grade, becomes unstable and more prone to rutting and/or shear failure.</p> <p>In line with these objectives, this interim report documents the research work completed in Year-1 of the study, namely: a) data search and literature review; b) computational modeling and shear stress-strain analysis; c) comparative evaluation of the Asphalt Mixture Performance Tester (AMPT) and the Universal Testing Machine (UTM); d) comparative evaluation of the Flow Number (FN), Dynamic Modulus (DM), and Repeated Load Permanent Deformation (RLPD) tests relative to the HWTT test method.</p>					
17. Key Words HMA, Rutting, Shear, Permanent Deformation (PD), Stress, Strain, Visco-elastic, Hamburg (HWTT), UTM, AMPT, Flow Number (FN), Dynamic Modulus (DM), Repeated Load Permanent Deformation (RLPD), Finite Element (FE), Shear Strength, Modulus			18. Distribution Statement No restrictions. This document is available to the public through NTIS: National Technical Information Service Alexandria, Virginia 22312 <a href="http://www.ntis.gov">http://www.ntis.gov</a>		
19. Security Classif.(of this report) Unclassified		20. Security Classif.(of this page) Unclassified		21. No. of Pages 152	22. Price



# **HMA SHEAR RESISTANCE, PERMANENT DEFORMATION, AND RUTTING TESTS FOR TEXAS MIXES: YEAR-1 REPORT**

by

Lubinda F. Walubita  
Research Scientist  
Texas A&M Transportation Institute

Abu NM Faruk  
Research Associate  
Texas A&M Transportation Institute

Sang Ick Lee  
Research Associate  
Texas A&M Transportation Institute

Stan Nguyen  
Student Technician II  
Texas A&M Transportation Institute

Jun Zhang  
Research Associate  
Texas A&M Transportation Institute

and  
Tom Scullion  
Senior Research Engineer  
Texas A&M Transportation Institute

Report 0-6744-1

Project 0-6744

Project Title: New HMA Shear Resistance and Rutting Test for Texas Mixes

Performed in cooperation with the  
Texas Department of Transportation  
and the  
Federal Highway Administration

Published: April 2014

TEXAS A&M TRANSPORTATION INSTITUTE  
College Station, Texas 77843-3135



## **DISCLAIMER**

The contents of this report reflect the views of the authors, who are responsible for the facts and the accuracy of the data presented herein. The contents do not necessarily reflect the official view or policies of the Federal Highway Administration (FHWA) or the Texas Department of Transportation (TxDOT). This report does not constitute a standard, specification, or regulation, nor is it intended for construction, bidding, or permit purposes. The United States Government and the State of Texas do not endorse products or manufacturers. Trade or manufacturers' names appear herein solely because they are considered essential to the object of this report. The researcher in charge was Lubinda F. Walubita.

## **ACKNOWLEDGMENTS**

This project was conducted for TxDOT, and the authors thank TxDOT and FHWA for their support in funding this research project. In particular, the guidance and technical assistance provided by the Project Manager, Darrin Jensen of TxDOT (RTI), proved invaluable. The following project advisors also provided valuable input throughout the course of the project: Joe Leidy, Gisel Carrasco, Ramon Rodriguez, and Mark Smith.

Special thanks are also extended to David Contreras, Jesus M. Ipina, Jason Huddleston, Tony Barbosa, and Lee Gustavus from the Texas Transportation Institute (TTI) for their help with laboratory and field work. A word of gratitude is also conveyed to Fujie Zhou for the assistance with the Asphalt Mixture Tester (AMPT) at TTI.

# TABLE OF CONTENTS

<b>List of Figures</b> .....	<b>x</b>
<b>List of Tables</b> .....	<b>xii</b>
<b>List of Notations and Symbols</b> .....	<b>xiii</b>
<b>Chapter 1 Introduction</b> .....	<b>1-1</b>
Research Objectives .....	1-1
Research Methodology and Work Plans .....	1-1
Report Contents and Organizational Layout .....	1-4
Summary.....	1-5
<b>Chapter 2 Data Search and Literature Review</b> .....	<b>2-1</b>
Laboratory Tests Reviewed.....	2-1
The HWTT Test.....	2-1
The RLPD Test.....	2-3
The Unconfined DM Test.....	2-5
The Unconfined FT and FN Tests .....	2-7
Other HMA Rutting and Shear Tests.....	2-9
Laboratory Tests Conducted in Study 0-6658.....	2-10
Summary.....	2-12
<b>Chapter 3 Computational Modeling and Shear Stress-Strain Analysis</b> .....	<b>3-1</b>
PLAXIS 2-D FE Modeling: Linear Elastic Analysis .....	3-2
The PLAXIS Software.....	3-2
PLAXIS Pavement Structures and Input Variables.....	3-3
PLAXIS Results: Vertical and Horizontal Displacements .....	3-5
PLAXIS Results: Shear Stress-Strain Distributions .....	3-6
PLAXIS Data Analysis: Identification of Critical Factors that Influence Shear Deformation.....	3-8
PLAXIS Data Analysis: Key Findings and Recommendations .....	3-10
ABAQUS 3D FE Modeling: VISCO-Elastic Analysis.....	3-11
The ABAQUS Software .....	3-11
ABAQUS Pavement Structures and Input Variables .....	3-12
ABAQUS Results: Effects of HMA Modulus on PVMNT Response .....	3-14
The ABAQUS Results: Effects of Tire Inclination (Cornering) on PVMNT Response .....	3-15
ABAQUS Results: Effects of Tire Inflation Pressure Variations.....	3-16
ABAQUS Data Analysis: Key Findings and Recommendations .....	3-17
Summary AND CURRENTLY ONGOING WORK.....	3-18
<b>Chapter 4 The AMPT Versus the UTM System</b> .....	<b>4-1</b>
The AMPT and UTM Systems.....	4-2
Load Cell Capacity and LVDT Span.....	4-3
LVDT Gluing Jigs and Sample Setup .....	4-4
Methodological Approach.....	4-5
Laboratory Experimentation Plan.....	4-6
Laboratory Test Methods.....	4-6

Work Plan and Procedural Steps .....	4-6
HMA Mix Details .....	4-7
The RLPD Test Method and Results.....	4-9
RLDP Data Analysis Models.....	4-9
HMA Sample Dimensions and AV Measurements for RLPD Testing .....	4-12
RLPD Test Results – Alpha ( $\alpha$ ) and Mu ( $\mu$ ) .....	4-12
RLPD Test Results – Statistical Analysis.....	4-13
RLPD Test Results – Key Findings and Recommendations .....	4-14
The FN Test Method and Results.....	4-14
FN Data Analysis Models.....	4-15
HMA Sample Dimensions and AV Measurements for FN Testing .....	4-17
FN Test Results and Statistical Analyses. ....	4-17
FN Test Results – Key Findings and Recommendations .....	4-18
The DM Test Method and Results.....	4-21
DM Data Analysis Models .....	4-21
HMA Sample Dimensions and AV Measurements for FN Testing .....	4-22
DM Test Results –  E*  Master Curves.....	4-23
DM Test Results – Statistics (COV and Stdev).....	4-23
DM Test Results – Key Findings and Recommendations .....	4-24
General Characteristic Features.....	4-27
HMA Sample and LVDT Setup .....	4-27
Temperature Consistency and Tolerances .....	4-27
LVDT Accuracy and Repeatability .....	4-29
Synthesis and Discussion of the Results .....	4-30
Summary.....	4-32
<b>Chapter 5 Comparative Evaluation of the RLPD, FN, AND DM Test Methods .....</b>	<b>5-1</b>
Laboratory Test Methods.....	5-1
Experimental Design Plan AND HMA MIXES.....	5-2
Laboratory Test Results and Analysis.....	5-2
The FN Test Results and Analysis.....	5-3
The DM Test Results and Analysis .....	5-5
The RLPD Test Results and Analysis .....	5-6
Comparison of the Test Results and Ranking of the HMA Mixes .....	5-7
Comparison of Laboratory Tests and Synthesis.....	5-12
Summary AND CURRENTLY ONGOING WORKS.....	5-18
<b>Chapter 6 Summary, Recommendations, and Future Work.....</b>	<b>6-1</b>
Key Findings and Recommendations.....	6-1
Ongoing and Future Work Plans .....	6-2

<b>References .....</b>	<b>R-1</b>
<b>Appendix A. List of Laboratory Tests Reviewed.....</b>	<b>A-1</b>
<b>Appendix B. The PLAXIS Software (2-D FE Linear Elastic Analysis) and Results .....</b>	<b>B-1</b>
<b>Appendix C. The ABAQUS Software (3-D FE Visco-Elastic Analysis) and Results.....</b>	<b>C-1</b>
<b>Appendix D. Comparative Evaluation of the AMPT and UTM Systems.....</b>	<b>D-1</b>
<b>Appendix E. Additional Data and Results for the FN, DM, and RLPD Tests .....</b>	<b>E-1</b>
<b>Appendix F. Workplans for Evaluating the HWTT Test Method, Tex-242-F Specification, and Preliminary Results .....</b>	<b>F-1</b>
<b>Appendix G. Work Plans for the Development of the Simple Punching Shear Test (SPST) and Preliminary Results.....</b>	<b>G-1</b>

## LIST OF FIGURES

Figure 1-1. Forensic Evaluations on US 79 (Bryan District) due to Premature SMA Rutting (about 1.2 inches Surface Rutting).....	1-2
Figure 1-2. Severe Surface Rutting on US 96 in Beaumont District (over 1.5 inches Rut Depth).....	1-2
Figure 1-3. Surfacing Rutting on Anderson Street in Bryan District (over 0.5 inches Surface Rutting).....	1-3
Figure 2-1. The HWTT Setup.....	2-2
Figure 2-2. RLPD Test Setup.....	2-3
Figure 2-3. RLPD Correlation with APT Field Data at NCAT - 10 Million ESALs.....	2-4
Figure 2-4. Example of a 5-Inches Long by 2-Inches Thick by 2-Inches Wide Prismatic Sample.....	2-4
Figure 2-5. Variability in the DM Test Results for a Type D Plant-Mix Material.....	2-7
Figure 2-6. A Typical Data Plot from the FT Test.....	2-8
Figure 2-7. A Typical Data Plot of the Flow Number Test.....	2-9
Figure 3-1. PLAXIS Software Main Input Screen Module.....	3-2
Figure 3-2. US 59 Pavement Structure in Atlanta District.....	3-3
Figure 3-3. Tire Loading Inclination at Vehicle Turning (P=100 psi).....	3-5
Figure 3-4. Vertical and Horizontal Displacements by Tire Inclination.....	3-6
Figure 3-5. Distribution of Shear Effect Zone by Tire Loading.....	3-7
Figure 3-6. Location of Max Shear Stress and Strain at 30° Tire Inclination.....	3-8
Figure 3-7. Maximum Shear Stress and Strain by Modulus (1.5-Inch HMA Overlay).....	3-9
Figure 3-8. Maximum Shear Stress and Strain by HMA (Overlay) Density (1.5-Inch Thick HMA Overlay with 147.7 ksi Modulus).....	3-9
Figure 3-9. Distribution of Shear Stress and Strain by Depth (2.0-Inch Thick HMA Overlay with 147.7 ksi Modulus).....	3-10
Figure 3-10. ABACUS/CAE Main Screen-User Interface.....	3-12
Figure 3-11. PVMNT Structure and Tire Loading Configuration.....	3-13
Figure 3-12. ABAQUS Tire and PVMNT Interaction.....	3-14
Figure 3-13. Shear and Vertical Stresses as a Function of PVMNT Depth and Temperature.....	3-14
Figure 3-14. Vertical Shear Strains Parallel to the Tire Moving Direction.....	3-15
Figure 3-15. Maximum Shear Stresses and Strains as a Function of Tire Inclination.....	3-16
Figure 3-16. PVMNT Response at 100 psi Tire Pressure.....	3-17
Figure 4-1. Pictures of the AMPT and UTM Units.....	4-2
Figure 4-2. Comparison of the Environmental Chambers.....	4-3
Figure 4-3. Comparison of the LVDT Gluing Jigs – UTM versus AMPT.....	4-4
Figure 4-4. Comparison of the LVDT Setup – UTM versus AMPT.....	4-5
Figure 4-5. Geographical Location of the Highway (SH 21).....	4-8
Figure 4-6. SH 21 PVMNT Structure.....	4-9
Figure 4-7. Plot of RLPD Strain versus Load Cycles.....	4-11
Figure 4-8. Log Plot of RLPD Strain versus Load Cycles.....	4-11
Figure 4-9. Graphical Illustration of the FN Concept.....	4-16
Figure 4-10. Accumulated Permanent Strain and Strain Rate as a Function of FN Load Cycles.....	4-16

Figure 4-11. Plot of the UTM-AMPT HMA $ E^* $ Master-Curves at 70°F.....	4-23
Figure 4-12. Plot of DM Stdev and COV—The UTM and AMPT Systems (Temperature Range = 40–130°F).....	4-26
Figure 4-13. Comparison of Temperature Consistency during RLPD Testing at 50°C.....	4-28
Figure 4-14. LVDT Variability Comparison for RLPD Testing at 40°C, 20 psi. ....	4-29
Figure 5-1. Graphical Comparison of the FN Parameters. ....	5-3
Figure 5-2. HMA $ E^* $ Master-Curves at 70°F.....	5-6
Figure 5-3. RLPD Accumulated Permanent Strain, $\epsilon_p$ , at 50°C. ....	5-7
Figure 5-4. Correlations between FN Cycles and $ E^* $ .....	5-9
Figure 5-5. Correlations between FN Index and $ E^* $ .....	5-9
Figure 5-6. Correlations between FN and $\epsilon_p$ , and FN Index and $\epsilon_p$ . ....	5-10
Figure 5-7. HWTT Graphical Rutting Results.....	5-11
Figure 5-8. Example of Variability in the DM Test Results (Type D Mix, Atlanta).....	5-14

## LIST OF TABLES

Table 2-1. Comparative Description of the DM, RLPD, and HWTT Tests.....	2-6
Table 2-2. Summary Review Findings of Laboratory Tests.....	2-13
Table 3-1. Pavement Structure and Moduli Values.....	3-4
Table 3-2. Density Variation.....	3-4
Table 3-3. Tire Loading Variation.....	3-5
Table 3-4. PVMNT Response as a Function of Tire Inflation Pressure.....	3-17
Table 4-1. Specification Features of the UTM and AMPT Units.....	4-3
Table 4-2. Type C HMA Mix-Design Characteristics.....	4-8
Table 4-3. The AMPT-UTM System Setups for the RLPD Test.....	4-10
Table 4-4. RLPD HMA Specimen Dimensions and AV Measurements.....	4-12
Table 4-5. RLPD Test Results – Alpha ( $\alpha$ ) and Mu ( $\mu$ ).....	4-12
Table 4-6. ANOVA Analysis at 95% Confidence Level-RLPD Test Data.....	4-13
Table 4-7. HSD Pairwise Comparison – RLPD Test Data.....	4-13
Table 4-8. The AMPT-UTM System Setups for the FN Test.....	4-14
Table 4-9. FN Data Analysis Models.....	4-15
Table 4-10. FN HMA Specimen Dimensions and AV Measurements.....	4-17
Table 4-11. FN Test Results and HSD Statistical Analyses.....	4-19
Table 4-12. FN Test Results and T-Test Statistical Analyses.....	4-19
Table 4-13. FN Test Results and HSD Statistical Analyses.....	4-20
Table 4-14. FN Test Results and T-Test Statistical Analyses.....	4-20
Table 4-15. The AMPT-UTM System Setups for the DM Test.....	4-21
Table 4-16. FN HMA Specimen Dimensions and AV Measurements.....	4-22
Table 4-17. Comparison of Sample and LVDT Setup Time.....	4-27
Table 4-18. Comparison of Temperature Heating Time.....	4-28
Table 4-19. Comparison of the AMPT and UTM Systems.....	4-31
Table 5-1. HMA Mix Characteristics.....	5-2
Table 5-2. Summary of FN Test Results.....	5-4
Table 5-3. HMA Mix Ranking Based on the FN, DM, and RLPD Test Results.....	5-7
Table 5-4. Summary of FN, DM, and RLPD Laboratory Test Results.....	5-8
Table 5-5. Comparisons of HWTT and RLPD Variability in the Test Results.....	5-12
Table 5-6. Statistics of the FN Index Results without the Outliers.....	5-13
Table 5-7. Comparison of the FN, DM, RLPD, and HWTT Test Methods.....	5-15

## LIST OF NOTATIONS AND SYMBOLS

2-D	Two-dimensional
3-D	Three-dimensional
AASHTO	American Association of State Highway and Transportation Officials
AMPT	Asphalt Mixture Test
APA	Asphalt Pavement Analyzer
AR	Asphalt-rubber
ASTM	American Society for Testing and Materials
AV	Air voids
Avg	Average
CAM	Crack attenuating mixtures
COV	Coefficient of variation
DOT	Department of Transportation
DM	Dynamic modulus
FE	Finite element
FN	Flow number
FSTCH	Frequency sweep test at constant height
HMA	Hot mix asphalt
HWTT	Hamburg Wheel Tracking Tester
Lab (lab)	Laboratory (laboratory)
LVDT	Linear variable displacement transducer
M-E	Mechanistic-empirical
MTS	Material testing system
OGFC	Open graded friction course
PD	Permanent deformation
PG	Performance grade
RAP	Reclaimed asphalt pavement
PD	Permanent deformation
RLPD	Repeated load permanent deformation test
PM	Plant-mix
PVMNT	Pavement

RAS	Recycled asphalt shingles
SGC	Superpave gyratory compactor
SMA	Stone mastic asphalt
SPST	Simple punching shear test
SPST-DL	Simple punching shear test in dynamic loading mode
SPST-ML	Simple punching shear test in monotonic loading mode
TTI	Texas A&M Transportation Institute
TxDOT	Texas Department of Transportation
UTM (UTM-25)	Universal Testing Machine
WMA	Warm mix asphalt
$G_f$	Specific fracture energy
$\sigma_t$	HMA tensile strength

## **CHAPTER 1 INTRODUCTION**

Routinely run at a single test temperature of 122°F in a water bath under Texas specification Tex-242-F, the Hamburg Wheel Tracking Test (HWTT) has a proven history of successfully identifying and screening hot-mix asphalt (HMA) mixes that are prone to rutting and/or susceptible to moisture damage (stripping) (TxDOT, 2009). However, with the record summer temperatures of recent years, several rutting failures have occurred with HMA mixes that had passed the HWTT test in the laboratory. These failures occurred mostly in high shear locations, in particular with slow moving (accelerating/decelerating) traffic at controlled intersections, in areas of elevated temperatures, heavy/high traffic loading, and/or where lower performance grade (PG) asphalt-binder grades have been used.

Earlier TxDOT studies had raised concerns about the HWTT test in that it is run at one temperature (122°F) and it provides high confinement to the test sample (TxDOT, 2009). Those studies also demonstrated that the repeated load permanent deformation (RLPD) test has a better correlation than the HWTT to field rutting performance. The RLPD test also provides material properties, which can be used in mechanistic-empirical (M-E) pavement thickness design procedures. However, the current RLPD test setup is relatively complex and not readily applicable for routine use. This makes it impractical to be used for routine HMA mix screening/acceptance and/or M-E structural design.

### **RESEARCH OBJECTIVES**

Based on the foregoing background and as a supplement to the HWTT test, this research study was initiated to develop a simpler and less time-consuming shear resistance and permanent deformation (PD)/rutting test that is also cost-effective, repeatable, and produces superior results in terms of correlation with field rutting performance. In particular, such a test should have the potential to discriminate HMA mixes for application in high shear stress areas (i.e., intersections) as well as being an indicator of the critical temperatures at which a given HMA mix, with a given PG asphalt-binder grade, becomes unstable and more prone to rutting and/or shear failure.

### **RESEARCH METHODOLOGY AND WORK PLANS**

Improper HMA mix selection due to poor laboratory screening can lead to costly premature pavement failures. Tying laboratory testing to field performance is thus very critical to

ensure optimal performance and minimization of maintenance/rehab costs. For rutting, this is particularly critical in areas of elevated temperatures (or in summer), heavy/high slow moving traffic with longer loading times, and/or where lower PG binder grades are used (for cost optimization purposes, etc.).

In the recent years where summer pavement temperatures have been over 110°F, several TxDOT districts including Bryan have experienced severe HMA rutting and shear failures for surface mixes (i.e., SMA, CAM, etc.), particularly at intersections; yet these mixes had satisfactorily passed the HWTT test in the lab. [Figure 1-1](#) through to [Figure 1-3](#) show some examples of severe summer surface rutting, mostly at intersections.



**Figure 1-1. Forensic Evaluations on US 79 (Bryan District) due to Premature SMA Rutting (about 1.2 inches Surface Rutting).**



**Figure 1-2. Severe Surface Rutting on US 96 in Beaumont District (over 1.5 inches Rut Depth).**



**Figure 1-3. Surfacing Rutting on Anderson Street in Bryan District (over 0.5 inches Surface Rutting).**

By contrast, however, most of these surface mixes shown in [Figure 1-1](#) through [Figure 1-3](#) had satisfactorily passed the HWTT at 122°F in the laboratory. The SMA in [Figure 1-1](#), for instance, had measured a rut depth of only 9.7 mm after 20,000 HWTT load passes at 122°F in the laboratory. Clearly, there is a need to revisit the HWTT and its associated Tex-242-F specification or otherwise explore other supplementary tests ([TxDOT, 2009](#)).

To address some of these problems, supplementary HMA shear resistance and PD/rutting tests in parallel with the HWTT should thus be developed that can be applicable for both laboratory molded and field core specimens. The research methodology for this study was therefore devised to focus on three key areas, namely:

- Should the HWTT criteria be modified for mixes to be used in these critical locations?
- Can practical supplementary HMA shear resistance and PD/rutting tests be developed to address these problems? Inevitably, such new test protocols should be applicable for both laboratory molded and field core specimens.
- What analytical models are available to help the designer at these critical locations?

As a minimum, the scope of work to address these aspects, over a two-year period, includes the following key activities:

- Data search and literature review.
- Computational modeling and shear stress-strain analysis.
- Evaluation of the existing rutting/PD tests such as the RLPD, FN, DM, etc., for possible improvements and modifications, relative to the HWTT test method.
- Comprehensive evaluation and possible modification of the HWTT test method and the Tex-242-F test specification.
- Development of new HMA rutting-shear tests.
- Sensitivity and statistical analyses of the test methods.
- Correlation with field data and development of test procedures/specifications.
- Test demonstration with a case study.

However, this interim report covers only the first three activities, namely literature review, computational modeling, and evaluation/modification of existing rutting/PD-related tests.

## **REPORT CONTENTS AND ORGANIZATIONAL LAYOUT**

As previously stated, this Year 1 report addresses three main activities of the study—namely, literature review, computational modeling, and laboratory test evaluations. The report is broken down into six chapters as follows:

- [Chapter 1](#) Introduction.
- [Chapter 2](#) Literature review.
- [Chapter 3](#) Computational modeling.
- [Chapter 4](#) Comparative evaluation of the UTM and AMPT systems.
- [Chapter 5](#) Comparative evaluation of the RLPD, FN, and DM tests.
- [Chapter 6](#) Summary, recommendations, and future work.

As noted above, [Chapter 6](#) provides a summation of the interim report including recommendations, ongoing work, and future work plans. Some appendices of important data are also included at the end of the report.

## **SUMMARY**

In this introductory chapter, the background and the research objectives of this project were discussed. The research methodology and scope of work were then described, followed by a summary of the project work plans. The chapter ended with a description of the report contents and the organizational layout.



## CHAPTER 2 DATA SEARCH AND LITERATURE REVIEW

The researchers conducted a literature review consisting of an extensive information search of electronic databases and their resulting publications to gather data on the currently existing HMA shear, PD, and rutting tests in the industry. This chapter discusses the findings of the literature review based on an extensive worldwide data search with a summary of the key findings and recommendations bullet-listed at the end of the chapter.

### LABORATORY TESTS REVIEWED

Over 10 different laboratory tests that are commonly used for HMA shear, PD, and rutting testing were comparatively reviewed, with particular emphasis on the following key characteristic attributes:

- Test type and schematic loading configuration.
- Test conditions and loading parameters.
- Output data and data analysis models.
- Advantages of each test method with emphasis on simplicity and tie to field performance.
- Limitations and challenges associated with each test method.
- Possible modification to the test method and its potential application for Texas mixes.

[Appendix A](#) of this interim report lists detailed evaluations of these characteristic attributes for each test method. However, some of the more commonly used HMA shear, PD, and rutting tests are discussed in the subsequent text and include the HWTT, RLPD, DM, and the FT/FN tests.

#### The HWTT Test

[Figure 2-1](#) defines the loading schematic of the HWTT in a TxDOT test procedure Tex-242-F (TxDOT, 2009). The HWTT is used for characterizing the rutting resistance potential and stripping susceptibility assessment (moisture damage potential) of HMA in the laboratory.



**Figure 2-1. The HWTT Setup.**

Although this test has performed satisfactorily in Texas for screening HMA mixes, particularly those susceptible to rutting/stripping, key challenges include high sample confinement and inability to generate material properties for M-E design and/or other analysis. Simulation of shear failure and impacts of traffic are also a challenge, particularly for surface HMA mixes placed at intersections. As indicated in [Appendix A](#) and discussed in the subsequent [Chapter 5](#) of this interim report, some of proposed modifications to improve this test method for continued Texas application include the following:

- Reviewing the HWTT test temperature to reflect the current field temperature regime and the asphalt-binder PG grades. This entails running the HWTT at multiple temperatures, ranging from 50°C to 70°C, depending on the asphalt-binder PG grade and climatic location of the candidate HMA mix.
- Reviewing the HWTT loading speed and other test parameters to better reflect field conditions, particularly at intersections.
- Reviewing and/or modifying the HWTT pass-fail screening criteria to address such scenarios as intersections, high temperature areas, slow moving traffic, etc.
- Running the HMA samples at multiple AV levels, ranging from 2 to 10 percent.
- Modifying the HWTT molds to relax the sample confinement during testing such as using rectangular molds.
- Exploring and/or devising other alternative HWTT data analysis parameters besides using the rut depth and number of passes as the only means to interpret the test results.

## The RLPD Test

The RLPD test is used to characterize the permanent deformation properties of HMA under repeated compressive Haversine loading (Zhou and Scullion, 2004; Walubita and Scullion, 2007). By measuring plastic strain of a HMA specimen due to the loading, the visco-elastic properties,  $\alpha$  and  $\mu$ , are determined as a function of a log-log plot of the accumulated plastic strain ( $\epsilon_p$ ) versus the number of load cycles ( $N$ ) as follows:

$$\epsilon_p = \alpha N^b \quad (\text{Equation 2-1})$$

$$\alpha = 1 - b; \mu = \frac{ab}{\epsilon_p} \quad (\text{Equation 2-2})$$

where  $a$  and  $b$  are the intercept and slope of the linear portion of the strain-load cycles curve on a log-log scale. The parameters  $\alpha$  and  $\mu$  are rutting parameters, with  $\mu$  computed at the 100th load cycle for this study (Zhou and Scullion, 2001). Figure 2-2 illustrates the pictorial setup of the RLPD test.

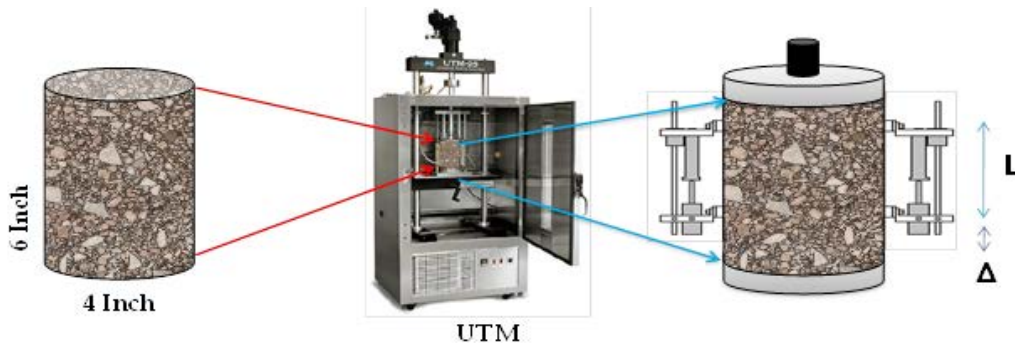


**Figure 2-2. RLPD Test Setup.**

Based on previous studies (Zhou et al., 2010) and as shown in Figure 2-3, the RLPD test has generally provided good correlation with field performance data and is also able to generate material properties for M-E design and other analyses; see also Appendix A. Major challenges are sample fabrication, testing of field cores or slabs, and high variability at high test temperatures such as 122°F. With the following proposed modifications/improvements, this test method exhibit potential for Texas applications:

- Test temperatures.
- Loading parameters.
- Specimen geometry.
- Analysis parameters.

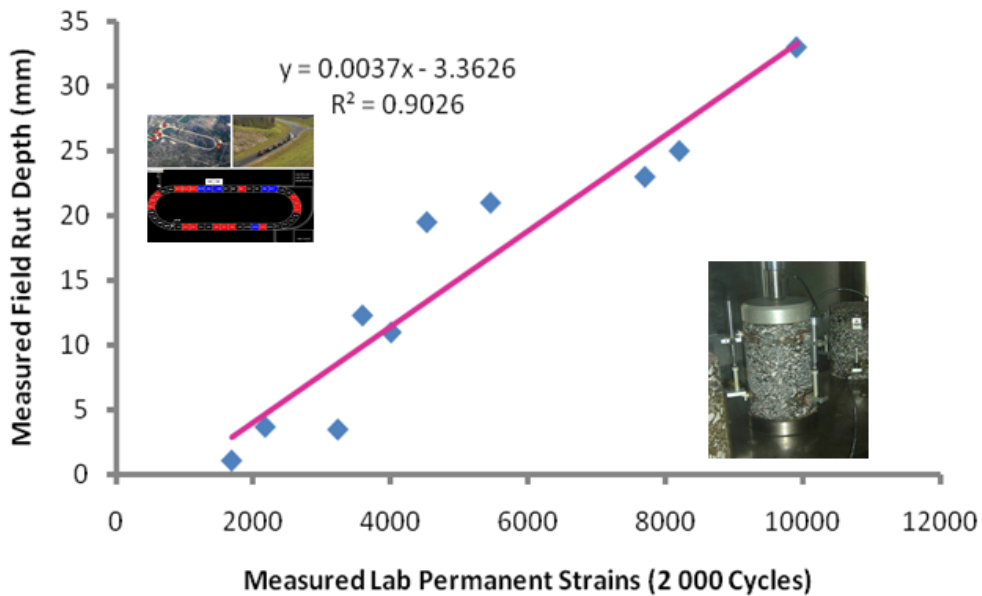


**Figure 2-3. RLPD Correlation with APT Field Data at NCAT - 10 Million ESALs.**

Figure 2-3 shows a good correlation between the RLPD lab and APT field data. Therefore, this test serves as a potential candidate for exploration and possible modification in this study. On the aspects of sample fabrication, Walubita et al. (2010) demonstrated that prismatic samples fabricated from field cores could easily be used provided the HMA layer thickness is equal to or greater than 2 inches. An example of a prismatic sample fabricated from a field core is shown in Figure 2-4.



**Figure 2-4. Example of a 5-Inches Long by 2-Inches Thick by 2-Inches Wide Prismatic Sample.**

Furthermore, the RLPD test parameters such as the stress and temperature could easily be modified to reflect the Texas field conditions. Also, unlike the HWTT, the RLPD does not provide high sample confinement and is also able to generate materials properties such as HMA modulus that can be used in M-E models/software.

### The Unconfined DM Test

Unconfined DM testing is an AASHTO standardized test method for characterizing the stiffness and visco-elastic properties of HMA mixes, measured in terms of the dynamic complex modulus,  $|E^*|$  (AASHTO, 2001). DM is a stress-controlled test involving application of a repetitive sinusoidal dynamic compressive-axial load (stress) to an unconfined specimen over a range of different temperatures and loading frequencies. The DM test setup is similar to the RLPD and major challenge is also sample fabrication and testing of field cores or slabs.

Table 2-1 provides a comparative description of the HWTT, RLPD, and DM tests (Walubita et al., 2012). The typical parameter that results from the DM test is the dynamic complex modulus,  $|E^*|$ , and is expressed as:

$$|E^*| = \frac{\sigma_0}{\varepsilon_0} \quad (\text{Equation 2-3})$$

where  $\sigma_0$  is the axial (compressive) stress, and  $\varepsilon_0$  is the axial (compressive) strain. For graphical analysis and easy interpretation of the DM data,  $|E^*|$  master-curves are also generated as a function of the loading frequency using time-temperature superposition sigmoidal model shown as (Pellinen and Witczak, 2002):

$$\log|E^*| = \delta + \frac{\alpha}{1+e^{\beta-\gamma\log(\xi)}} \quad (\text{Equation 2-4})$$

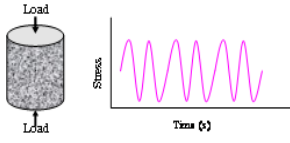
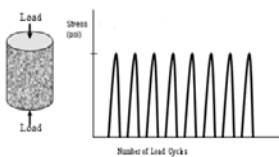
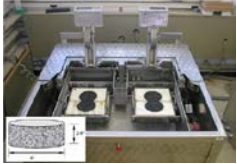
$$\log(\xi) = \log(f) + \log(a_T) \quad (\text{Equation 2-5})$$

where  $\xi$  is the reduced frequency (Hz),  $\delta$  is the minimum dynamic modulus value,  $\alpha$  is the span of modulus values, and  $\beta$  and  $\gamma$  are shape parameters. Parameters  $f$  and  $a_T$  are the loading frequency and temperature shift factor to temperature T, respectively.

The  $|E^*|$  determined from this test defines the stiffness (visco-elastic modulus) of the HMA mix and its PD/rutting resistance potential. Running this test at a limited temperature and

frequency range may practically serve to indicate the PD and rut susceptibility of HMA mixes as well as generate materials properties for M-E analysis. This can be done on a limited scale for specific scenarios and/or where data are required for input into M-E models.

**Table 2-1. Comparative Description of the DM, RLPD, and HWTT Tests.**

Feature\ Test	Dynamic Modulus (DM)	Uniaxial Repeated Load Permanent Deformation (RLPD)	Hamburg Wheel Tracking Test (HWTT)
Schematic			
Sample loading configuration			
Specimen size	4 in $\phi$ $\times$ 6 in H	4 in $\phi$ $\times$ 6 in H	6 in $\phi$ $\times$ 2.5 in H
Sample coring	Yes	Yes	No
Sample LVDT gluing/curing	Yes ( $\geq$ 12 hrs)	Yes ( $\geq$ 12 hrs)	No
Lab sample AV	7 $\pm$ 1%	7 $\pm$ 1%	7 $\pm$ 1%
Loading mode	Compressive repeated sinusoidal (stress-controlled)	Compressive repeated Haversine (stress-controlled)	Compressive repeated passing load
Test parameters	Loading: 0.5–250 psi Frequency: 0.1–25 Hz Recoverable strain: 50–150 $\mu\epsilon$	Loading: 10–30 psi Frequency: 1 Hz (0.1 s loading, 0.9 s rest time) Load passes: 5000 or 10,000	Loading: 158 lb Rate: 52 passes/min
Test temperature	-10°C, 4.4°C, 21.1°C, 37.8°C, 54.4°C	25°C, 40°C, 50°C	50°C in water bath
Output data	Load (stress), deformation, phase angle, and dynamic modulus	Axial permanent deformation, strains ( $\epsilon_p$ ), stress, number of load passes, time, temperature, frequency, visco-elastic properties ( $\alpha$ , $\mu$ ), and resilient modulus ( $M_r$ )	Number of load passes, applied load, temperature (water bath), time, and vertical permanent deformation (rut depth)
Terminate pass-failure criterion	N/A	10,000 cycles (for this study 5,000 cycles; some selected mixture were tested up to 10,000 cycles) or 25,000 microstrains	$\leq$ 0.5 in rut depth at: 10,000, 15,000, and 20,000 load passes for mixes with PG 64-XX, PG 70-XX, and PG 76-XX asphalt-binders, respectively
Reference or standard used	AASHTO TP-03, 2001	Walubita et al., 2012	Tex-242-F (2009)

Legend:  $\phi$  = diameter; H = height; AV = air voids; in = inches  $\cong$  25 mm; LVDT = linear variable differential transducer

As shown in [Figure 2-5](#), caution should be exercised with the DM test method because of the likelihood occurrence of high variability in the test results at elevated test temperatures.

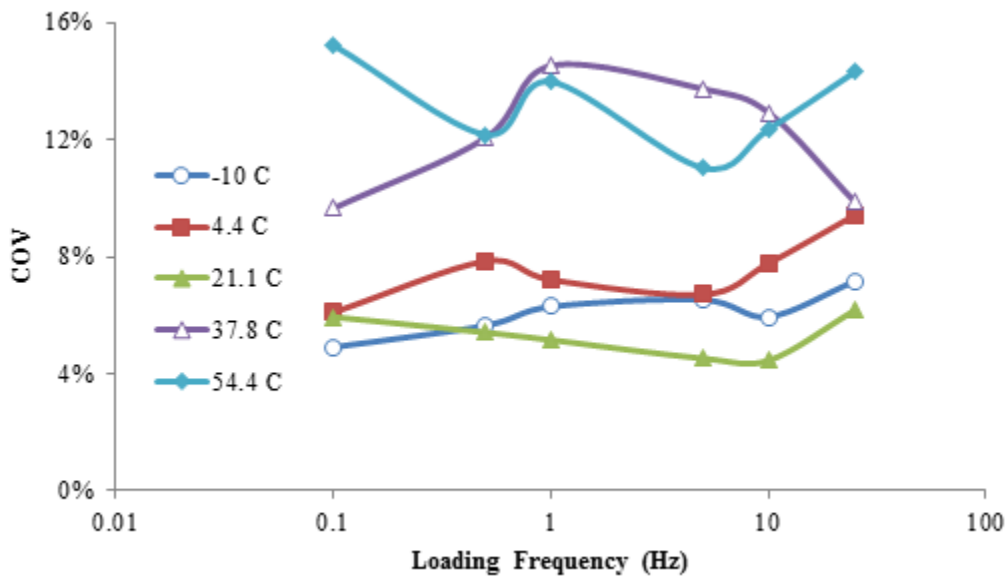


**Figure 2-5. Variability in the DM Test Results for a Type D Plant-Mix Material.**

In addition to the high temperature variability issues shown in [Figure 2-5](#), [Appendix A](#) also lists the following challenges as being associated with the DM test:

- Specimen fabrication (very laborious and requires experienced technicians).
- Inability to readily test field cores, particularly for thin PVMNT structures.
- Problematic getting the test temperature to  $-10^{\circ}\text{C}$ .
- Lengthy test time.

Therefore, modification and/or improvement of this test method will entail looking at the following aspects as a minimum:

- Test temperatures.
- Loading parameters, i.e., stress levels and frequencies.
- Specimen geometry.

### The Unconfined FT and FN Tests

This is a static uniaxial creep test in which an HMA cylinder is axially loaded and the total sample compliance versus loading time is measured ([Witczak et al., 2002](#)). A constant

stress of 207 kPa (30 psi) is applied on a specimen with a diameter of 100 mm and a height of 150 mm at the temperature of 140°F.

Three basic zones in a typical plot of log compliance versus log time have been identified as indicators of HMA response:

- The primary zone—the portion in which strain rate decreases with loading time.
- The secondary zone—the portion in which strain rate is constant with loading time.
- The tertiary zone—the portion in which strain rate increases with loading time.

Ideally, a large increase in compliance occurs within the tertiary zone while the sample remains at relatively constant volume. In theory, this is due to shear deformation and the time it takes a sample to reach this shear deformation, called flow time (FT), can indicate an HMA mix's rutting resistance (Witczak et al., 2002). This is shown subsequently in Figure 2-6. Lower laboratory flow times should correspond to greater permanent deformation in the field.

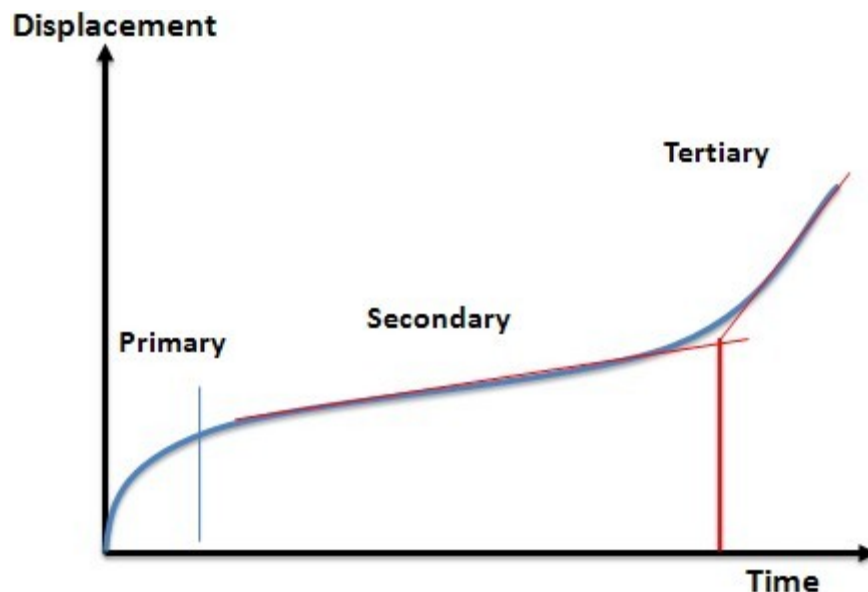


**Figure 2-6. A Typical Data Plot from the FT Test.**

The FN follows a similar concept and setup as the FT except that the horizontal X-axis is a plot of load cycles instead of time (see Figure 2-7). Appendix A lists the pros and cons of both the FT and FN test methods.

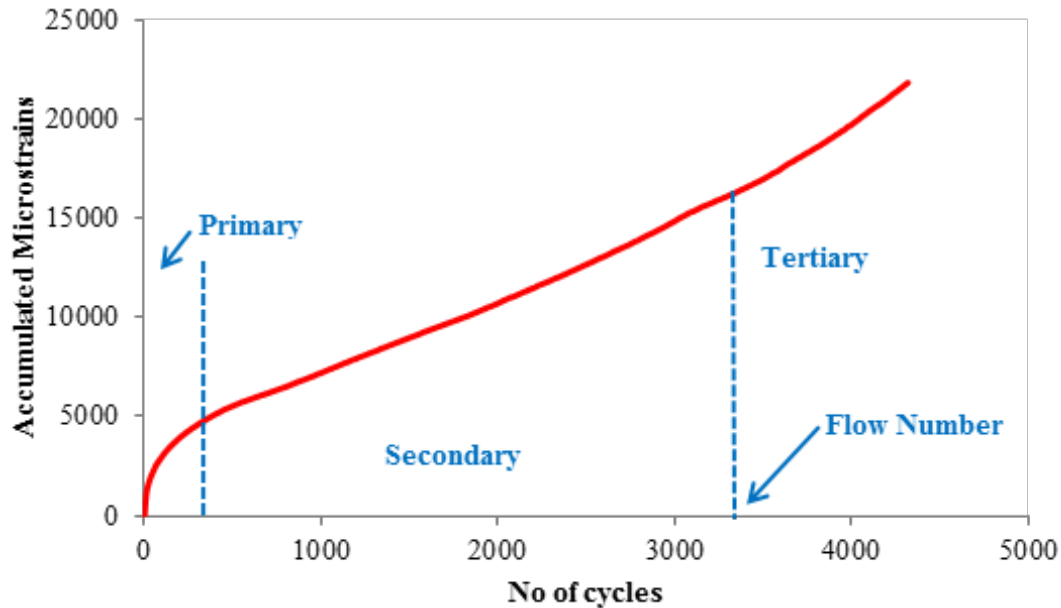


**Figure 2-7. A Typical Data Plot of the Flow Number Test.**

Key challenges associated with these tests include the following:

- Sample fabrication process is both laborious and long.
- Confined testing may be required for open-graded mixes.
- May not simulate field dynamic phenomena.
- Problematic testing field cores obtained from thin PVMNT structures.

Like the DM test, modification and/or improvement of these test methods will entail looking at the following aspects as a minimum:

- Test temperatures.
- Loading parameters, i.e., stress levels and frequencies.
- Specimen geometry.
- Data analysis models/parameters.

### **Other HMA Rutting and Shear Tests**

[Appendix A](#) shows the other available tests currently in use such as the Asphalt Pavement Analyzer (APA), the Repeated Shear Test at Constant Height (RSTCH), and the Frequency Sweep Test at Constant Height (FSTCH). The APA concept is similar to the HWTT and for most part, presents similar challenges as those for the HWTT ([PTI, 2012](#); [George DOT, 2012](#)). The Repeated Shear Test at Constant Height (RSTCH) is outlined in the AASHTO T320-03

Procedure C (AASHTO, 2003; Sousa et al., 1994). A Haversine shear stress of 10 psi for 0.1 sec with a 0.6 sec rest period is applied to a HMA specimen (6 inches diameter by 2 inches height) while the height of the specimen is maintained constant throughout the test.

Experiences with a wide range of mixes tested at different temperatures and stress levels in SHRP Report A-698 (Sousa et al., 1994) have defined the shear stress of 10 psi for the RSTCH test. The test is conducted until 5 percent shear strain is reached or up to 5,000 cycles. HMA mixes that reach 5 percent shear strain before 5,000 cycles of loading may be susceptible to rutting. While the test can be executed at any temperature, AASHTO recommends the use of the maximum 7-day pavement temperature for a selected depth.

The RSTCH is a strain-controlled repeated test where the resultant stress is measured over a range of temperatures and frequencies (Chowdhury and Button, 2002). Actually, the test method is used to measure the shear dynamic modulus by the visco-elastic behavior of HMA mixes. Test specimen is 6 inches diameter by 2 inches height. Horizontal strain is applied at different ranges from 0.1 to 10 Hz using a Haversine loading while the specimen height is maintained constant by compressing or pulling it vertically. The applied strain and the stress response are measured during the test and used to compute the shear modulus and the shear phase angle. While a higher complex modulus indicates a stiffer mix that is more resistant to rutting, a lower shear phase angle indicates more elastic behavior that is more resistant to rutting. The test machine is expensive and requires a highly trained operator to run the test. Thus, it may be unfeasible to consider it in this study.

Appendix A shows the other tests reviewed include the IDT, the punching test, and the indentation test. Specifically, the punching and indentation tests will be utilized as a basis for developing a new HMA shear test that will be executed and reported in Year 2 of this study.

## **LABORATORY TESTS CONDUCTED IN STUDY 0-6658**

These researchers are currently conducting various rutting and PD tests in the ongoing Study 0-6658 (Walubita et al., 2012), including:

- HWTT.
- The RLPD.
- The FN.
- The DM.

Based on the preliminary comparative analysis of these tests, the major findings as related to Study 0-6658 include the following:

- The HWTT exhibits the best repeatability and lowest variability in the test results;  $COV < 10$  percent. For the DM and RLPD tests, variability generally appeared to increase with increasing temperature; but exhibited no definitive trend with the loading frequency.
- Because of its simplicity, practicality, repeatability, and lowest variability, the HWTT appears to be the best suited for daily routine HMA mix-design and screening, including stripping assessment and rutting performance prediction. One major challenge with the HWTT is its inability to directly generate most of the typical HMA input data and material properties (e.g., modulus) required for pavement structural designs and M-E analyses. High sample confinement during testing and characterization of the HMA shear resistance properties are other aspects that need to be addressed with this test.
- Because of their potential to comprehensively characterize the HMA modulus (stiffness) and visco-elastic properties as well as predict rutting performance, the DM and RLPD tests appears to be better suited for HMA structural design applications such as generating input data for M-E design models. Compared to the HWTT, a challenge exists in applying these tests for daily routine HMA mix-designs and screening due to the complexity of the sample fabrication process and the length test-time requirement, particularly for the DM test. Addressing these challenges, specifically the RLPD can easily serve as a routine screening test and characterization of the HMA shear properties to supplement the HWTT. Hence, the RLPD is a potential test candidate for this study next to the HWTT.
- With the FN test, derivation of new parameters to analyze and interpret the test data proved very promising in the ongoing Study 0-6658. The newly derived parametric ratio (FN Index) was able to successfully distinguish and differentiate mixes. Thus, this test is also a potential candidate for further evaluation in this study.

## SUMMARY

Based on literature search findings of this chapter and the review analysis presented in [Table 2-2](#) and [Appendix A](#), the following laboratory tests and setup systems were found to be feasible for evaluation and possible modification/improvement in this study:

- The HWTT test.
- The RLPD test.
- The FN test.
- The DM test.
- The APA test.
- The punching and indentation tests.
- The AMPT system in comparison to UTM system.

[Chapter 4](#) of this interim report documents a comparative evaluation of the AMPT and UTM systems. [Chapter 5](#) presents a comparative evaluation of the RLPD, the FN, and DM tests relative to the HWTT test method. However, no extensive laboratory evaluation was conducted on the APA during this reporting period as it shares almost the same shortfalls and challenges as the HWTT test method.

The punching and indentation tests were all used as a reference basis for developing a new HMA shear test that will be executed in Year 2 of this study. This work will all be documented and published in the future Year 2 report of this study.

**Table 2-2. Summary Review Findings of Laboratory Tests.**

<b>Test Type</b>	<b>Parameter</b>	<b>Test Condition</b>	<b>Advantages</b>	<b>Disadvantages</b>	<b>Proposed Modification</b>
HWTT	Rut/passess	50°C and 158 lb	<ul style="list-style-type: none"> <li>-Simplicity and practicality.</li> <li>-Can test both laboratory made samples and field cores.</li> <li>-Reasonable test time (&lt; 8 hrs).</li> <li>-Repeatability and low variability in results</li> <li>-Rutting and moisture damage (stripping) assessment.</li> <li>-Applicable for daily routine mix-design.</li> <li>-Good correlation to field performance.</li> </ul>	<ul style="list-style-type: none"> <li>-Cannot readily generate HMA material properties for structural design and M-E analyses.</li> <li>-High sample confinement during testing that may at times negatively impact the test results and rutting performance of the mixes.</li> <li>-Inability to sufficiently capture the shear resistance characteristics of the mixes.</li> </ul>	Temperature, wheel speed, confinement conditions, etc.
DM	E*	-10, 4.4, 21.1, 37.8, 54.4°C	<ul style="list-style-type: none"> <li>-Characterization of dynamic modulus,  E* , and visco-elastic properties (E', E'', δ).</li> <li>-HMA stiffness and rutting performance prediction.</li> <li>-Generation of HMA material properties for structural design, Mechanistic-Empirical (M-E) models, and performance prediction (MEPDG, PerRoad, etc.)</li> </ul>	<ul style="list-style-type: none"> <li>-Specimen fabrication process is laborious and long.</li> <li>-Cannot readily test field cores.</li> <li>-Lengthy test time (minimum 3 days).</li> <li>-High variability at high test temperatures.</li> <li>-Problematic getting the temperature to below 0°C (i.e., -10°C)</li> <li>-Problematic maintaining LVDT studs at high temperatures.</li> </ul>	Temperature and loading frequency
RLPD	$\alpha, \mu$	50°C and 10 psi, 40°C and 20 psi	<ul style="list-style-type: none"> <li>-Reasonable test time (<math>\cong</math> 24 hrs).</li> <li>-HMA permanent deformation and visco-elastic properties.</li> <li>-HMA material properties for structural design.</li> <li>-HMA rutting performance prediction.</li> </ul>	<ul style="list-style-type: none"> <li>-Sample fabrication process is both laborious and long.</li> <li>-Cannot readily test field cores.</li> <li>-High variability at high test temperatures.</li> <li>-Problematic maintaining LVDT studs at high temperatures.</li> </ul>	Temperature, load, specimen geometry
Flow Number (FN)	FN	Not specified	Good correlation to field rutting	In some cases, FN cannot represent field situation	Temperature, load, analysis parameters, etc.
FT	FT	60°C and 30 psi	<ul style="list-style-type: none"> <li>-Simple test and inexpensive.</li> <li>-Best correlation of experimental sites to field rutting for confined conditions.</li> </ul>	<ul style="list-style-type: none"> <li>-Sample fabrication process is both laborious and long.</li> <li>-Confined testing may be required for open-graded (SMA) mixtures.</li> <li>-May not simulate field dynamic phenomena.</li> </ul>	

**Table 2.2. Summary Review Findings of Laboratory Tests (cont'd).**

APA	Rut	100 psi (Temp. not specified)	<ul style="list-style-type: none"> <li>-Good correlation to field performance and widely used.</li> <li>-It is reasonable, repeatable, and reliable.</li> <li>-Can evaluate moisture damage.</li> </ul>	<ul style="list-style-type: none"> <li>-Rut depth is sensitive to changes in air voids content</li> </ul>	
RSTCH	$a, b$	10 psi with max. 7-day pavement temperature	<ul style="list-style-type: none"> <li>-Good correlation to field performance.</li> <li>-HMA material properties for structural design.</li> </ul>	<ul style="list-style-type: none"> <li>-Sample fabrication process is both laborious and long.</li> <li>-Cannot readily test field cores.</li> <li>-High variability at high test temperatures.</li> </ul>	test temperature and load
FSTCH	$ G^* , \delta$	0.1 to 10 Hz of horizontal strain	<ul style="list-style-type: none"> <li>-HMA permanent deformation and visco-elastic properties.</li> <li>-Useful to predict both rutting and fatigue cracking.</li> <li>-Generation of HMA material properties for structural design, M-E models and performance prediction.</li> </ul>	<ul style="list-style-type: none"> <li>-Sample fabrication process is both laborious and long.</li> <li>-Cannot readily test field cores.</li> <li>- Need a highly trained operator.</li> <li>- Impractical for field use.</li> </ul>	Test temperature and frequency

## CHAPTER 3      COMPUTATIONAL MODELING AND SHEAR STRESS-STRAIN ANALYSIS

As an integral component of this study, computational modeling was imperative, at a minimum, to address the following two key aspects:

- Shear stress-strain distribution analysis to determine the critical zones of plastic deformation and shear failure in a pavement structure.
- Computational and sensitivity analysis to determine the critical factors that influence rutting and shear deformation when the pavement structure is subjected to the worst case scenario in terms of traffic loading (low speed/heavy trucks), intersections/turning traffic, traffic go-stop sections (i.e., at traffic lights), and extreme temperatures.

Overall, the ultimate intent is to be able to compare and relate the HMA shear strength properties to the shear stresses that heavy trucks produce on pavement structures under the aforementioned extreme conditions to mitigate HMA shear failures in the field. To accomplish these objectives, the researchers used 2-D elastic and 3-D visco-elastic FE analysis with the PLAXIS and ABAQUS software, respectively.

Computational modeling and numerical analysis was executed to help identify the critical factors that influence rutting and shear deformation in terms of:

- Stress-strain impacts on pavement (PVMNT) response and performance.
- Generation of a matrix of critical factors to aid in establishing the lab test parameters.
- Establishment of preliminary limits and thresholds for critical shear deformation zones and occurrence of maximum plastic strains.
- Establishing and relating the analytical displacements and stress-strain results to the lab tests and field data in terms of HMA shear resistance, PD, and rutting characterization.

This chapter provides a documentation of the computational work completed to date and the analytical results based on the 2-D PLAXIS and 3-D ABAQUS FE modeling. [Appendices B](#) and [C](#) have additional software data and detailed analytical results. The chapter then concludes with a summary of the key findings and recommendations.

## PLAXIS 2-D FE MODELING: LINEAR ELASTIC ANALYSIS

This section of the chapter discusses the PLAXIS 2-D FE linear-elastic analysis and is broken into the following subsections:

- Description of the PLAXIS software.
- Pavement structures analyzed and input variables.
- PLAXIS modeling results and analysis – displacements, shear stresses, and strains.
- Key findings and recommendations.

### The PLAXIS Software

The PLAXIS software is based on finite element technology and intended for civil engineers for the two-dimensional analysis. The software provides several material models such as linear elastic, mohr-coulomb, soil model, etc. The software package consists of:

- The input module for defining geometry, material properties, and loading.
- The calculation module for setting up analysis options.
- The output module for presenting analysis results.

Figure 3-1 shows an example of the PLAXIS main input screen module. Appendix B shows other details such as the calculation and output screen modules.

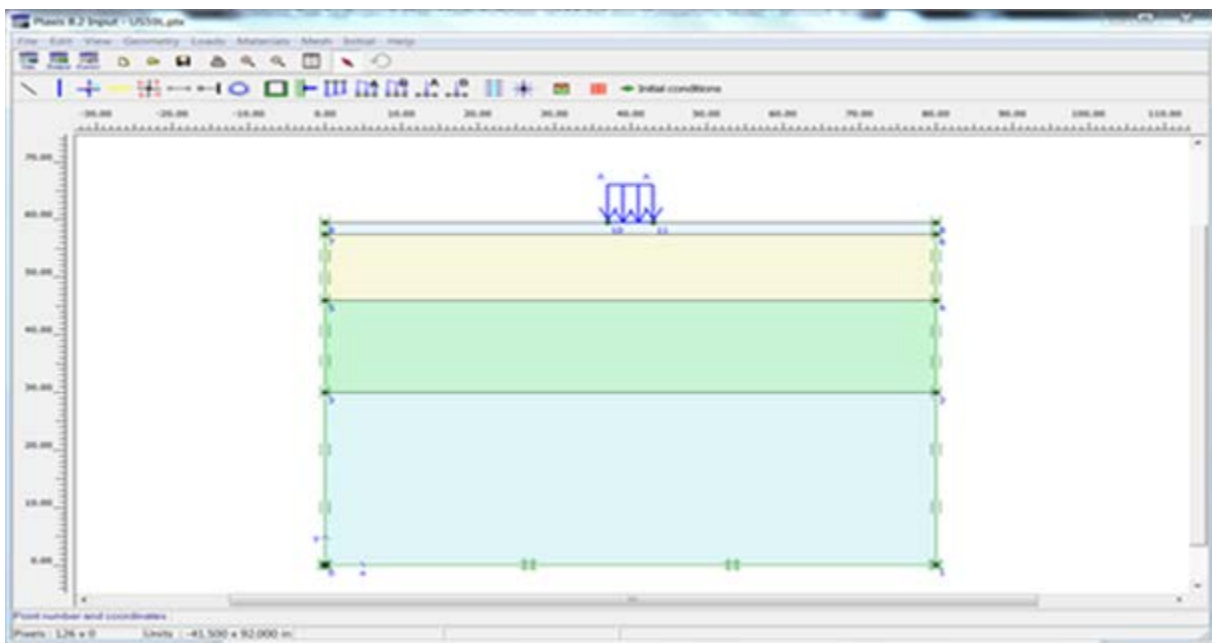


**Figure 3-1. PLAXIS Software Main Input Screen Module.**

## PLAXIS Pavement Structures and Input Variables

To identify the shear deformation effect zone when subjected to traffic loading and temperature, the researchers conducted the 2-D finite element analysis using PLAXIS software and considering various range of pavement structures (HMA layer thickness), HMA layer modulus (as a function of actual measured temperature), and traffic loading condition. For this analysis, the US 59 highway in the Atlanta District—a test section in Study 0-6658, with known material properties and climatic data—was utilized as the reference PVMNT structure (see [Figure 3-2](#)).



**Figure 3-2. US 59 Pavement Structure in Atlanta District.**

Based on the US 59 PVMNT structure data, the following variables were included in the analysis matrix:

- Layer thickness variations from 1.5 to 2.0 inches for the HMA (AC) surfacing overlay.
- Climatic influence in terms of field temperatures and HMA modulus variation.
- Air void (AV) effects in terms of the HMA density variations from 140 to 150 pfc.
- Tire inclination variations from 0 to 30° angles to simulate turning traffic at intersections.
- Tire pressure (100 psi).

Table 3-1 shows the variations of layer thickness and HMA modulus influenced by field temperature. The temperatures 112 and 92°F represent actual measured field temperatures in summer and fall, respectively, in 2012 at 1 inch PVMNT depth. The following equation was used to correct the HMA back-calculated modulus to 77°F (Walubita et al., 2012):

$$E_{77^{\circ}\text{F}} = (T^{2.81}/200,000) * E_{\text{FWD}} \quad (\text{Equation 3-1})$$

where  $E_{77^{\circ}\text{F}}$  is the corrected HMA modulus to 77°F in ksi,  $E_{\text{FWD}}$  is the back-calculated FWD modulus in ksi without any temperature corrections, and  $T$  is the pavement temperature in °F during FWD test that was measured at 1-inch depth.

**Table 3-1. Pavement Structure and Moduli Values.**

Layer	Thickness (in.)			Modulus (ksi) by Temperature (°F)		
HMA Overlay (Type D)	1.50	1.75	2.00	147.7 (112°F)	256.7 (92°F)	423.3 (77°F)
Existing HMA	11.5			478.5		
LFA Base (Lime fly-ash treated)	16.0			129.8		
Subgrade	-			44.0		

To investigate the AV effects in terms of the HMA density, the density variation listed in Table 3-2 was analyzed using the PLAXIS software. The 1.5 inches instead of the in-situ 2.0 inches was utilized for the density variation because it represented the worst-case scenario in terms of shear stress-strain responses based on Table 3-1 analysis.

**Table 3-2. Density Variation.**

PVMNT Layer	Density (pcf)			Thickness (Inch)	Modulus (ksi)
HMA Overlay (Type D)	140	145	150	1.5	147.7
Existing HMA	145			11.5	478.5
LFA Base (Lime fly-ash treated)	135			16	129.8
Subgrade	125			-	44.0

To simulate turning traffic at an intersection zone, the tire forces were applied in a manner of shearing by inclining the tire loading from 0 to 30° angles. Table 3-3 lists various tire inclinations used for the analysis. The tire pressure components in the X and Y directions were determined as a vector sum of 100 psi based on the tire inclination angles shown in Table 3-3 and demonstrated in Figure 3-3, i.e., P = 100 psi.

**Table 3-3. Tire Loading Variation.**

Tire Inclination ( $\alpha$ )		0° (Vertical only)	5°	10°	15°	20°	30°
Tire Pressure (psi)	X-axis	0	8.72	17.36	25.88	34.20	50.00
	Y-axis	100	99.62	98.48	96.59	93.97	86.60

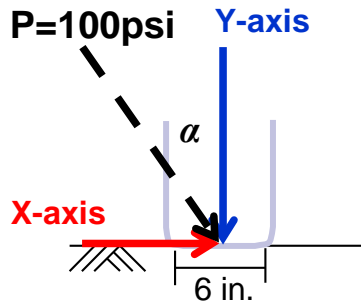


**Figure 3-3. Tire Loading Inclination at Vehicle Turning (P=100 psi).**

### PLAXIS Results: Vertical and Horizontal Displacements

To assess the displacements occurring on the surface of the PVMNT structure subjected to traffic loading, the research team evaluated the vertical and horizontal displacements by inclining the tire loading at various angles. As theoretically expected, the displacements were greater in magnitude when the traffic loading was applied only in the vertical direction (i.e., 0° tire inclination angle).

However, the horizontal displacement increases along with inclining the tire loading (see Figure 3-4). That is the horizontal displacement increased with an increase in the tire inclination angle and vice versa for the vertical displacement. This increase in horizontal displacement could potentially contribute to shear failures at intersections due to turning traffic. The movement of displacement effect from vertical to horizontal direction due to the tire inclination may also possibly contribute to the buckling and/or shoving of HMA surface at high temperatures.

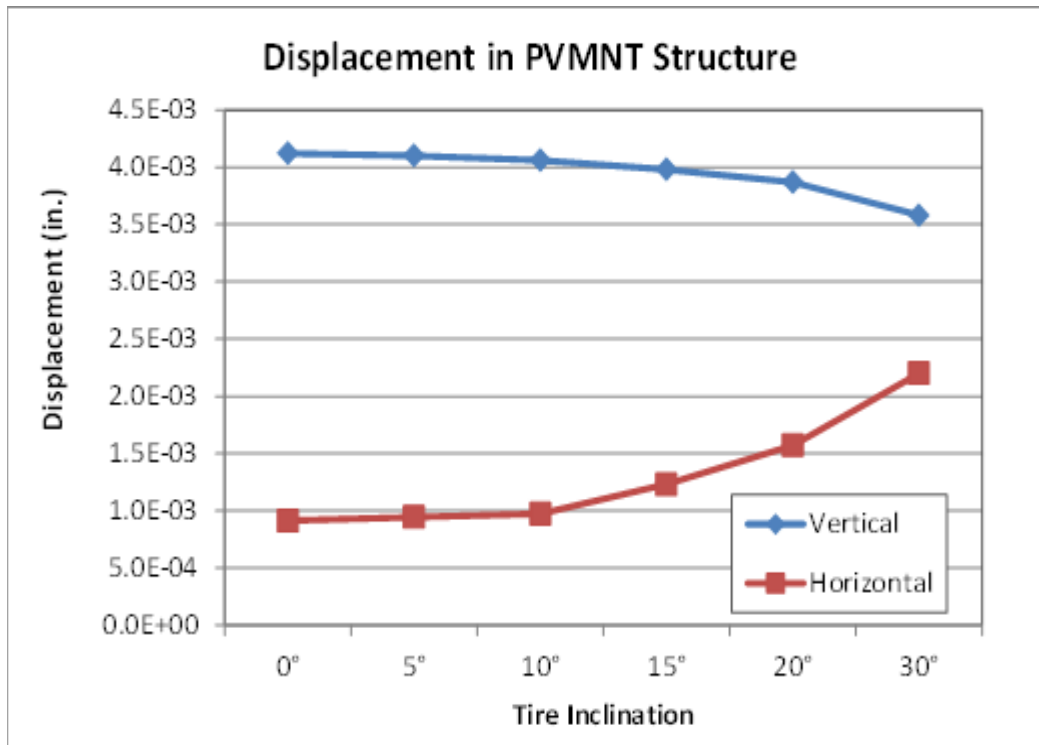
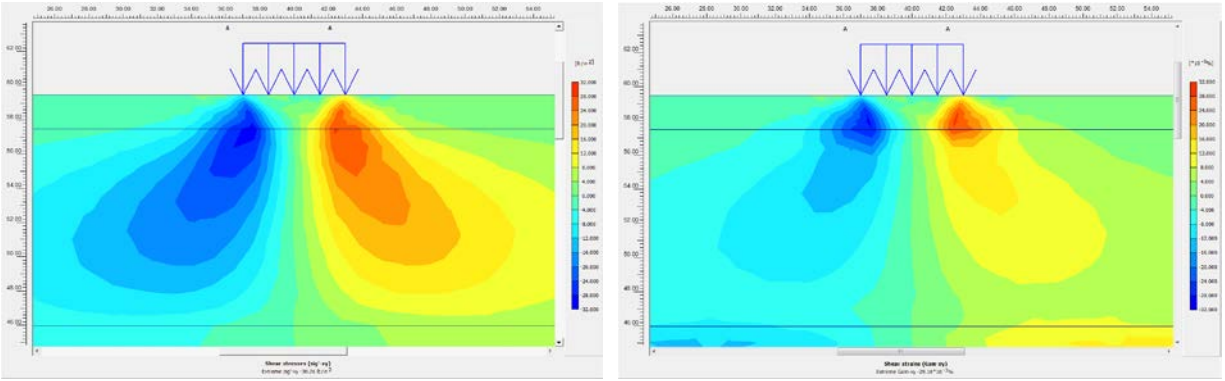


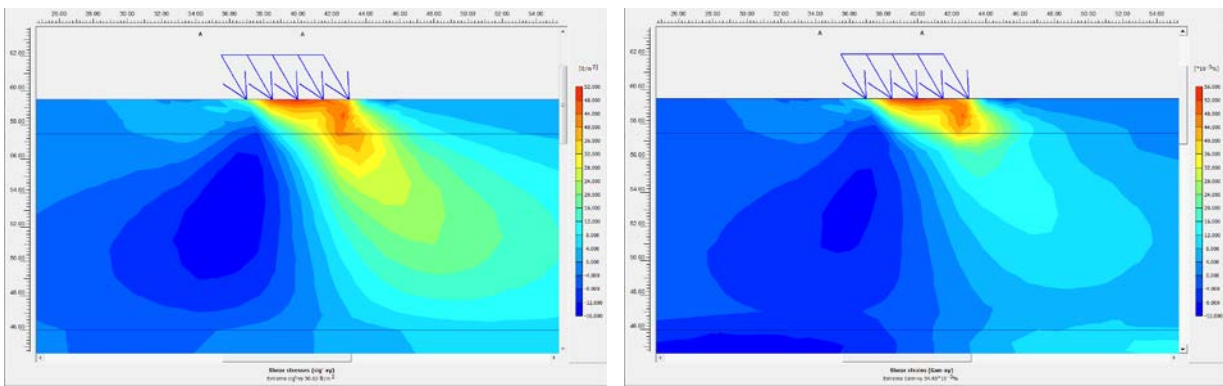
**Figure 3-4. Vertical and Horizontal Displacements by Tire Inclination.**

#### **PLAXIS Results: Shear Stress-Strain Distributions**

When the traffic loading was applied only in the vertical direction (0° tire inclination), the most severe shear stress-strain distribution within the HMA layer, as theoretically expected, occurred near the edge of the tire load as shown in [Figure 3-5\(a\)](#). However, the distribution of the shear effect zone moved from the edge to underneath the tire by inclining the tire loading along with an increase in the maximum shear stress and strain (see [Figure 3-5\(b\)](#) for the 30° tire inclination). The movements of the shear effect zone due to tire inclination are illustrated in [Figure B-4](#) through [B-9](#) in [Appendix B](#).



**(a) Shear Stress and Strain at Vertical Tire Loading of 0° Inclination**



**(b) Shear Stress and Strain at 30° Inclination Tire Loading**

**Figure 3-5. Distribution of Shear Effect Zone by Tire Loading.**

The relocation of the shear effect zone might indicate that the critical shear failure zone extends to the entire range of the tire contact area as a function of the tire inclination, which may partly contribute to the buckling or shoving of the surfacing HMA or overlay. In the case of the 30° tire inclination, the maximum shear stress and strain occurred at the middle of the surface of the AC overlay layer (see [Figure 3-6](#)). This means that the surface of the HMA layer such as the top 0.5 inches should be considered as a critical shear and rutting failure zone at an intersection where vehicles are turning and/or stopping. In [Appendix B, Figure B-10 through Figure B-15](#) presents the location of the maximum shear stress and strain on each tire inclination.

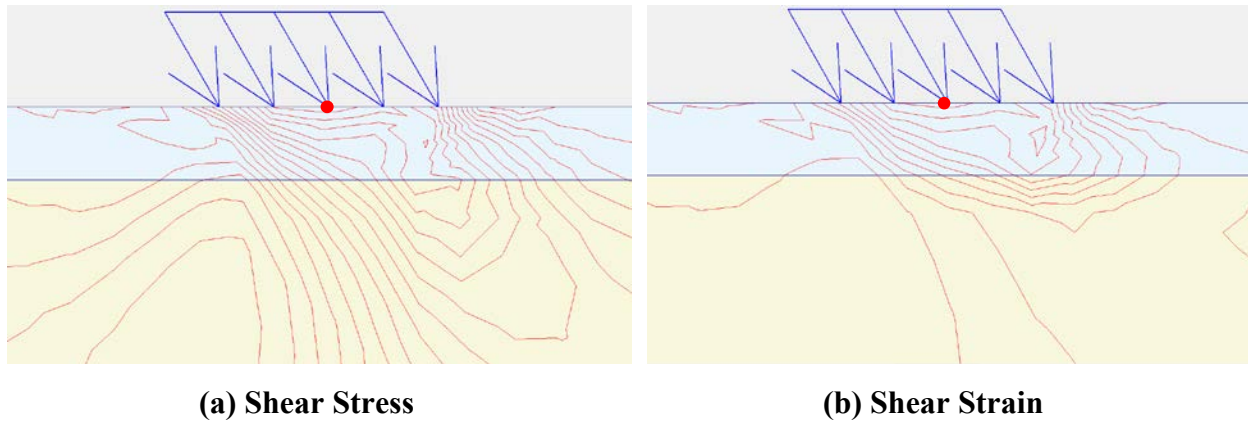


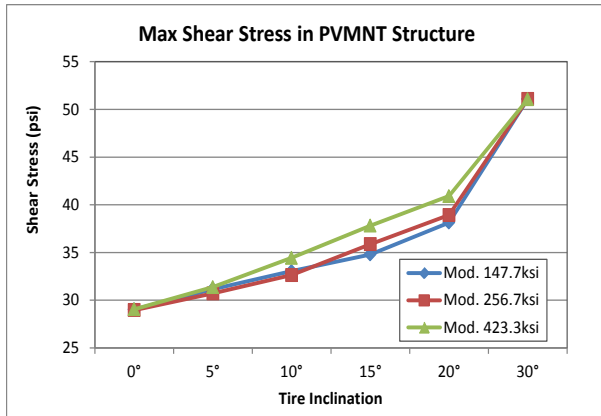
**Figure 3-6. Location of Max Shear Stress and Strain at 30° Tire Inclination.**

**PLAXIS Data Analysis: Identification of Critical Factors that Influence Shear Deformation**

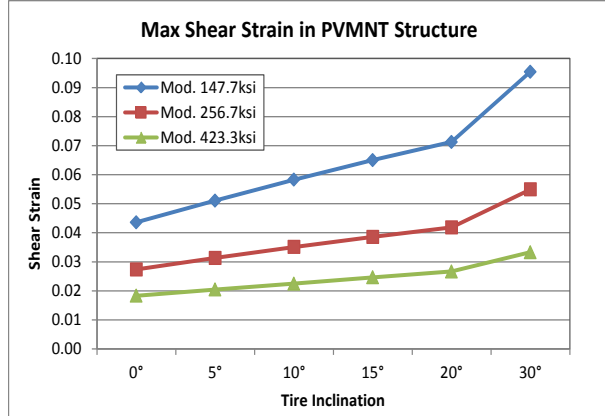
To identify critical factors that significantly impact HMA shear deformation, partly to aid in the development of new HMA shear resistance and rutting tests, PLAXIS sensitivity analyses were conducted, taking into account the effects of thickness and temperature of the HMA layer, pavement-tire interaction, and density of the HMA layer. As shown in [Figure 3-7\(a\)](#), the shear stress in each HMA pavement is increasing significantly with a rise in the degree of tire inclination. However, the modulus shows less influence on the shear stress response as compared to the tire inclination. That is, the pavement-tire interaction has a significant influence on controlling the shear stress response within the HMA structure.

On the other hand, both the tire inclination and the modulus of HMA (overlay) layer have significantly affected the shear strain response (see [Figure 3-7\[b\]](#)). From these comparisons, it is noted that both traffic loading conditions simulated by tire inclination and temperature representing HMA modulus variation have significant impact on the shear strain response in HMA pavements. This effect should possibly be considered in the developmental process of new HMA shear resistance and rutting test methods. [Figure B-16](#) through [Figure B-18](#) ([Appendix B](#)) presents a comparison on all the HMA overlay thicknesses.

Note that the shear stresses in [Figure 3-7\(a\)](#) are synonymous to the shear resistance developed within the HMA in when subjected to loading. So, high stress development should theoretically result into lower strain values and vice versa.



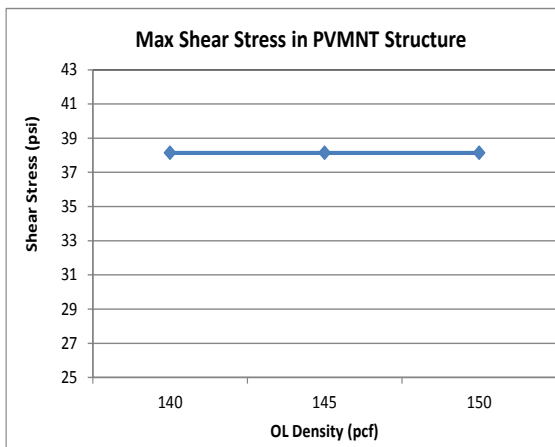
(a) Shear Stress



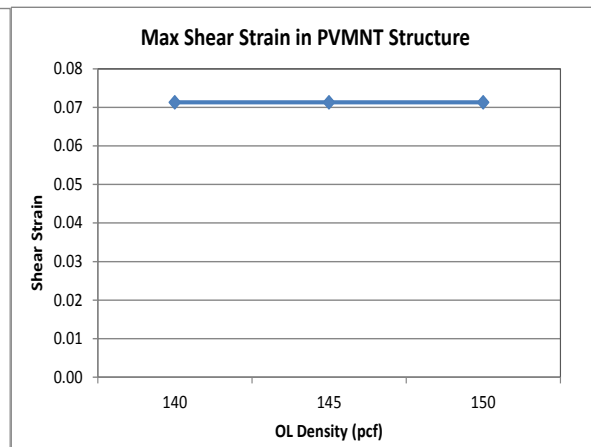
(b) Shear Strain

**Figure 3-7. Maximum Shear Stress and Strain by Modulus (1.5-Inch HMA Overlay).**

For the effects of HMA (overlay) density variations, the research team conducted a sensitivity analysis with the worst-case scenario (thin surface layer, low modulus corresponding to high temperature, and 20° tire inclination). Surprisingly however, the 2-D PLAXIS elastic analysis did not detect any influence on the shear stress-strain responses due to HMA (overlay) density variations (see Figure 3-8). A similar unexpected shear stress-strain response trend was also noted for the surfacing layer (HMA overlay) thickness variation in Figure B-19 through B-21 in Appendix B, further reinforcing the need for 3-D FE visco-elastic analysis.



(a) Shear Stress



(b) Shear Strain

**Figure 3-8. Maximum Shear Stress and Strain by HMA (Overlay) Density (1.5-Inch Thick HMA Overlay with 147.7 ksi Modulus).**

The shear stress-strain distribution in Figure 3-9 shows a theoretically expected decreasing magnitude with PVMNT depth. The overlay (surfacing) layer is the most severely affected, especially at the higher angles of tire inclination that is synonymous with turning traffic at intersections. Thus, the surfacing layer, particularly at intersections under high summer temperatures, will likely be more susceptible to shear failure and permanent deformation.

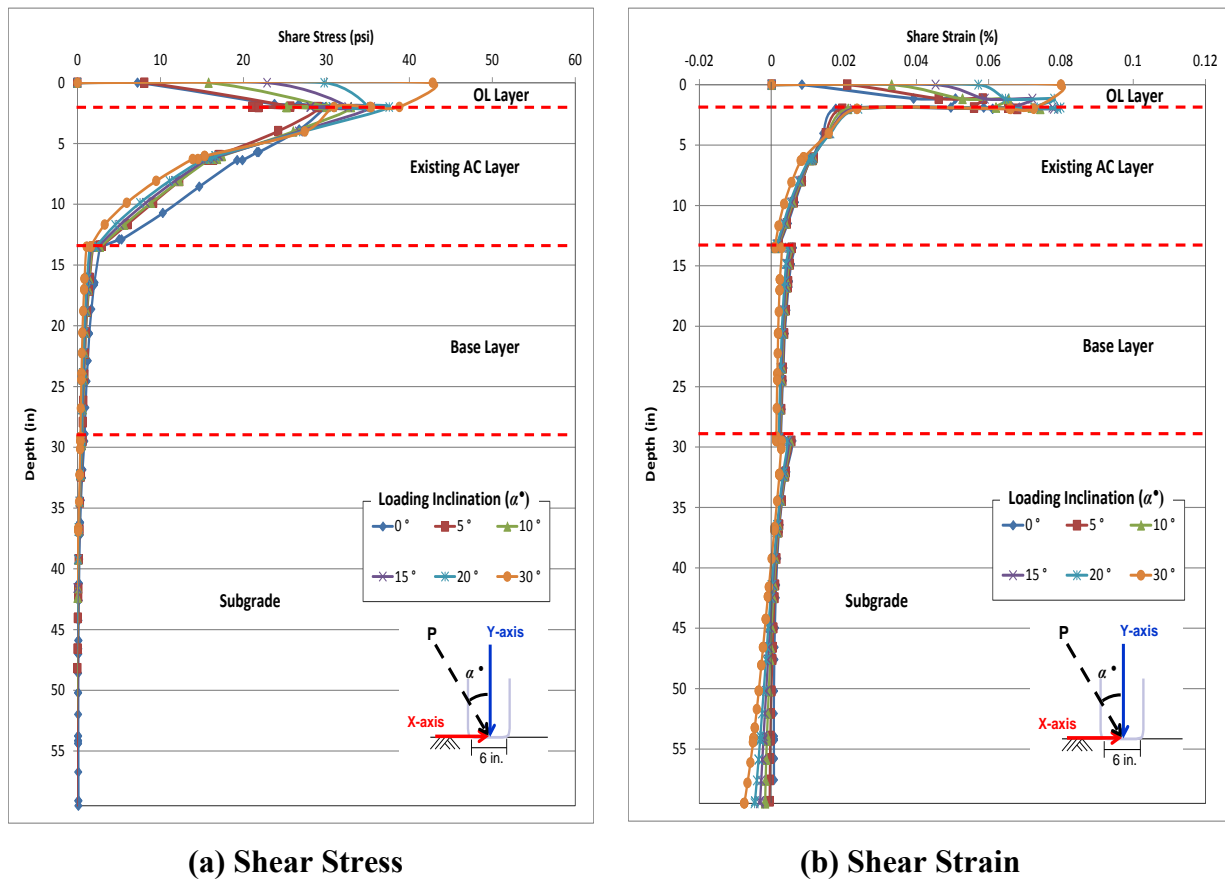


**Figure 3-9. Distribution of Shear Stress and Strain by Depth (2.0-Inch Thick HMA Overlay with 147.7 ksi Modulus).**

### PLAXIS Data Analysis: Key Findings and Recommendations

Overall, the 2-D PLAXIS analysis indicated that tire inclination, temperature, and HMA modulus have a significant impact on both the location and magnitude of the shear stress-strain responses within a PVMNT structure. At intersections with turning traffic that represents the worst-case scenario in terms of tire inclination angle, the maximum shear stresses and strains occur at the surface and are more critical under low HMA moduli values that is a function of the high summer temperatures. Therefore, intersections are more susceptible to surface shear failure

and permanent deformation compared to other sections of the road. As discussed subsequently, 3-D FE visco-elastic analysis with ABAQUS is ongoing to supplement and verify the PLAXIS results.

### **ABAQUS 3D FE MODELING: VISCO-ELASTIC ANALYSIS**

The 3-D visco-elastic modeling with ABAQUS modeling is presented and discussed in the subsequent text. As ABAQUS is relatively a complex and time-consuming, but very versatile software, only limited results are presented in this interim report. Numerical modeling is still currently ongoing and complete results with varied PVMNT structures and input variables will be presented in future Tech Memos and report publications.

#### **The ABAQUS Software**

ABAQUS is a suite of finite element analysis modules used for stress, heat transfer, and other types of analysis in mechanical, structural, civil, and related engineering applications. The ABAQUS system consists of several modules, and the key modules for mechanical purposes are ABAQUS/Standard and ABAQUS/Explicit, which are complementary and integrated analysis tools:

- ABAQUS/Standard: a general purpose finite element module
- ABAQUS/Explicit: an explicit dynamic finite element module
- ABAQUS/CAE: an analysis module in to a Complete ABAQUS Environment (CAE) for modeling, managing, and monitoring ABAQUS analysis and visualizing results. Integrated ABAQUS/Standard and ABAQUS/Explicit.

The FE program used in this study was ABAQUS/CAE, which is an intuitive and consistent user interface throughout the system. [Figure 3-10](#) shows the main user interface screen for the ABAQUS/CAE software. In addition to the data discussed in the subsequent text, some ABAQUS results are also included in [Appendix C](#).

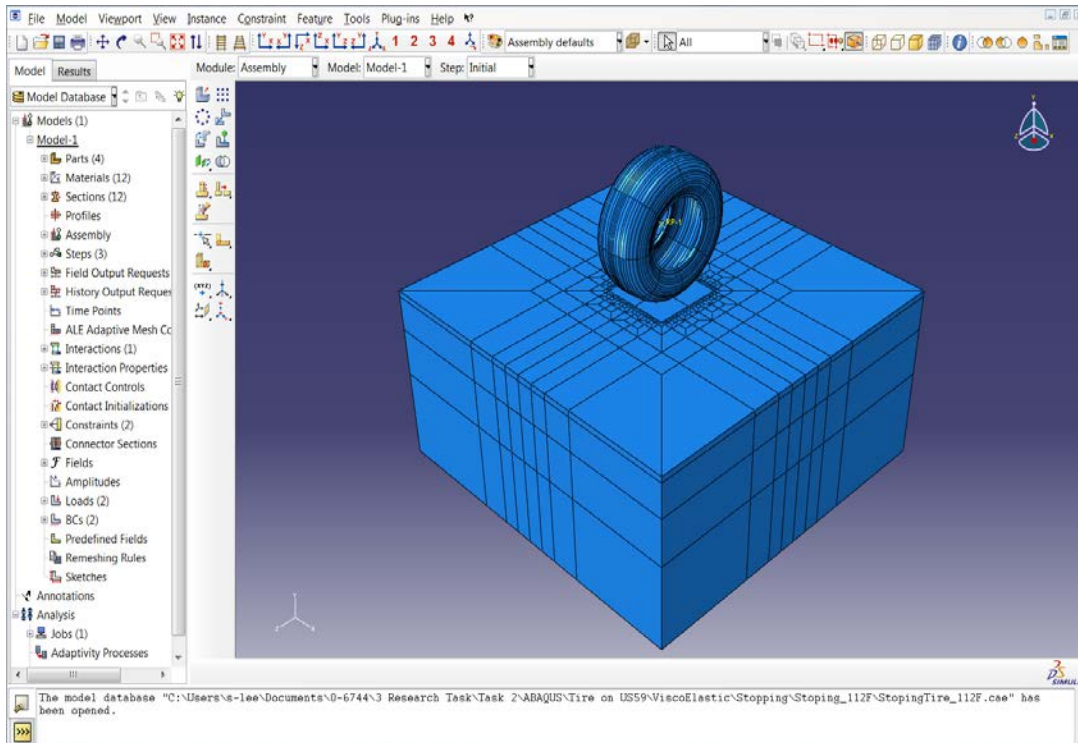


**Figure 3-10. ABAQUS/CAE Main Screen-User Interface.**

### **ABAQUS Pavement Structures and Input Variables**

Since the behavior of HMA materials on loading and climatic effects is based on the visco-elastic property, the 2-D PLAXIS simulation using the elastic analysis method showed limited behavior of the HMA materials. Therefore, to verify and supplement the PLAXIS results, 3-D FE visco-elastic modeling was conducted with the ABAQUS software.

Similar to the 2-D PLAXIS simulation, the US 59 PVMNT structure in Atlanta District, was used for the 3-D analysis as well. The HMA surface layer was modeled as an isotropic visco-elastic medium and the rest of layers, existing HMA, base, and subgrade, was modeled as elastic medium as shown in [Figure 3-11](#). For simulating traffic loading on the pavement, a tire was modeled inclusive of the rubber, steel wires, and threads.

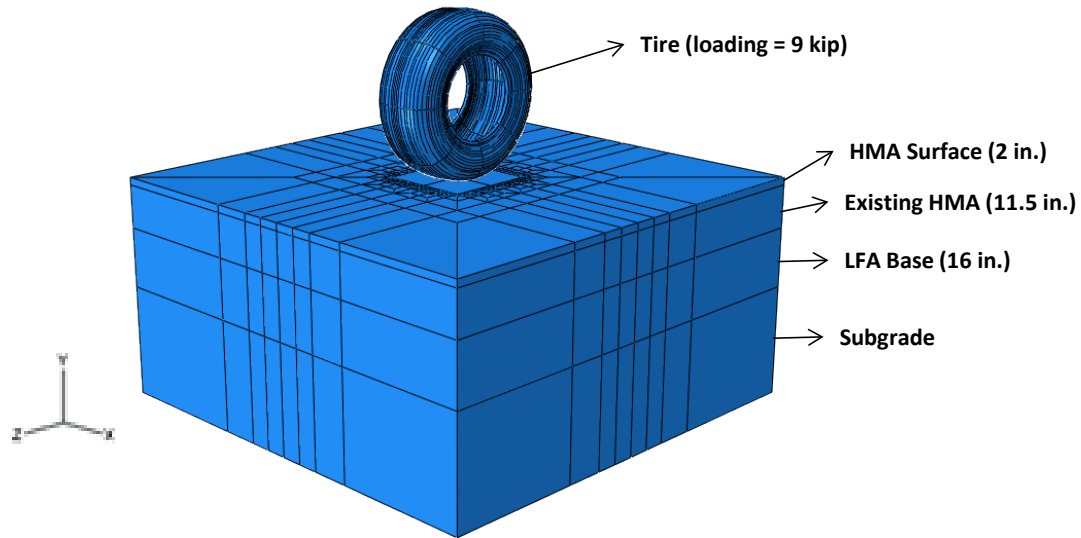


**Figure 3-11. PVMNT Structure and Tire Loading Configuration.**

The material property of the HMA surface layer was obtained from the dynamic modulus test conducted in Study 0-6658 and converted into time domain visco-elasticity using Prony series expansion (Walubita et al., 2012, Chebab, 2002).

Based on the elastic 2-D PLAXIS analysis, the following variables were included in ABAQUS analysis matrix:

- HMA visco-elastic effects (i.e. temperature effects on HMA modulus variation) defined by dynamic modulus master curves (112°F, 92°F, and 77°F)
- Tire loading configurations (tire inclination variations form 0° to 30° angle).
- Tire inflation pressure variations (80 to 120 psi)
- Tire loading (9 kips)

For this analysis, a single tire loading configuration was modeled, consisting of inner- and outer-rubber, steel belts, and threads, based on a radial-ply tire as shown in Figure 3-12.

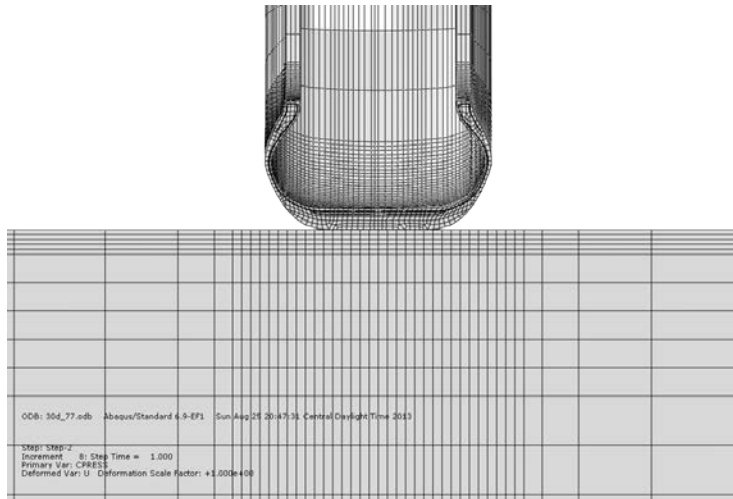


**Figure 3-12. ABAQUS Tire and PVMNT Interaction.**

**ABAQUS Results: Effects of HMA Modulus on PVMNT Response**

The linear visco-elastic model was used in this analysis to investigate the effects of surface HMA modulus as a function of temperature while the other layers (existing HMA, LFA Base, and subgrade) were considered as elastic materials having constant moduli values. [Figure 3-13](#) compares the in-depth distribution of shear and vertical stresses in the PVMNT structure under the vertical tire loading at 77°F, 92°F, and 112°F, respectively. Additional results are listed in [Appendix C](#).

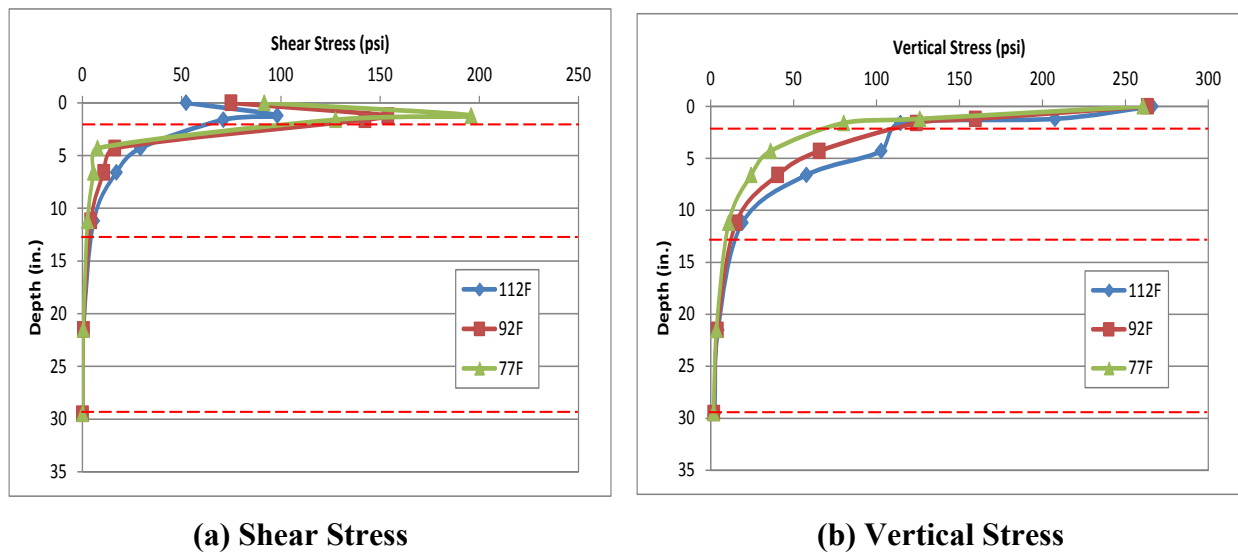


**Figure 3-13. Shear and Vertical Stresses as a Function of PVMNT Depth and Temperature.**

The 3-D ABAQUS analysis results in Figure 3-13 shows that the shear stress at the lower temperature (77°F) is about 80~90 percent greater than that at the higher temperature (112°F) on HMA surface layer. This result depicts a different phenomenon on the shear stress response because the HMA moduli variation did not exhibit as much as influence on the shear stress response in the 2-D PLAXIS analysis (elastic).

### The ABAQUS Results: Effects of Tire Inclination (Cornering) on PVMNT Response

Figure 3-14 compares the in-depth distribution of the vertical shear strains (parallel to the tire moving direction) at various tire inclination angles when carrying the same load (9 kips). The tire-pavement interaction was modeled using 0.8 as the surface friction coefficient at 0°, 20°, and 30° slip angle. The shear strain parallel to the tire moving direction is mainly contributing to rutting while the shear strain in the plane perpendicular to the tire moving direction is responsible for the shoving/corrugation (Wang, 2011). The tire inclination cause a little higher shear strain compared to static loading because the tire inclination results in greater vertical and transverse contact stresses and the peak contact stress shifts toward one side of the contact patch. Thus, it can be inferred that tire inclination will predominantly increase the shear and PD potential in the top to the middle zone of the HMA surfacing layer.

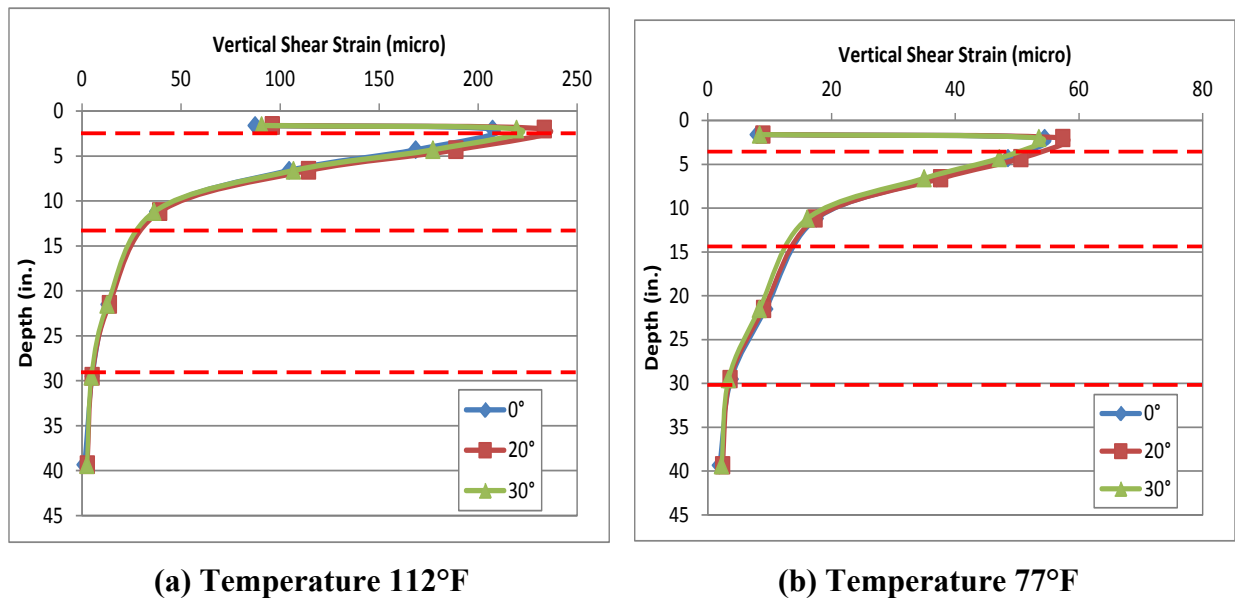
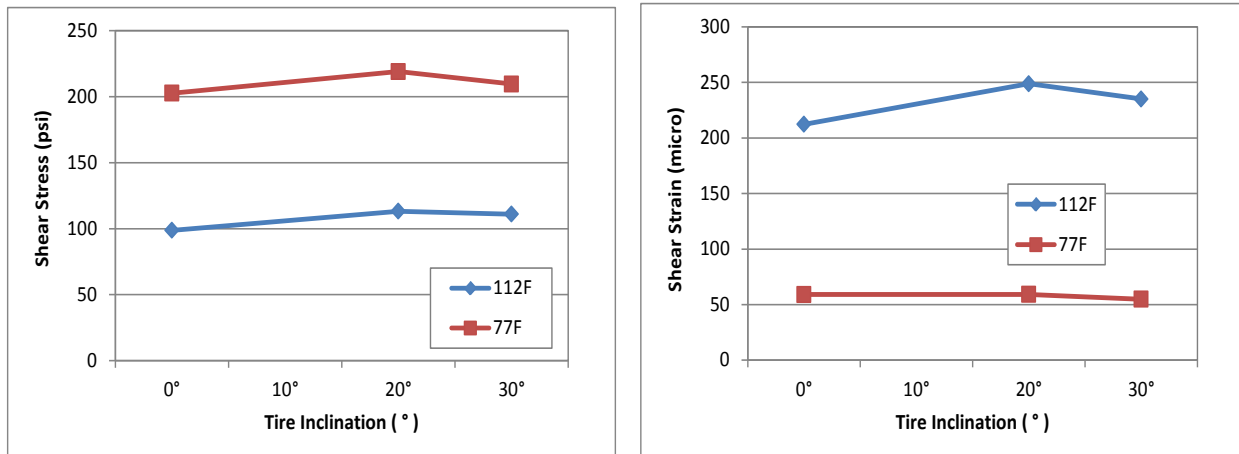


Figure 3-14. Vertical Shear Strains Parallel to the Tire Moving Direction.

In the 2-D PLAXIS elastic analysis, the shear stress and strain exhibited a consistently increasing trend with an increase in the tire inclination angle. In the 3-D ABAQUS visco-elastic analysis, however, the maximum shear stress and strain occurred at 20° tire inclination with lower values at 0° and 30°, respectively; see [Figure 3-15](#). Detailed results are also tabulated in [Appendix C](#) of this interim report.



(a) Shear Stress

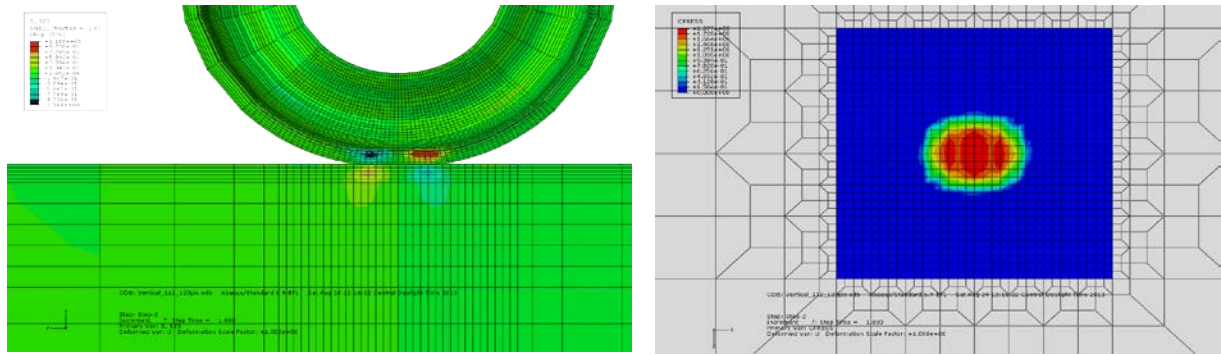
(b) Shear Strain

**Figure 3-15. Maximum Shear Stresses and Strains as a Function of Tire Inclination.**

From these ABAQUS results ([Figure 3-15b](#)), it can be inferred that 20° may be the critical tire inclination angle for shear deformation in HMA. In the case of PLAXIS elastic analysis, however, there was no distinct differentiation of the critical tire inclination angle; the shear strains constantly increased with an increase in the tire inclination angle. Nonetheless, additional ABAQUS modeling is currently ongoing with different PVMNT structures and input variables to further substantiate these results.

### ABAQUS Results: Effects of Tire Inflation Pressure Variations

To assess the effects of tire inflation pressure on the PVMNT response, the research team evaluated the vertical displacement, shear stress and strain, and contact pressure at the surface by varying the tire pressures as follows: 80, 100, and 120 psi. The tire loading was applied vertically on the PVMNT structure. [Figure 3-16](#) shows an example of the shear stress distribution and contact pressure at the surface for 100 psi tire pressure. The computational results are listed in [Table 3-4](#).



(a) Shear Stress

(b) Tire Contact Pressure on Surface

Figure 3-16. PVMNT Response at 100 psi Tire Pressure.

Table 3-4. PVMNT Response as a Function of Tire Inflation Pressure.

Tire Pressure (psi)		80	100	120
Vertical displacement (inch)		3.364E-3	3.366E-3	3.368E-3
Stress (psi)	Shear	98.66	98.82	98.96
	Vertical	267.16	267.16	267.16
Strain	Shear	2.121E-04	2.123E-04	2.125E-04
	Vertical	3.309E-05	3.312E-05	3.314E-05
Contact pressure at surface (psi)		271.95	272.10	272.24

For the PVMNT structure and materials considered the results in Table 3-4 shows that tire pressure variation did not significantly impact the shear and vertical stress-strain responses. Additional results of these computational analyses can be found in Appendix C.

### ABAQUS Data Analysis: Key Findings and Recommendations

From the 3-D ABAQUS analysis, it was noted that HMA modulus and temperature have a significant influence on the shear stress-strain response of the PVMNT structure. Since, 3-D analysis utilized the visco-elasticity for the surface HMA material; the most significant impact on shear stress response was HMA modulus, which is a function of the temperature variations; an aspect that is not prominent in the 2-D analysis. By contrast, however, the effect of tire pressure variation on the shear stress-strain responses was marginal. For the tire inclination angle, 20° was observed to be the critical angle at which the maximum shear stress-strain responses were computed. Overall, the 3-D ABAQUS analysis indicated that the maximum shear stress and strains occur at low HMA modulus value that is function of the high summer temperature regime.

## SUMMARY AND CURRENTLY ONGOING WORK

The computational modeling and shear stress-strain analyses documented in this chapter were predominately based on a 2-D FE elastic analysis with the PLAXIS software. To supplement and verify the results, limited 3-D FE visco-elastic modeling with ABAQUS software was also conducted. A similar in-service PVMNT structure (US 59 in Atlanta District) was used in both the PLAXIS and ABAQUS analysis under a single tired load. The key findings and conclusions drawing from this chapter are as follows:

- From the elastic 2-D analysis (PLAXIS), the shear stress in HMA pavement increased significantly with an increase in the tire inclination angle. However, the HMA modulus showed less influence on the shear stress response. In general, the shear strain increased with an increase in temperature and tire inclination angle.
- The 3-D visco-elastic analysis (ABAQUS) indicated that the maximum shear stress and strains occurred at the lower HMA modulus values that are a function of the high summer temperatures. Ultimately, these findings suggest that for the same traffic loading, the HMA would be more susceptible to shear deformation failure in summer when PVMNT temperatures are extremely high.
- Unlike the 2-D elastic analysis which showed an increasing trend with the tire inclination angle, the 3-D ABAQUS visco-elastic analysis preliminarily suggested that the critical tire inclination angle for HMA shears deformation is 20°. Thus, this angle should be considered as basis for future designs. Nonetheless, additional numerical modeling is recommended to validate these results.
- When modeled as a function of PVMNT depth, both the 2-D elastic and 3-D visco-elastic FE analyses indicated that the shear stress-strain responses were more critical in the topmost HMA layer. The results suggested that the top 0.5 inches should be considered as the potential critical shear and PD failure zone.
- Overall, the results indicated that intersections are more susceptible to surface shear failure and permanent deformation compared to other sections of the road, partly attributed to the higher tire inclination angle due to turning traffic.

As stated in the introductory section of this chapter, one of the intents of this numerical modeling is to get to a point where we can compare the shear strength of various HMA mixes to the shear stresses and strains produced by heavy trucks under extreme conditions (i.e., at intersections in summer). In view of these preliminary results, findings, and recommendations drawn from this chapter, the following works are currently ongoing based on the 3-D FE visco-elastic modeling with ABAQUS:

- PVMNT structures, i.e., thin, overlays, multi-layered, and new construction with varying HMA layer thickness and base type (granular, CTB, LTB, etc.).
- Single versus dual tired wheels. The results reported in this chapter were based on a single tire loading (6-inch of contact width with varying tire pressure), which is assumed to be more critical for the same loading. Therefore, efforts will be made to try dual tired wheels as well as multiple axles.
- Vertical tire load variations (i.e., 9, 10, 15 kips, etc).
- Tire loading configurations on straight sections and at intersections.
- Moving/bouncing and stopping wheel including the tractive or breaking frictional forces caused by heavy trucks accelerating/decelerating.
- Density effects, i.e., 2 to 10 percent AV.
- Re-simulation for some cases that did not converge in the current analysis.
- Correlations and tying the numerical results (PLAXIS and ABAQUS) to laboratory and field data.

Results and findings of this work, as bullet-listed above, will be documented in future Tech Memos and report publications.



## CHAPTER 4 THE AMPT VERSUS THE UTM SYSTEM

Performing reliable and repeatable laboratory testing for HMA mixes constitutes an indispensable element for proper HMA mix-design characterization to ensure satisfactory field performance. Different systems are currently available for HMA performance testing and material property characterization.

Recently, TTI acquired a new unit of the Asphalt Mixture Tester (AMPT) system in 2012 for laboratory HMA performance testing such as the RLPD, FN, and DM. Historically, TTI has used the traditional Universal Testing Machines (UTM) system for conducting these tests with satisfactory results. With the acquisition of the new AMPT unit however, three fundamental questions arose, namely:

- Now that TTI has bought the AMPT unit, should we discontinue using the traditional UTM system that we have used satisfactorily for the past decades or use them both?
- What is the impact of using the new AMPT system in relation to all the previous results that we have been getting with the traditional UTM? Will using the AMPT cause a significant difference in the results compared to the traditional UTM?
- How do the results from the two systems compare and what is the difference between the AMPT and the UTM in terms of accuracy, repeatability, and reliability?

To address these questions, the researchers undertook the work described in this chapter with the following objectives:

- To comparatively evaluate if given the same material (HMA) and test conditions, both the new AMPT and the traditional UTM will yield statistically comparable results or not.
- To comparatively evaluate the accuracy, operational efficiency, and practicality of the new AMPT system relative to the traditional UTM system.
- To make recommendations as to which system to use for future HMA performance testing, or if both systems could be used concurrently or in lieu of the other.

In the subsequent text, the two systems (AMPT and UTM) are described, and the research methodology and laboratory experimentation plan follow. Laboratory test results for the RLPD, FN, and DM tests are then presented and comparatively analyzed, after which an evaluation of the

systems' general characteristic attributes follows. The chapter then concludes with a synthesis and summary of the key findings and recommendations. [Appendix D](#) includes additional data patterning to this chapter.

## THE AMPT AND UTM SYSTEMS

[Figure 4-1](#) shows pictures of both the AMPT and UTM systems; one outstanding difference is the size of the temperature chambers of the two units. The chamber of the UTM is over ten times the size of the AMPT in volume and, therefore, can permit conditioning of multiple specimens at a single given time without the need for an external chamber (see [Figure 4-2](#)). However, this means longer time for conditioning the specimens, i.e., reaching the target temperature. By contrast, the smaller chamber size of the AMPT means better temperature control and consistency during testing; but it would need an external chamber for conditioning multiple specimens.

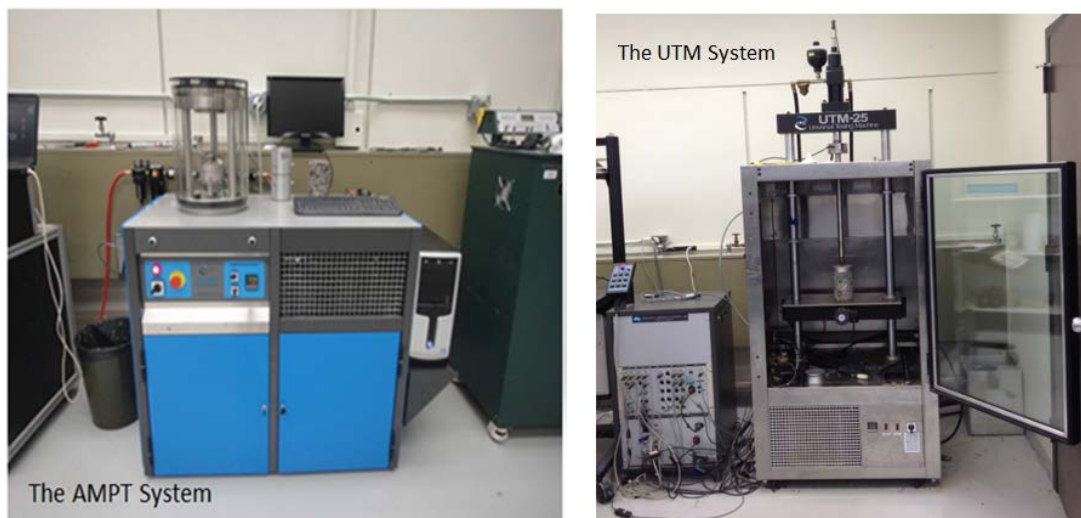


**Figure 4-1. Pictures of the AMPT and UTM Units.**



**Figure 4-2. Comparison of the Environmental Chambers.**

### Load Cell Capacity and LVDT Span

The AMPT has a load cell capacity of 13.5 kN (3.035 kips), while the UTM is capable of applying up to 25 kN (5.620 kips) vertical dynamic force; hence, the designation UTM-25. Each system has multiple LVDTs for displacement measurements with the following maximum span movements: 1) AMPT  $\leq \pm 0.5$  mm (i.e., 1 mm total movement) and 2) the UTM  $\leq \pm 5$  mm (i.e., 10 mm total movement). Both systems are servo hydraulic operated. [Table 4-1](#) comparatively lists the specification details.

**Table 4-1. Specification Features of the UTM and AMPT Units.**

Characteristic Feature	UTM	AMPT
Load cell (kN) (static)	25 (5.620 kips)	15 (3.372 kips)
Load cell (kN) (dynamic)	20 (4.496 kips)	13.5 (3.035 kips)
Frequency (Hz) - up to	60	70
Loading mechanism	Hydraulic	Hydraulic
LVDT span	Varies ( $\pm 5$ mm)	$\pm 0.5$ mm
LVDT accuracy	-	Meets NCHRP 9-29 Specs, resolution better than 0.0002 mm (0.04%)
Approximate chamber dimensions (internal)	H $\cong$ 1045 mm; W $\cong$ 750 mm; B $\cong$ 475 mm Can handle most specimen dimensions and configurations	$\phi \cong 285$ mm ; H $\cong$ 290 mm Designed for 150 mm tall x 100 mm diameter specimens
Temperature range	-40°C to +100°C (-40°F to +212°F)	4°C to 60°C (+39.2°F to 140°F)
LVDT gluing jigs and setup	Manual	Automatic

*Legend: LVDT = linear variable differential transducer; H = height, W = width; B = breadth;  $\phi$  = diameter*

As evident in [Figure 4-1](#), the AMPT unit is more compact with a higher flexibility for mobility than the UTM. However, some evident limitations of the AMPT in [Table 4-1](#) include the lower load cell capacity, shorter LVDT span (i.e., 10 times shorter than that used in the UTM), and shorter temperature range; i.e., the AMPT cannot be used for testing below +4 °C or above +60 °C. On the contrary, as can be noted from [Table 4-1](#), the shorter LVDT span of the AMPT means better resolution and higher accuracy.

**LVDT Gluing Jigs and Sample Setup**

[Figure 4-3](#) presents the gluing jigs for the LVDT studs and shows that the AMPT jigs are automated while the UTM are not. Therefore, one can infer to an element of simplicity and better accuracy for the AMPT jigs than the UTM gluing jigs that are manually handled. In both cases, however, a minimum of three LVDTs are used with the studs at typically 4 inches spacing for standard DM, FN, and RLPD testing; [Figure 4-4](#) illustrates the sample setups.

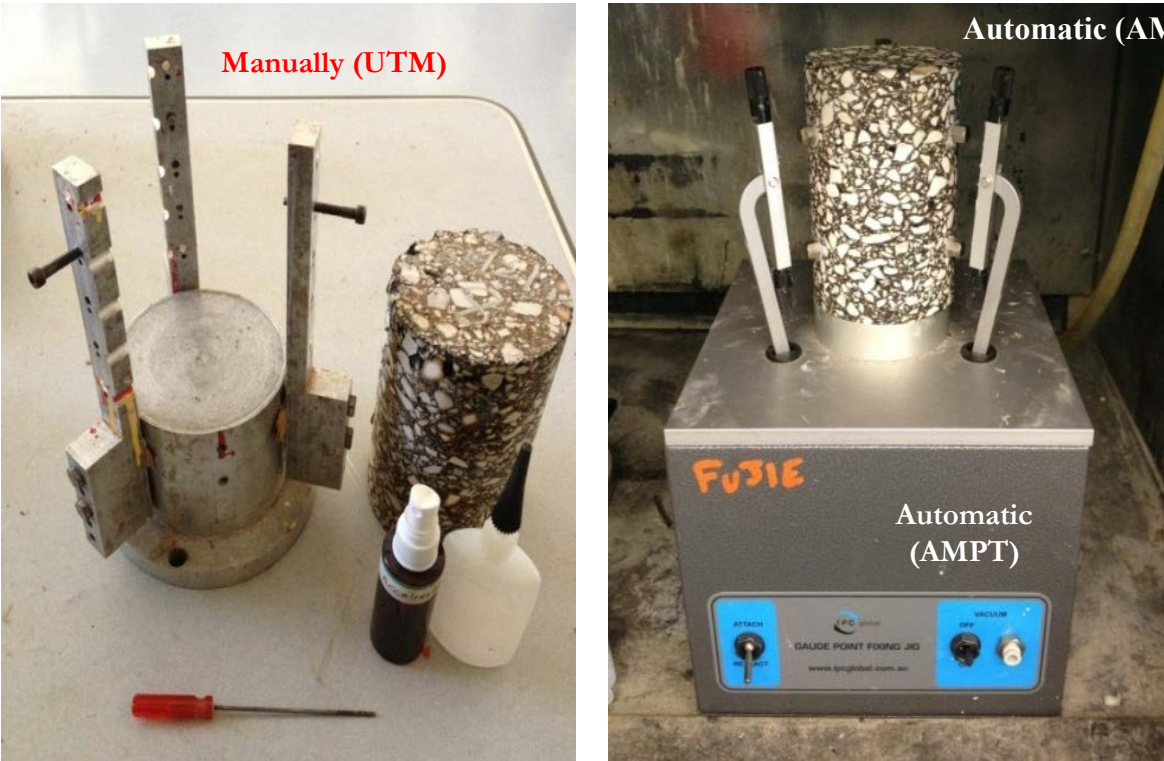


**Figure 4-3. Comparison of the LVDT Gluing Jigs – UTM versus AMPT.**



**Figure 4-4. Comparison of the LVDT Setup – UTM versus AMPT.**

#### **METHODOLOGICAL APPROACH**

For both the AMPT and UTM systems, the research team adapted the following methodological approach to ensure similar conditions and consistency in the results without any bias:

- Used the same HMA mixes.
- Used the same number of sample replicates.
- Molded and fabricated the samples exactly to same target density (AV) and dimensions.
- Used the same test methods, conditions, and loading parameters.
- Ensured that both the AMPT and UTM were well calibrated.
- Used the same operator/technician (trained).
- Used the same data analysis methods.
- Used different personnel to analyze the data.

## **LABORATORY EXPERIMENTATION PLAN**

The experimental design plan consisted of selecting the appropriate test methods and thereafter, devising an appropriate work plan to execute the task. These aspects along with the HMA mix details are discussed in the subsequent text.

### **Laboratory Test Methods**

Using similar HMA mixes, similar test conditions, similar test loading parameters, and the same operator, the researchers drew up a work plan to accomplish this particular assignment that involved parallel testing in both the AMPT and UTM systems. Thereafter, the research team compared the HMA test results for the following three commonly used laboratory test methods for HMA performance testing:

- RLPD = Repeated Load Permanent Deformation test.
- FN = Flow Number test.
- DM = Dynamic Modulus test.

Details of these test methods including the loading configuration and test parameters are discussed in the subsequent text ([Walubita et al., 2012](#)). Note, however, that all three tests were based on dynamic loading mode using standard 6 inches height by 4 inches diameter HMA specimens.

### **Work Plan and Procedural Steps**

The plan was to evaluate at least one HMA mix type at three replicate samples per test type per test condition in each system, at a target AV level of  $7\pm 1$  percent. As previously outlined, the research team undertook a streamlined methodological approach to accomplish this task, namely:

- For the same Type C plant-mix, a minimum of three different HMA sample replicates was fabricated and subjected each to FN, RLPD, and DM testing in both the UTM and AMPT systems, respectively, using similar test conditions and the same operator for each test type. A minimum of 24 HMA replicates were fabricated and tested.
- All the samples were molded and fabricated by the same technician/operator.

- For the FN data from both the UTM and AMPT systems, similar models and mathematical equations were utilized to compute the FN parameters, namely FN,  $\epsilon_p(F)$ ,  $t(F)$ , and FN Index; that are used to characterize the permanent deformation (PD) properties of HMA at 50°C.
- Likewise, similar models and mathematical equations were utilized to analyze the DM data from both the UTM and AMPT systems; and compute the  $|E^*|$  parameter that characterizes the HMA moduli values and stiffness properties as a function of temperature (40–130°F) and loading frequency (0.1–25 Hz).
- All the lab test data were statistically analyzed at 95 and 90 percent confidence levels, with 30 percent COV as the acceptable level of variability in the test results (i.e., COV < 30 percent). Both t-tests and Tukey's HSD statistical methods were employed to analyze and comparatively interpret the results.
- To discount the operator effect as well as minimize human errors, the same operator/technician was used throughout the laboratory work component of the task, namely sample preparation, setup, lab testing, etc. However, different personnel were engaged to analyze/verify the data and interpret the results including drawing conclusions.

### **HMA Mix Details**

A Type C mix from SH 21 in Bryan District (Brazos County) was used for all the testing (RLPD, FN, and DM) in this task. [Table 4-2](#) lists the HMA mix-design characteristics. [Figure 4-5](#) and [Figure 4-6](#) show the highway (SH 21) location and PVMNT structure where the mix has been used. [Appendix D](#) has the mix-design sheet details.

**Table 4-2. Type C HMA Mix-Design Characteristics.**

#	Item	Details
1	HMA mix	Type C (Coarse Surface – Item SS3224)
2	Mix-design	4.8% PG 64-22 (Jebro) + Limestone/Dolomite + 1% Lime + 17% RAP + 3%RAS
3	Rice	2.432
4	VMA	14.0%
5	Lab TGC design density	97%
6	Field density (construction)	94%
7	Hwy where used	SH 21
8	District (County)	Bryan (Brazos)
9	Environment	Wet-warm
10	HMA sample replicates per test method per unit	
11	Sample type	Plant-mix
12	Target sample AV	7±1%

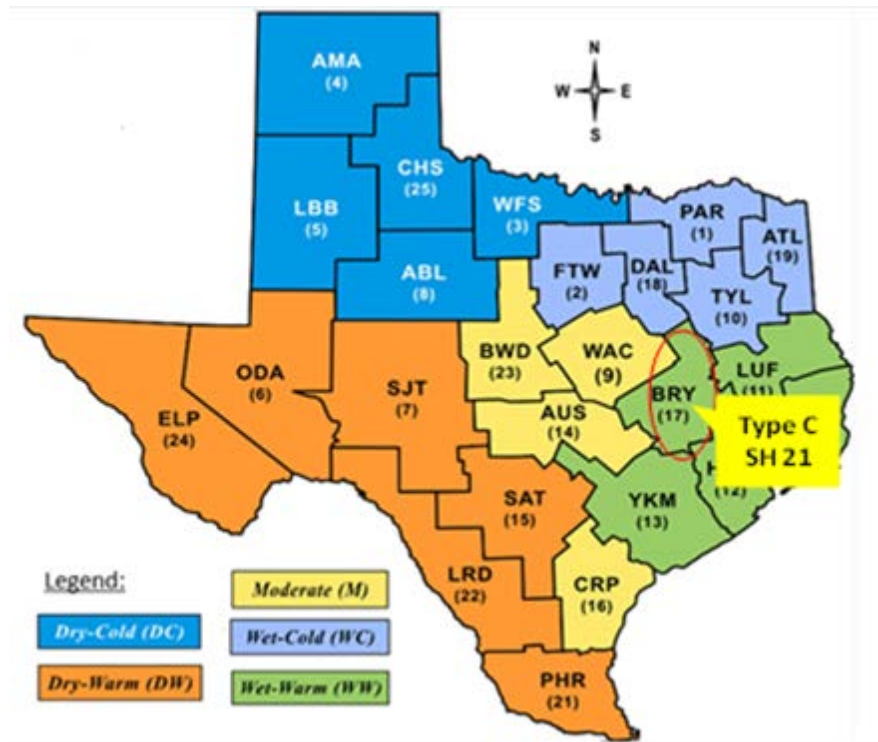


**Figure 4-5. Geographical Location of the Highway (SH 21).**



Layer#	Thickness (inch)	Layer Material	Year Constructed
3	5.0	HMA Type C	2012
2	7.0	Flex Base	2012
1	8.0	4.5% Cement Treated Subgrade	2011
0	∞	Compacted Raw Subgrade Soil	2011

**Figure 4-6. SH 21 PVMNT Structure.**

## THE RLPD TEST METHOD AND RESULTS

Table 4-3 lists the RLPD test setup for both the AMPT and UTM systems. Essentially, similar loading and test conditions were applied for the same number of replicate specimens. The RLPD data analysis models, HMA sample AV measurements, results, and key findings are presented and discussed in the subsequent subsections.

### RLDP Data Analysis Models

The RLPD test is used to characterize the permanent deformation properties of HMA under repeated compressive Haversine loading (Zhou and Scullion, 2004). For the purpose of this task, the visco-elastic properties  $\alpha$  and  $\mu$  were determined as a function of a log-log plot of the accumulated plastic strain ( $\epsilon_p$ ) versus the number of load cycles ( $N$ ) as follows:

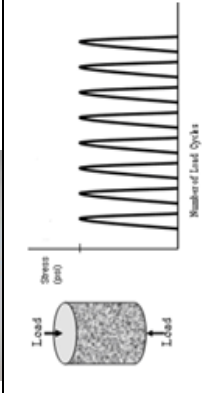
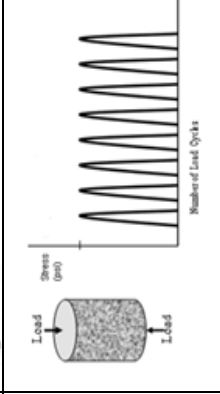
$$\epsilon_p = aN^b \quad (\text{Equation 4-1})$$

$$\alpha = 1 - b \quad (\text{Equation 4-2})$$

$$\mu = \frac{ab}{\epsilon_{r(r200)}} \quad (\text{Equation 4-3})$$

Regression parameters  $a$  and  $b$  are the intercept and slope of the “linear portion” of the strain-load cycles curve on a log-log scale. Alpha ( $\alpha$ ) and mu ( $\mu$ ) are the HMA rutting parameters, with  $\mu$  computed at the 200<sup>th</sup> load cycle for this study.  $\epsilon_{r(r200)}$  is the resilient microstrain obtained at the 200<sup>th</sup> RLPD load cycle (Zhou et al., 2009); see examples in Figure 4-7 and Figure 4-8.

**Table 4-3. The AMPT-UTM System Setups for the RLPD Test.**

# Item	The AMPT System	The UTM System
1 Pictorial setup		
2 Sample loading configuration		
3 Sample dimensions	4" $\phi$ $\times$ 6" H	4" $\phi$ $\times$ 6" H
4 Target test temperatures	40°C (104°F) 50°C (122°F)	40°C (104°F) 50°C (122°F)
5 Target temperature tolerance	$\pm 2^\circ\text{C}$	$\pm 2^\circ\text{C}$
6 Loading mode	Compressive repeated Haversine (stress-controlled mode)	Compressive repeated Haversine (stress-controlled mode)
7 Loading frequency	1 Hz (0.1 sec loading and 0.9 sec rest)	1 Hz (0.1 sec loading and 0.9 sec rest)
8 Stress level @ 40 $\pm$ 2°C	20 psi (vertical-dynamic)	20 psi (vertical-dynamic)
9 Stress level @ 50 $\pm$ 2°C	10 psi (vertical-dynamic)	10 psi (vertical-dynamic)
10 Confining pressure	0 psi	0 psi
11 Test termination criterion	10,000 load repetitions or 25,000 microstrains	10,000 load repetitions or 25,000 microstrains
12 Test time	$\leq 3$ hrs	$\leq 3$ hrs
13 Measurable & output data	Axial permanent deformation, permanent & resilient strains ( $\epsilon_p$ , $\epsilon_r$ ), stress, number of load passes, time, temperature, frequency, visco-elastic properties ( $\alpha$ , $\mu$ ), and resilient modulus ( $M_r$ )	Axial permanent deformation, permanent & resilient strains ( $\epsilon_p$ , $\epsilon_r$ ), stress, number of load passes, time, temperature, frequency, visco-elastic properties ( $\alpha$ , $\mu$ ), and resilient modulus ( $M_r$ )
14 References	Zhou et al., 2001, 2009, 2010; Walubita et al. 2011	Zhou et al., 2001, 2004, 2009, 2010, Walubita et al., 2011, 2012

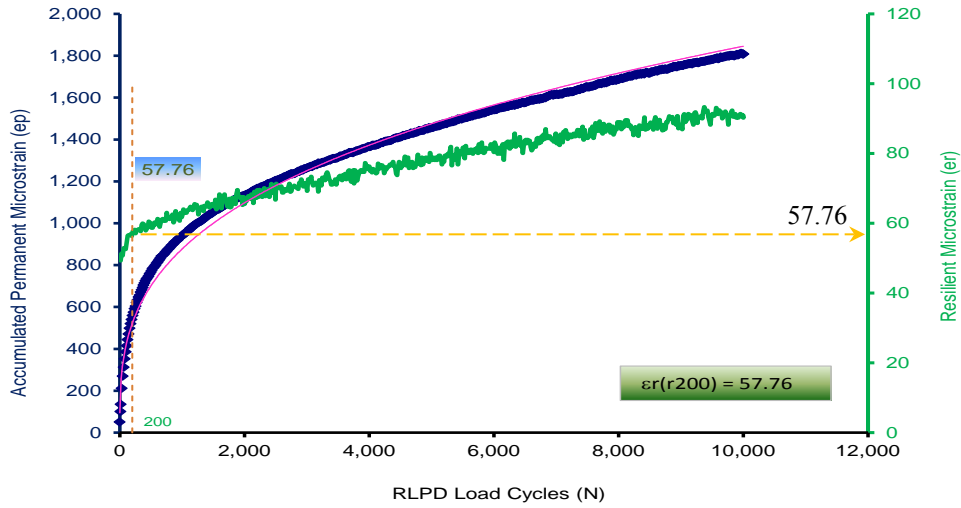


**Figure 4-7. Plot of RLPD Strain versus Load Cycles.**

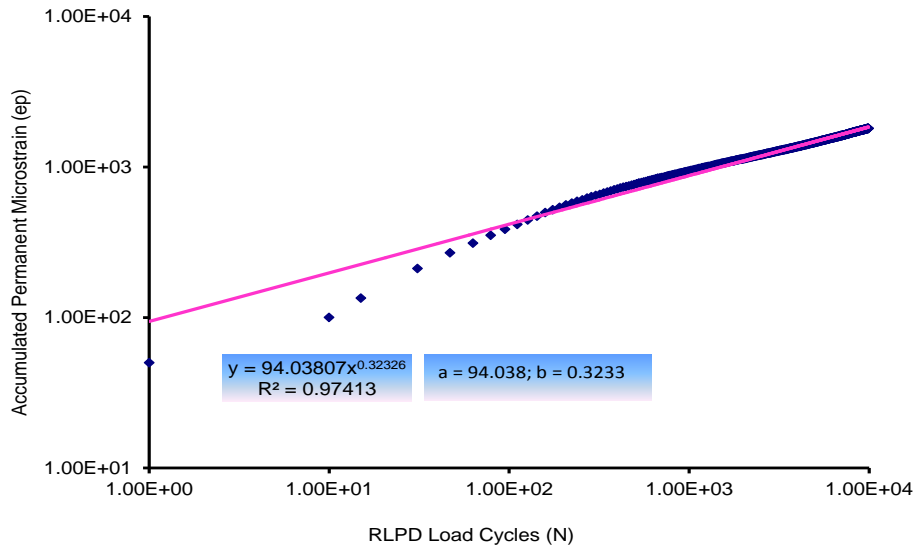


**Figure 4-8. Log Plot of RLPD Strain versus Load Cycles.**

For the example shown in [Figure 4-7](#) and [Figure 4-8](#), the  $\alpha$  and  $\mu$  parameters would be determined as follows:

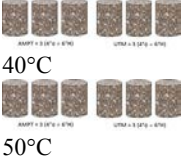
- $a, b, \epsilon_r(r200) = 94.0380, 0.3233, 57.76$
- $\alpha, \mu = 0.6767, 0.5264$

These HMA rutting parameters, alpha ( $\alpha$ ) and mu ( $\mu$ ), are input data into the M-E models such as the TxACOL, TxM-E, and related software.

## HMA Sample Dimensions and AV Measurements for RLPD Testing

For a systems (i.e., AMPT versus UTM) comparative study of this nature, it is imperative that both the sample dimensions and AV are consistently similar and within a set tolerance limit to avoid any biasness in the final results. As shown in [Table 4-4](#), both the HMA specimen dimensions and AV are fairly consistent and within tolerable limits. [Appendix D](#) has more detailed results for the HMA specimen dimension and AV measurements.

**Table 4-4. RLPD HMA Specimen Dimensions and AV Measurements.**

Samples	Item	AMPT			UTM		
		H (Inches)	$\phi$ (Inches)	AV	H (Inches)	$\phi$ (Inches)	AV
 40°C 50°C	Avg	6.06	3.97	7.17%	6.06	3.97	7.13%
	COV	0.23%	0.26%	4.40%	0.23%	0.26%	5.60%
	Range	6.04–6.08	3.95–3.98	6.90–7.57%	6.04–6.07	3.95–3.98	6.59–7.72%
	Target	6.00±0.10 "	4.08±0.08"	7±1%	6.00±0.10 "	4.08±0.08 "	7±1%

## RLPD Test Results – Alpha ( $\alpha$ ) and Mu ( $\mu$ )

[Table 4-5](#) shows that the overall RLPD test results in terms of the computed  $\alpha$  and  $\mu$  are insignificantly different between the two systems. The magnitudes of these HMA rutting parameters are very comparable and, therefore, justifies that both systems can be reliably and accurately used for RLPD testing to characterize the HMA permanent deformation properties at the given test conditions. [Appendix D](#) has graphical plots of these results.

**Table 4-5. RLPD Test Results – Alpha ( $\alpha$ ) and Mu ( $\mu$ ).**

Sample Replicate#	Parameters	RLPD @ 40°C & 20 psi		RLPD @ 50°C & 10 psi	
		UTM	AMPT	UTM	AMPT
Sample1	alpha ( $\alpha$ )	0.6922	0.7198	0.7873	0.7258
	mu ( $\mu$ )	0.6276	0.5997	0.9800	0.6382
Sample2	alpha ( $\alpha$ )	0.7462	0.7185	0.7922	0.7262
	mu ( $\mu$ )	0.8218	0.6182	0.9403	0.4750
Sample3	alpha ( $\alpha$ )	0.6354	0.7508	0.7540	0.6671
	mu ( $\mu$ )	0.2086	0.5691	0.7580	0.4406
Average	alpha ( $\alpha$ )	0.6913	0.7297	0.7779	0.7064
	COV	8.02%	2.51%	2.67%	4.82%
	mu ( $\mu$ )	0.5527	0.5957	0.8928	0.5179
	COV	10.03%	2.76%	2.16%	5.81%

## RLPD Test Results – Statistical Analysis

Statistical variability, as measured in terms of the COV, for the computed  $\alpha$  and  $\mu$  parameters in both systems, was also reasonably acceptable and comparable. All of the COV values computed based on three replicate RLPD tests in [Table 4-5](#) are below 15 percent, suggesting that both the AMPT and UTM systems are fairly repeatable and comparable for RLPD testing at 40°C and 50°C, respectively; see [Appendix D](#) for additional data. Likewise, ANOVA and Tukey’s HSD analysis at 95 percent confidence level also reaffirmed that the results ( $\alpha$  and  $\mu$ ) from both systems were statistically indifferent (see [Table 4-6](#) and [Table 4-7](#). That is, the AMPT 40°C and AMPT 50°C results are statistically indifferent from the UTM 40°C and UTM 50°C results, respectively.

**Table 4-6. ANOVA Analysis at 95% Confidence Level-RLPD Test Data.**

Groups	Count	alpha ( $\alpha$ )			mu ( $\mu$ )		
		Sum	Avg	Variance	Sum	Avg	Variance
UTM 40°C	3	2.0738	0.6913	0.0031	1.6580	0.5527	0.0982
AMPT 40°C	3	2.1891	0.7297	0.0003	1.7870	0.5957	0.0006
UTM 50°C	3	2.3336	0.7779	0.0004	2.6783	0.8928	0.0140
AMPT 50°C	3	2.1191	0.7064	0.0012	1.5537	0.5179	0.0111

**Table 4-7. HSD Pairwise Comparison – RLPD Test Data.**

Parameter	Are the Results Statistically Different @ 95% Confidence Level?	
	AMPT versus UTM @ 40°C	AMPT versus UTM @ 50°C
Alpha ( $\alpha$ )	No	No
mu ( $\mu$ )	No	No

Undoubtedly, the consistency and repeatability in these test results may also have been attributed to the consistency in the HMA sample dimensions and AVs (7±1 percent); see [Table 4-4](#) and [Appendix D](#). Therefore, it is imperative to always ensure consistent AV in the HMA samples when conducting comparative studies of this nature.

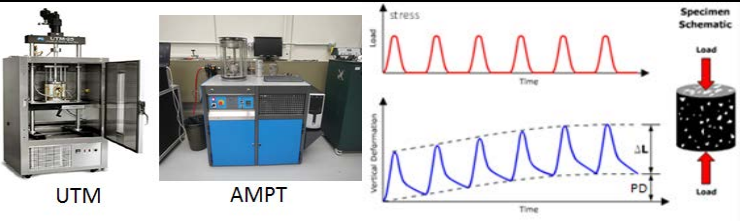
## RLPD Test Results – Key Findings and Recommendations

For the HMA mix and test conditions considered in this task, the overall RLPD test results were statistically comparable and acceptable. Thus, either system (AMPT or UTM) can be confidently used in lieu of the other to generate similarly quality and reliable results of a comparable statistical degree of accuracy at 95 percent confidence level with acceptable variability (i.e., COV < 30 percent). The choice/preference is basically on the user.

## THE FN TEST METHOD AND RESULTS

Table 4-8 lists the FN test setup for both the AMPT and UTM systems. As evident in the table, similar loading and test conditions were applied for the same number of replicate specimens. The FN data analysis models, HMA sample AV measurements, results, and key findings are presented and discussed in the subsequent subsections.

**Table 4-8. The AMPT-UTM System Setups for the FN Test.**

#	Item	FN Loading and Test Parameters
1	Pictorial setup & sample loading configuration	 <p>The figure shows two testing machines: UTM (left) and AMPT (right). To the right are two graphs: the top one shows 'stress' vs 'Time' with a repeating square wave, and the bottom one shows 'Vertical Deformation' vs 'Time' with a repeating sawtooth wave. A 'Specimen Schematic' on the far right shows a cylindrical specimen with 'Load' arrows pointing down and up.</p>
2	Sample dimensions	 <p>4" <math>\phi</math> <math>\times</math> 6" H.            AMPT = 3 (4" <math>\phi</math> <math>\times</math> 6" H)            UTM = 3 (4" <math>\phi</math> <math>\times</math> 6" H)</p>
3	Target test temperatures	50°C (122°F)
4	Target temp. tolerance	$\pm 2^\circ\text{C}$
5	Sample temperature conditioning time	2~3 hrs
6	Loading mode	Compressive repeated Haversine (stress-controlled mode)
7	Loading frequency	1 Hz (0.1 sec loading and 0.9 sec rest)
8	Vertical stress level (dynamic)	30 psi (207 kPa)
9	Confining pressure	0 psi
10	Test termination criterion	10,000 load repetitions or 30,000 microstrains
11	Test time	$\leq 3$ hrs
12	Measurable & output data	Flow number (cycles), time to tertiary flow (minutes), temperature, frequency, accumulated microstrain at tertiary flow (microns), and microstrain-flow number ratio
13	References	<a href="#">Walubita et al. 2012</a>

## FN Data Analysis Models

For the purpose of this comparative study, models in the publication by [Adrian et al. \(2007\)](#), as shown in [Table 4-9](#), were used to analyze both the UTM and AMPT FN data. However, other methods including the Francken's model ([Raj et al., 2009](#)) are available for analyzing the AMPT FN data. Example plots of the FN concept and output data are graphically illustrated in [Figure 4-9](#) and [Figure 4-10](#).

**Table 4-9. FN Data Analysis Models.**

#	Item/Parameter	Model	Description
1	General relationship between the accumulated permanent strain and the number of load cycles	$\varepsilon_p = aN^b$	$\varepsilon_p$ is the accumulated permanent strain due to dynamic vertical loading, $N$ is the number of load cycles to produce $\varepsilon_p$ , and $a$ and $b$ are regression constants that depend on the material and stress state conditions.
2	Probabilistic distribution (Weibull) model for the relationship between $\varepsilon_p$ and $N$	$N = \gamma[1 - e^{-(\beta\varepsilon_p)^\alpha}]$	$\beta$ , $\alpha$ , and $\gamma$ are the probability distribution and shape parameters. The parameter $\gamma$ has the simple interpretation of being the maximum number of load cycles that the specimen would last if the testing machine could apply an arbitrary deformation to the sample (i.e., the number of load cycles at which the rate $d\varepsilon_p/dN \rightarrow \infty$ )
3	Predicted permanent strains ( $\varepsilon_p(\text{Predicted})$ )	$\varepsilon_p(\text{Predicted}) = \frac{1}{\beta} \times \left( -\ln\left(1 - \frac{N}{\gamma}\right) \right)^{1/\alpha}$	$\varepsilon_p(\text{Predicted})$ is the predicted accumulated permanent strain as a function of $N$ ; where $N$ , $\beta$ , $\alpha$ , and $\gamma$ are as previously defined.
4	Flow number (FN; cycles)	$\text{FN} = \gamma \left[ 1 - \exp\left(\frac{1}{\alpha} - 1\right) \right]$	FN = flow number or number of load cycles at the onset of tertiary zone; at which $d^2\varepsilon_p/d^2N = 0$
5	Accumulated permanent strain at tertiary flow ( $\varepsilon_p(F)$ ; microns)	$\varepsilon_{p\text{flow}} = \frac{1}{\beta} \left( 1 - \frac{1}{\alpha} \right)^{1/\alpha}$	$\varepsilon_p(F)$ = accumulated permanent strain at the onset of tertiary flow, i.e., at $d^2\varepsilon_p/d^2N = 0$
6	Time to tertiary flow ( $t(F)$ ; minutes)	$t(F) = \text{FN}/60$	$t(F)$ = time at the onset of tertiary flow (based on a loading frequency of 1 Hz) or time count in minutes at $d^2\varepsilon_p/d^2N = 0$
7	FN Index (microstrains/ cycle)	$\text{FN Index} = \varepsilon_p(F)/\text{FN}$	Derived composite parametric ratio that simultaneously incorporates the strain at tertiary flow, $\varepsilon_p(F)$ , and flow number (FN) at tertiary flow.
8	References	<a href="#">Adrian et al., 2007</a> ; <a href="#">Walubita et al., 2012</a>	

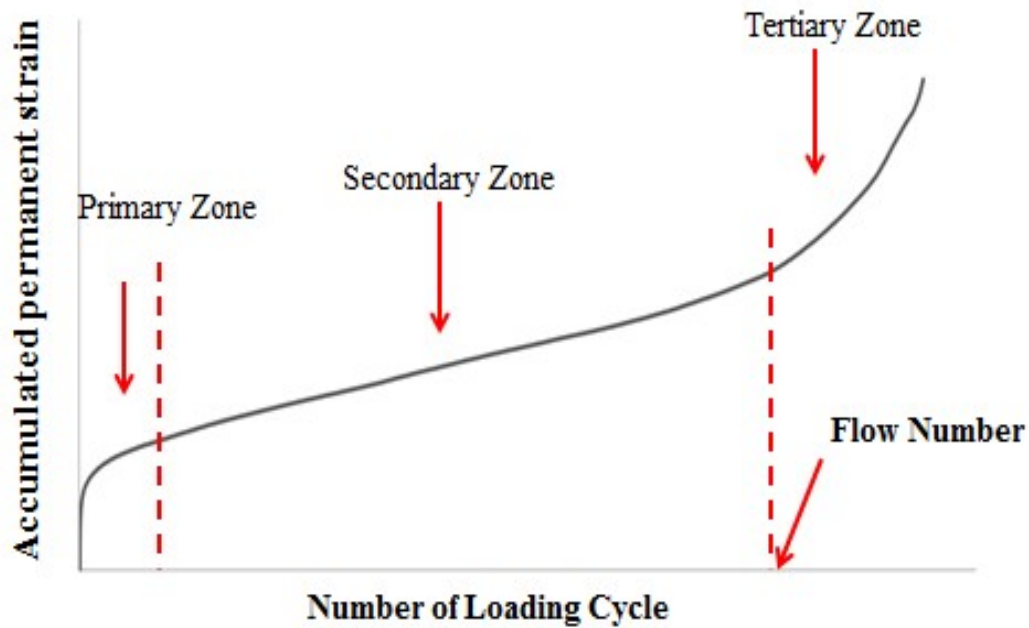


Figure 4-9. Graphical Illustration of the FN Concept.

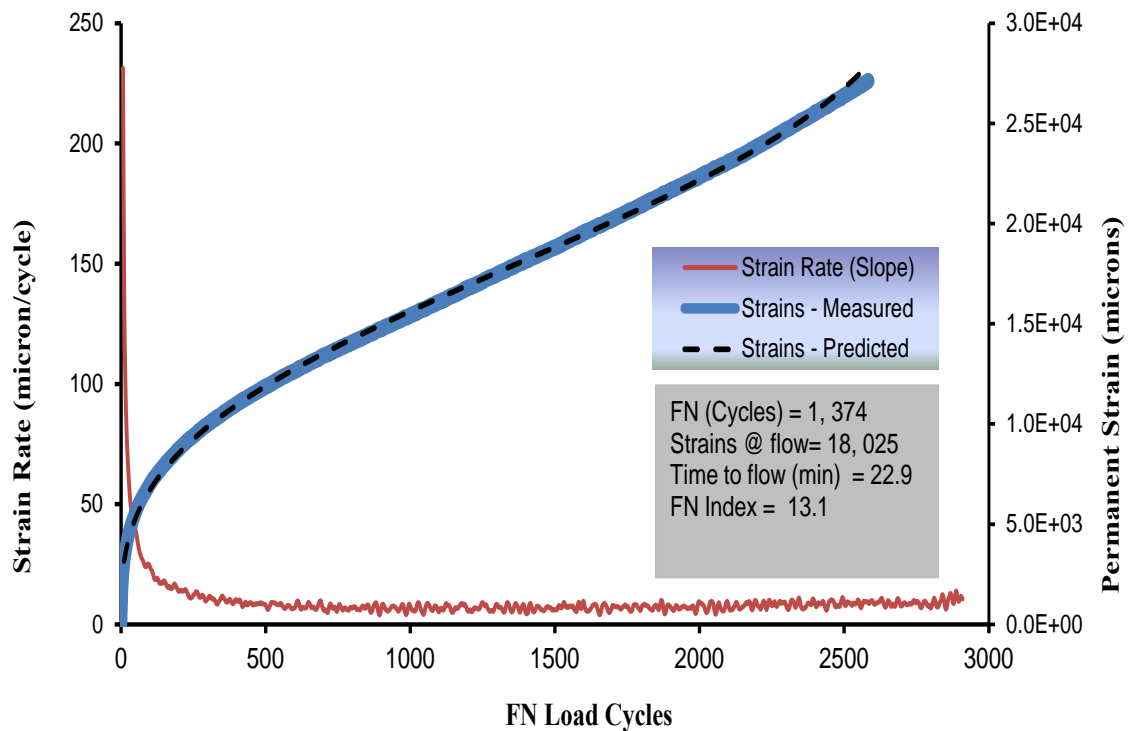


Figure 4-10. Accumulated Permanent Strain and Strain Rate as a Function of FN Load Cycles.

## HMA Sample Dimensions and AV Measurements for FN Testing

Similar to the RLPD tests, [Table 4-10](#) shows that both the HMA specimen dimensions and AV are fairly consistent and within the tolerable limits for the FN tests. [Appendix D](#) gives more detailed results for the HMA specimen dimensions and AV measurements.

**Table 4-10. FN HMA Specimen Dimensions and AV Measurements.**

Samples	Item	AMPT			UTM		
		H (Inches)	$\phi$ (Inches)	AV	H (Inches)	$\phi$ (Inches)	AV
 50°C	Avg	6.06	3.97	7.21	6.06	3.97	7.36
	COV	0.34%	0.25%	5.49%	0.17%	0.39%	3.65%
	Range	6.04–6.08	3.96–3.98	6.80–7.59%	6.05–6.07	3.95–3.98	7.15–7.66%
	Target	6.00±0.10 "	4.08±0.08 "	7±1%	6.00±0.10 "	4.08±0.08 "	7±1%

### FN Test Results and Statistical Analyses.

[Table 4-11](#) through [Table 4-14](#) show the FN test results based on the computations with models listed in [Table 4-9](#) along with statistical analysis based on both the actuator (RAM) and LVDT displacement measurements. [Appendix D](#) gives graphical plots of the FN test results. Both the HSD and t-tests were performed to evaluate any statistical differences between the AMPT and UTM FN test results at 90 and 95 percent confidence levels, respectively. Based on the results shown in [Table 4-11](#) through [Table 4-14](#), the following can be inferred:

- In terms of statistical variability, all the FN results are statistically acceptable and comparable, with COV values less than 30 percent. Thus, both systems (UTM and AMPT) exhibit acceptable in-laboratory repeatability for the FN test and can be used with a fairly similar level of reliability. However, although the COV results between the systems are comparable, the COV values for the FN (cycles) parameter are higher than the [AASHTO TP 79-12 \(2012\)](#) specification.
- With the exception of the FN Index parameter, however, the AMPT generally exhibits lower variability based on its lower COV values; indicating superior repeatability. This is not unexpected among others due to the better temperature consistency of the relatively smaller temperature chamber of the new AMPT; see [Table 4-1](#) and [Figure 4-2](#).

- Both the HSD and t-test statistical analyses show that the results are insignificantly different at 90 and 95 percent confidence levels, with the exception of the FN Index parameter at 95 percent. Therefore, either system (UTM or AMPT) can be confidently and reliably used in lieu of the other. In general, both the LVDT and axial RAM (actuator) deformation measurements can satisfactorily be used to characterize the HMA PD properties and compute the FN parameters using the UTM system. Furthermore, the use of either the AMPT or the UTM does not significantly impact or change the FN test results. Nonetheless, caution should be exercised with the FN Index computation, particularly at higher confidence levels such as 95 percent and that it is best if data analysis is based on actuator (RAM) displacement measurements in both systems.
- For UTM-AMPT comparison purposes, however, FN data analysis should preferably be based on axial RAM (actuator) deformation measurements. This is because, unlike the UTM with longer span LVDTs, the current AMPT setup uses only the actuator deformation measurements (without LVDTs) when running the destructive FN test that is associated with relatively larger HMA vertical deformations. Consideration for the provision of longer span LVDTs (> 1 mm) in the AMPT system is recommended.

### **FN Test Results – Key Findings and Recommendations**

Overall, the FN test results from both the AMPT and UTM systems were statistically comparable and acceptable at 95 and 90 percent confidence levels. However, the newer AMPT with a smaller temperature chamber exhibited superior repeatability, as the lower COV values show. Nonetheless, all the FN test results had COV values acceptably less than 30 percent. Thus, either system (AMPT or UTM) can be confidently used in lieu of the other to generate similarly quality and reliable FN results of a comparable statistical degree of accuracy with acceptable variability. The choice/preference is basically on the user.

**Table 4-11. FN Test Results and HSD Statistical Analyses.**

HMA Characteristic Parameter	UTM (RAM)		AMPT (RAM)		Avg		Statistics - COV		Statistics - HSD PairWise Comparison Are UTM-AMPT Results Significantly Different @ 90 & 95% Confidence Levels??
	Sample#1	Sample#2	Sample#1	Sample#2	UTM	AMPT	UTM	AMPT	
FN (cycles)	4,538	5,115	4,125	4,373	4,206	3,855	26.45%	17.99%	NO
$\epsilon_p$ (flow) (microstrain)	13,757	14,463	13,127	11,335	13,522	12,618	7.97%	8.86%	NO
Time (flow) (min)	76	85	69	73	70	64	26.45%	17.99%	NO
FN Index (microstrain/cycle)	3.03	2.83	3.18	2.59	3.34	3.38	21.53%	26.72%	NO

**Table 4-12. FN Test Results and T-Test Statistical Analyses.**

HMA Characteristic Parameter	UTM (RAM)		AMPT (RAM)		$t = \frac{\bar{x}_1 - \bar{x}_2}{SE}$	Are the Results Significantly Different ??			
	Avg ( $x_{i,bar}$ )	Stddev ( $s_i$ )	Avg ( $x_{i,bar}$ )	Stddev ( $s_i$ )		At 90% CL	At 95% CL7		
FN (cycles)	4206	1112	3855	1460	1297.82	1059.66	0.331	No	No
$\epsilon_p$ (flow) (microstrain)	13522	1078	12618	1634	1384.10	1130.11	0.800	No	No
Time (flow) (min)	70	19	64	24	21.63	17.66	0.331	No	No
FN Index (microstrain/cycle)	3.34	0.72	3.38	0.47	0.61	0.49	0.080	No	No

**Table 4-13. FN Test Results and HSD Statistical Analyses.**

HMA Characteristic Parameter	UTM (LVDT)		AMPT (RAM)		Avg		Statistics - COV		Statistics - HSD Pairwise Comparison Are UTM-AMPT Results Significantly Different @ 90 & 95% Confidence Level??
	Sample#1	Sample#2	Sample#1	Sample#2	UTM	AMPT	UTM	AMPT	
FN (cycles)	5,074	5,069	3,004	3,067	4,382	3,855	27.23%	17.99%	NO
$\epsilon_p$ (flow) (microstrain)	11,870	10,528	8,217	13,390	10,205	12,618	18.11%	8.86%	NO
Time (flow) (min)	85	84	50	51	73	64	27.23%	17.99%	NO
FN Index (microstrain/cycle)	2.34	2.08	2.74	4.37	2.38	3.38	13.90%	26.72%	NO

**Table 4-14. FN Test Results and T-Test Statistical Analyses.**

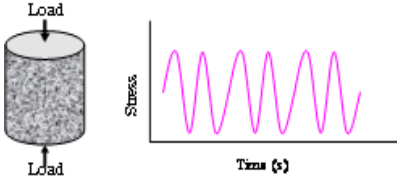
HMA Characteristic Parameter	UTM (LVDT)		AMPT (RAM)		$f = \frac{\bar{x}_1 - \bar{x}_2}{SE}$	Are the Results Significantly Different ??		
	Avg ( $x_{1bar}$ )	Stdev ( $s_1$ )	Avg ( $x_{2bar}$ )	Stdev ( $s_2$ )			At 90% CL	At 95% CL?
FN (cycles)	4382	1193	3855	1460	1333.32	0.484	No	No
$\epsilon_p$ (flow) (microstrain)	10205	1848	12618	1634	1744.11	1.694	No	No
Time (flow) (min)	73	20	64	24	22.22	0.484	No	No
FN Index (microstrain/cycle)	2.38	0.33	3.38	0.47	0.40	3.019	No	Yes

Legend: CL = Confidence Level

## THE DM TEST METHOD AND RESULTS

The DM test setups for both the AMPT and UTM systems are listed in [Table 4-15](#). As evident in [Table 4-15](#), similar loading and test conditions were applied for the same number of replicate specimens. The DM data analysis models, HMA sample AV measurements, results, and key findings are presented and discussed in the subsequent subsections.

**Table 4-15. The AMPT-UTM System Setups for the DM Test.**

#	Item	FN Loading and Test Parameters
1	Pictorial setup	 <p style="text-align: center;">UTM                      AMPT</p>
2	Sample loading configuration	
2	Sample dimensions	 <p style="text-align: center;">4" <math>\phi</math> <math>\times</math> 6" H.      AMPT = 3 (4" <math>\phi</math> <math>\times</math> 6" H)      UTM = 3 (4" <math>\phi</math> <math>\times</math> 6" H)</p>
3	Target test temperatures	4.4, 21.1, 37.8, 54.4°C
4	Target temp. tolerance	$\pm 2^\circ\text{C}$
5	Sample temperature conditioning time	$\geq 3$ hrs (4.4°C), 2 hrs (21.1°C), 2 hrs (37.8°C), and 2 hrs (54.4°C)
6	Loading mode	Compressive repeated Haversine (stress-controlled mode)
7	Loading frequency	0.1–25 Hz
8	Stress level (vertical-dynamic)	0.5–250 psi
9	Confining pressure	0 psi
10	Test termination criterion	Variable preset number of cycles per stress level per loading frequency
11	Test time	$\geq 3$ days
12	Measurable & output data	Load (stress), deformation, phase angle, & dynamic modulus
13	References	<a href="#">AASHTO 2001</a> ; <a href="#">Walubita et al., 2012</a>

### DM Data Analysis Models

The typical parameter that results from the DM test is the dynamic complex modulus of the HMA, denoted as  $|E^*|$ , and is expressed as shown in [Equation 4-4](#) ([AASHTO, 2002](#)):

$$|E^*| = \frac{\sigma_0}{\varepsilon_0} \quad (\text{Equation 4-4})$$

where  $\sigma_0$  is the axial (compressive) stress, and  $\varepsilon_0$  is the axial (compressive) strain. For graphical analysis and easy interpretation of the DM data,  $|E^*|$  master-curves were also generated as a function of the loading frequency using [Pellinen et al.'s \(2012\)](#) time-temperature superposition sigmoidal model shown in [Equations 4-5 and 4-6](#):

$$\text{Log } |E^*| = \delta + \frac{\alpha}{1 + e^{\beta - \gamma \log(\xi)}} \quad (\text{Equation 4-5})$$

$$\text{Log}(\xi) = \log(f) + \log(a_T) \quad (\text{Equation 4-6})$$

where  $\xi$  is the reduced frequency (Hz),  $\delta$  is the minimum dynamic modulus value (ksi or MPa),  $\alpha$  is the span of modulus values, and  $\beta$  and  $\gamma$  are shape parameters. Parameters  $f$  and  $a_T$  are the loading frequency and temperature shift factor to temperature  $T_{ref}$ , respectively. For this study, the temperature of reference,  $T_{ref}$ , was 70°F (21.1°C); see [Appendix D](#) for some examples.

### HMA Sample Dimensions and AV Measurements for FN Testing

Similar to the RLPD and FN tests, [Table 4-16](#) shows that both the HMA specimen dimensions and AV are fairly consistent and within the tolerable limits for DM testing; see [Appendix D](#) for more detailed results.

**Table 4-16. FN HMA Specimen Dimensions and AV Measurements.**

Samples	Item	AMPT			UTM		
		H (Inches)	$\phi$ (Inches)	AV	H (Inches)	$\phi$ (Inches)	AV
 4.4–54.4°C	Avg	6.07	3.96	7.45	6.06	3.96	7.46
	COV	0.25%	0.39%	2.58%	0.25%	0.25%	4.00%
	Range	6.05–6.08	3.95–3.98	7.28–7.66%	6.06–6.07	3.95–3.97	7.26–7.80%
	Target	6.00±0.10 "	4.08±0.08 "	7±1%	6.00±0.10 "	4.08±0.08 "	7±1%

## DM Test Results – $|E^*|$ Master Curves

As evident in Figure 4-11, the  $|E^*|$  master-curves shows a reasonably comparable moduli overlap among the HMA replicate specimens from the UTM and AMPT systems, particularly at the high moduli values corresponding to the low temperature domain. As theoretically expected, the overlap is not very pronounced at the high temperature domain due partly to HMA's visco-elastic nature. Therefore, caution should be exercised when analyzing and interpreting the results at the high temperature domain. However, the need to accurately calibrate the equipment and use of trained operators is also imperative to generating quality laboratory DM test results.

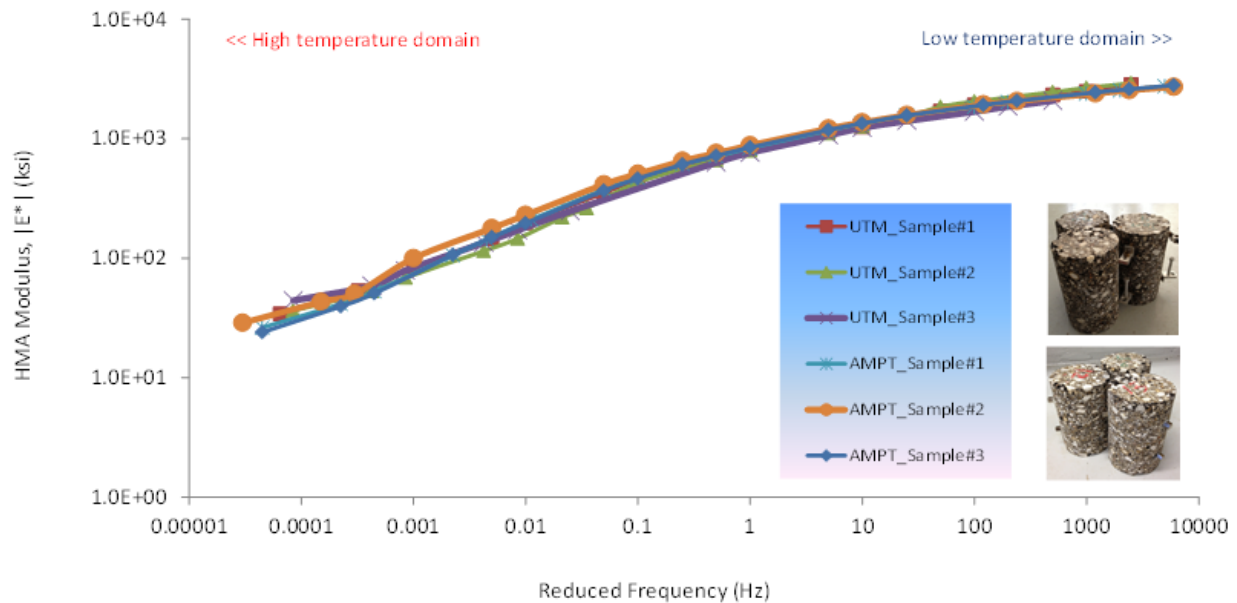


**Figure 4-11. Plot of the UTM-AMPT HMA  $|E^*|$  Master-Curves at 70°F.**

## DM Test Results – Statistics (COV and Stdev)

In terms of statistical variability and considering a COV threshold of 30 percent for the 40–130°F temperature range, all the results were statistically acceptable and comparable (see Figure 4-12). Thus, either system can be used to yield comparable and statistically acceptable results. However, operator proficiency should not be ignored. As theoretically expected due to HMA's visco-elastic nature, the AMPT\_COV trend line shows an increasing level of variability with increasing temperature.

In [Figure 4-12](#), the lower COV values (i.e., overall average of 3.70 percent versus 13.06 percent for the UTM) of the AMPT indicate superiority in terms of repeatability and lower variability in the moduli values than the UTM. This observation was not unexpected, partly attributed to the better accuracy in the automated LVDT setup and better temperature consistency in the smaller chamber of the new AMPT unit. Thus, the newer AMPT unit would be given preference over the traditional UTM as it provides more confidence and reliability in the test results. Additionally, the AMPT COV results are also consistent with the [AASHTO TP 79-12 \(2012\)](#) specification for DM testing with the AMPT.

### **DM Test Results – Key Findings and Recommendations**

Overall, the DM test results from both the AMPT and UTM systems were statistically comparable and acceptable with COV values less than 30 percent.

- The  $|E^*|$  master-curves showed a reasonable overlap in the moduli values, particularly at the low temperature domain, indicating that the results are fairly comparable. However, the AMPT exhibited a better overlap among the three HMA replicate specimens at the high moduli values corresponding to the low temperature domain. The minor scatter at the high temperature domain is theoretically expected due to HMA's visco-elastic nature; but emphasizes the need for caution when analyzing/interpreting the DM data at high temperatures.
- In terms of statistical variability, all the DM results are statistically acceptable and fairly comparable, i.e., all the COV values are less than 30 percent. Thus, both systems (UTM and AMPT) exhibit acceptable in-laboratory repeatability for the DM test and can be utilized with a fairly similar level of reliability to yield statistically repeatable results with acceptable variability.
- Based on its lower COV values (i.e., an overall average of 3.70 percent versus 13.06 percent for the UTM), the AMPT generally exhibits lower variability, thus indicating superiority in terms of repeatability than the UTM. Like the FN test, this is partly due to the better accuracy in the automated LVDT stud setup, LVDT measurement consistency, and better temperature consistency of the relatively smaller chamber of the new AMPT; see subsequent discussions. Additionally, the automatic load adjustment

based on the strain response during DM testing also contributes to the better accuracy of the AMPT; this feature is unavailable in the UTM.

Overall, the key finding and conclusion are that both the UTM and AMPT can be used concurrently or in lieu of the other for DM testing to generate quality results of acceptability reliability. The choice/preference is basically on the user.

Statistics - Variability	
UTM_COV	AMPT_COV
17.71%	1.70%
18.15%	1.31%
18.94%	1.51%
20.01%	1.52%
21.77%	2.46%
24.44%	4.03%
8.49%	0.41%
2.71%	1.14%
3.92%	1.96%
4.77%	2.87%
4.64%	3.28%
6.64%	4.53%
22.77%	3.90%
20.34%	4.98%
19.86%	6.44%
14.74%	8.26%
14.68%	9.02%
16.45%	9.82%
9.24%	2.44%
7.94%	0.91%
7.94%	0.67%
7.44%	2.46%
5.95%	4.31%
13.91%	8.93%
<b>Avg= 13.06%</b>	<b>3.70%</b>

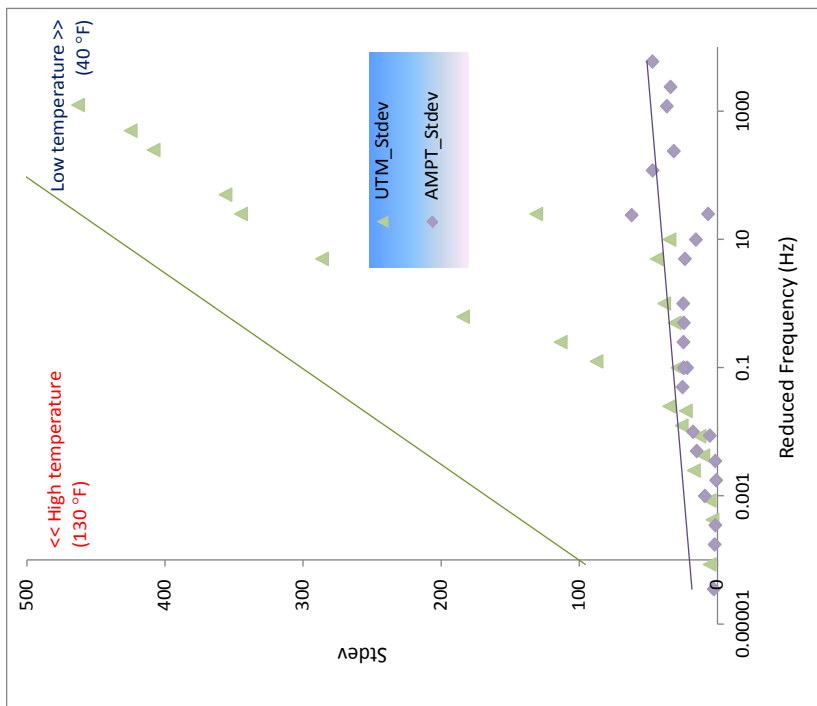
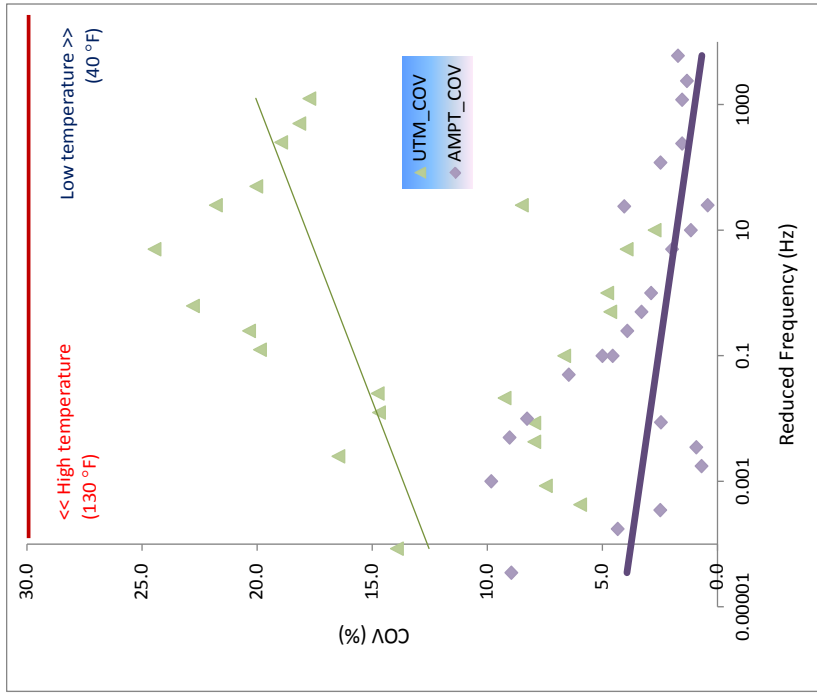


Figure 4-12. Plot of DM Stdev and COV—The UTM and AMPT Systems (Temperature Range = 40–130°F).

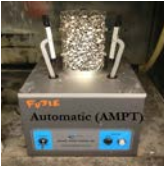
## GENERAL CHARACTERISTIC FEATURES

General characteristic features such as LVDT setup, LVDT accuracy, temperature consistency, etc., were also comparatively evaluated. These aspects are discussed under this section in the subsequent text.

### HMA Sample and LVDT Setup

HMA mix sample and LVDT setting up (including gluing the studs, cleaning, etc.) is much simpler and faster with the automated AMPT jigs than with the UTM's manually operated jigs (see [Table 4-17](#)). For instance, it takes approximately 10 minutes to glue the studs and set up the LVDTs with the AMPT system for one HMA specimen. As shown in [Table 4-17](#), the same processes take nearly 80 minutes with the UTM system. Thus, the AMPT system would be considered to be more efficient and cost-effective in this aspect.

**Table 4-17. Comparison of Sample and LVDT Setup Time.**

Machine Setup	Avg Time Requirement (Minutes)		
	Cleaning LVDT Studs	Gluing the Studs	Setting up the LVDTs
 <p>Manual (UTM)</p> <p>UTM</p>	40–60	30–60	20
 <p>Automatic (AMPT)</p> <p>AMPT</p>	≅ 5	≅ 5	≅ 5

### Temperature Consistency and Tolerances

Because of the smaller chamber (less than one-tenth that of the UTM chamber in volume), it is much quicker to obtain and maintain temperature consistency with the AMPT than the UTM system. For instance, it takes over twice the time to heat from room temperature (approximately 25°C) to 40°C and about 1.5 times more to heat from 40°C to 50°C for the UTM system as compared to the AMPT system (see [Table 4-18](#)).

**Table 4-18. Comparison of Temperature Heating Time.**

Temperature Change/Heating	Time (Hrs)	
	UTM	AMPT
From room temperature to 40°C	2.5–3.0	< 2.5
From 40°C to 50°C	1.5	< 1.5

For all the tests performed, the AMPT system exhibited better temperature consistency than the UTM system, attributed mainly to its smaller chamber size in volume. In case of the RLPD test, for instance, while both systems were within the  $50\pm 2^\circ\text{C}$  temperature tolerance range, the example in Figure 4-13 shows less temperature fluctuations with the AMPT system (COV of 0.01 percent with a temperature range from  $49.98^\circ\text{C}$  to  $50.00^\circ\text{C}$ ) than with the UTM system (COV of 0.46 percent with a temperature range of  $49.90^\circ\text{C}$  to  $50.60^\circ\text{C}$ ). The need for an external chamber for multiple sample conditioning may, however, negate these AMPT characteristics in terms of cost-effectiveness, which is not the case with the UTM.

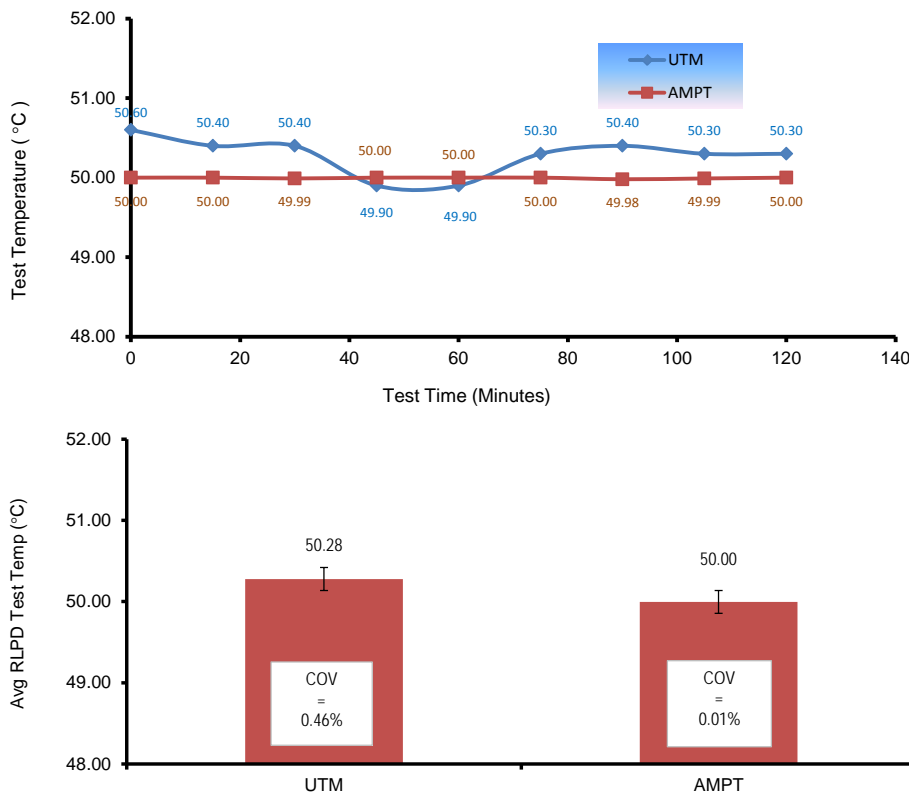


**Figure 4-13. Comparison of Temperature Consistency during RLPD Testing at 50°C.**

Considering all the tests conducted in this task, the following temperature operational tolerances were noted:  $AMPT \leq \pm 0.25^{\circ}C$  and  $UTM \leq \pm 1.0^{\circ}C$ . Compared to the UTM, these results suggest that the AMPT system is superior and more cost-effective in terms of temperature operational efficiency. In turn, this may have also positively contributed to more consistent LVDT readings for the AMPT system that are discussed in the subsequent text.

### LVDT Accuracy and Repeatability

As shown in Figure 4-14 and Appendix D for the RLPD test as a demonstration example, the LVDT measurements from the AMPT system exhibited more consistency and repeatability than the UTM system. The COV values computed based on the average LVDT measurements from three individual LVDTs (LVDT1, LVDT2, and LVDT3) are comparatively higher for the UTM than those computed from the AMPT system at both test temperatures, e.g., 34.64 percent versus 14.67 percent at 40°C (Figure 4-14) and 39.50 percent versus 21.99 percent at 50°C (Appendix D). Therefore, while the overall  $\alpha$  and  $\mu$  results may be comparable and acceptable, the LVDT readings suggest that there is more statistical confidence and reliability in using the AMPT system than the UTM system.

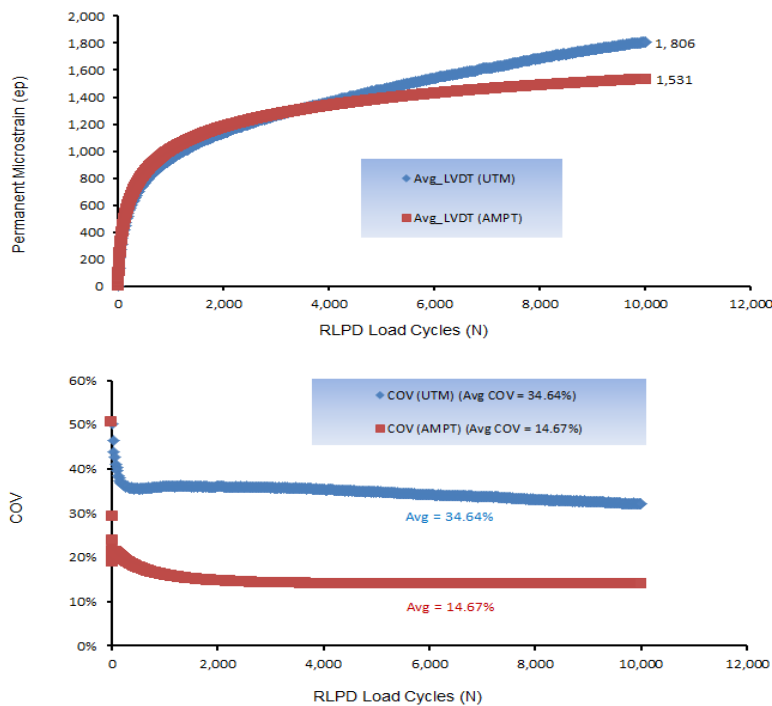


**Figure 4-14. LVDT Variability Comparison for RLPD Testing at 40°C, 20 psi.**

As observed in other studies (Walubita et al., 2012), variability in the LVDT measurements was generally higher at the high 50°C test temperature compared to 40°C; see the COV values in Figure 4-14 and Appendix D. This is in part attributed to the HMA visco-elastic behavior, particularly at elevated temperatures. Nonetheless, the AMPT system still exhibited statistical superiority with the LVDT variability having COV values less than 30 percent. The COV values were higher than 30 percent for the UTM for both of the two RLPD test temperatures evaluated, i.e., 40°C and 50°C.

However, the magnitude of the LVDT measurements indicates relatively less HMA permanent deformation in the AMPT than the UTM system, e.g., 1,531 (AMPT) versus 1,806 (UTM) microstrains at 40°C (Figure 4-14) and 1,745 (AMPT) versus 2,613 (UTM) microstrains at 50°C (see Appendix D). This may partly be attributed to the smaller AMPT chamber that may be acting as confinement to the HMA sample. The AMPT test chamber is less than one-tenth the size of the UTM chamber (see Figure 4-2). For the RLPD test, however, this does not significantly affect the final results because computation of the  $\alpha$  and  $\mu$  parameters is predominantly dependent on the shape characteristics of the strain-cycle response curve than the strain magnitude.

## **SYNTHESIS AND DISCUSSION OF THE RESULTS**

In addressing the fundamental questions and study objectives raised in the opening paragraphs of this chapter, a synthesis of the results presented here indicates the following findings, conclusions, and recommendations:

- All test (RLPD, FN, and DM) results were statistically comparable and acceptable at 95 percent confidence level in both the UTM and AMPT systems.
- Test repeatability /variability in both the UTM and AMPT systems were also statistically acceptable with low COV values less than 30 percent.
- Either system (AMPT or UTM) can be confidently used in lieu of the other to generate similar quality and reliable results of a comparable statistical degree of accuracy at 95 percent or 90 percent confidence levels with acceptable variability (i.e., COV < 30 percent).

Overall, it should be emphasized here that the use of trained operators/technicians and well-calibrated equipment is one of the key ingredients to obtaining quality, reliable, and consistent laboratory test results, whether with the AMPT or UTM system. [Table 4-19](#) provides a subjective comparison of the AMPT and UTM based solely on the HMA mixes evaluated in this study and on the authors' experience with these test methods.

**Table 4-19. Comparison of the AMPT and UTM Systems.**

<b>Unit</b>	<b>Advantages and Applications</b>	<b>Limitations and Challenges</b>
AMPT	<ul style="list-style-type: none"> <li>- Compact system for easy mobility.</li> <li>- Small chamber for better temperature consistency.</li> <li>- Automatic LVDT setup jigs for improved efficiency and accuracy.</li> <li>- Robust LVDTs with high resolution and accuracy.</li> </ul>	<ul style="list-style-type: none"> <li>- Relatively low load cell capacity.</li> <li>- Shorter span LVDTs limit the measurements of larger deformations in destructive tests such as FN.</li> <li>- Requires external chamber for conditioning multiple specimens.</li> <li>- Designed for 6" tall by 4" diameter specimens.</li> </ul>
UTM	<ul style="list-style-type: none"> <li>- High load cell capacity for high load applications.</li> <li>- Longer span LVDT for large deformation measurements.</li> <li>- Wider temperature range that permits testing below zero and over 140°F (from -40° to 100°C).</li> <li>- Big temperature chamber permits the conditioning of multiple specimens.</li> <li>- Bigger temperature means no need for external chamber.</li> <li>- Both the actuator (RAM) and LVDTs can sufficiently be used to measure deformations under most test methods.</li> <li>- Can accommodate different specimens dimensions and configurations.</li> </ul>	<ul style="list-style-type: none"> <li>- Manually operated LVDT setup jigs means longer setup time.</li> <li>- Bigger chambers means longer time in reaching target temperature and difficult in maintaining temperature consistency.</li> </ul>

Aside from the limitations and challenges listed in [Table 4-17](#), the new AMPT system, as theoretically expected, generally exhibited superiority in terms of:

- Operational efficiency.
- Temperature consistency (i.e.,  $\pm 0.25^\circ\text{C}$  vs.  $\pm 1.0^\circ\text{C}$  tolerance for the UTM).
- LVDT measurement consistency (about twice the accuracy of the UTM in terms of the variability [COV] in the three LVDT readings).
- Simplicity of sample setup and practicality.

- Statistical reliability (lowest COV values).
- Cost-effectiveness, i.e., setup time (at least 40 percent shorter than for the UTM and temperature heating/cooling time (at least 30 percent more efficient than the UTM).

Thus, if users were given the choice, the new AMPT system would be preferred over the traditional UTM. Compared to the UTM, the limitations associated with the AMPT include the lower load cell capacity, shorter LVDT span, shorter temperature range, and the need for an external chamber for conditioning multiple specimens. Thus, if feasible, provision and installation of longer span LVDTs (> 1 mm) without compromising resolution and accuracy for the AMPT system to accommodate destructive testing such as FN would be a welcome undertaking. The other added advantages of the UTM include the potential to simultaneously use both LVDTs and the actuator (RAM) in destructive testing such as FN and the ability to accommodate different specimen dimensions and configurations that allows for performing different tests. Overall, the key findings and recommendations drawn from this study are as follows:

- Previously obtained UTM results are still good and the use of the new AMPT system should not affect these.
- Both the UTM and AMPT can be used concurrently or in lieu of the other with comparable accuracy and reliability.
- The biggest challenge is to always use trained operators/technicians and ensuring that all equipment is well-calibrated.
- Be cautious when comparing DM testing at the high temperature domain; variability could occur due partly to the HMA's visco-elastic nature.
- If feasible, provide and install longer span LVDTs (> 1 mm) for the AMPT system to accommodate destructive testing such as FN ( $\geq 5$  mm).

## **SUMMARY**

For the HMA mix evaluated, the test (RLPD, FN, and DM) results from the UTM and AMPT were statistically comparable and acceptable at 95 percent and 90 percent confidence levels. The test repeatability and variability in both the UTM and AMPT systems were also statistically acceptable with low COV values less than 30 percent. Thus, either system (AMPT

or UTM) can be confidently used in lieu of the other to generate similarly quality and reliable results of a comparable statistical degree of accuracy with acceptable variability. The choice/preference is basically on the user; as was listed in [Table 4-19](#), each system has its own merits and limitations.

However, operator/technician proficiency and equipment calibration are some of the most critical factors not to ignore in laboratory studies of this nature. Cautiousness should also be exercised when comparing DM testing at the high temperature domain as variability in the test results could occur due partly to the HMA's visco-elastic nature.



## **CHAPTER 5 COMPARATIVE EVALUATION OF THE RLPD, FN, AND DM TEST METHODS**

The objective of work presented in this chapter was to comparatively evaluate the FN, DM, and RLPD test methods in terms of characterizing the PD response of HMA mixes in the laboratory, relative to the traditional HWTT test method. Secondly, the researchers aimed to investigate if these test methods are correlated with each other in terms of screening and ranking HMA mixes for rutting resistance potential and if, based on these correlations, a single test method can be satisfactorily used in lieu of the others. Lastly, the third objective was to comparatively assess if these test methods and/or the data generated could be related to the HMA shear resistance by way of computing or estimating the HMA shear properties such as shear strength, shear modulus, shear strain, etc. The ultimate goal is to be able to relate these HMA shear properties to the HMA shear deformation/rutting in the field under extreme traffic and temperature conditions, particularly at stop-go intersections.

To address these objectives, various HMA mixes were evaluated in each test method (RLPD, FN, and RLPD), and the results were compared and correlated to each other. The advantages and disadvantages associated with the test methods were also comparatively reviewed and are discussed in this chapter.

In terms of the chapter organization, overviews of the FN, DM, and RLPD test methods are discussed in the subsequent sections. Thereafter, the experimental design plan—including characteristics of the HMA mixes used for the laboratory tests—is discussed. Results obtained from each test method are then presented and statistically analyzed, followed by a discussion and synthesis of the findings. The chapter then concludes with a summary of the key findings and recommendations. [Appendix E](#) includes additional data patterning to this chapter.

### **LABORATORY TEST METHODS**

The FN, DM, and RLPD tests were conducted using the UTM following the test procedures described in [Chapter 4](#) of this interim report; refer to [Table 4-4](#), [Table 4-9](#), and [Table 4-15](#). [Chapter 4](#) also presented the data analysis models associated with these test methods, and are therefore, not discussed in this chapter. The HWTT was conducted according to the Tex-242-F test procedure ([TxDOT, 2009](#)).

## EXPERIMENTAL DESIGN PLAN AND HMA MIXES

To compare the three test methods, seven HMA mixes, ranging from fine-graded to open-graded, that are commonly used in Texas were evaluated in each test method. [Table 5-1](#) presents the mix-design characteristics for these mixes.

**Table 5-1. HMA Mix Characteristics.**

#	HMA Mix	Aggregate Gradation	Mix-Design	Field Project Where Used
1	CAM	Fine-graded ( $\frac{3}{8}$ " NMAS)	7.0% PG 64-22 + Igneous/limestone	SH 121 (Paris)
2	Type B	Coarse-graded ( $\frac{3}{4}$ " NMAS)	4.6% PG 64-22 + Limestone + 30% RAP	IH 35 (Waco)
3	Type C	Dense-graded ( $\frac{3}{4}$ " NMAS)	4.8% PG 64-22 + Limestone/Dolomite + 1% Lime + 17% RAP + %RAS	SH 21 (Bryan)
4	Type D	Fine-graded ( $\frac{3}{8}$ " NMAS)	5.1% PG 64-22 + Quartzite + 20% RAP	US 59 (Atlanta)
5	Type F	Fine-graded ( $\frac{3}{8}$ " NMAS)	7.4% PG 76-22 + Sandstone	US 271 (Paris)
6	PFC	Open-graded ( $\frac{3}{4}$ " NMAS)	6.0% PG 76-22 + Igneous/limestone	SH 121 (Paris)
7	SMA	Gap-graded ( $\frac{3}{4}$ " NMAS)	6.0% PG 76-22 + Limestone	IH 35 (Waco)

*Legend: CAM = crack attenuating mix; PFC = permeable friction course; SMA = stone matrix asphalt; NMAS = nominal maximum aggregate size; RAP = reclaimed asphalt pavement material; PG= performance grade.*

For each HMA mix and test type/condition, a minimum of three replicate specimens were molded, using the SGC with HMA obtained from the plant. As per Texas specification, all HMA test specimens were molded to a target AV content of  $7\pm 1$  percent, except for the PFC mix specimens that were molded to a higher total AV content of  $20\pm 2$  percent ([TxDOT, 2004](#)). To avoid any biasness, the same technician was used to mold and fabricate all the HMA test specimens for all the three test methods (FN, DM, RLPD, and HWTT).

## LABORATORY TEST RESULTS AND ANALYSIS

This section presents each laboratory test result from the FN, DM, RLPD, and HWTT tests and a comparison of the ranking of the HMA mixes based on the results of these test methods. In addition, graphical correlations for the laboratory results are provided.

## The FN Test Results and Analysis

Table 5-2 presents the FN test results of six different HMA mixes and Figure 5-1 shows a graphical summary of these data including both the FN (cycles) and FN Index. Both parameters indicate that the SMA has the lowest susceptibility to rutting. However, based on the FN (cycles) parameter, the CAM has higher rutting resistance potential than the Type D mix, while the FN Index indicates that CAM has much lower rutting resistance; its FN Index is twice as much as that for the Type D. The subsequent results of the DM, RLPD, and HWTT tests further verify that the CAM has lower rutting resistance potential, which is consistent with the FN Index results. Therefore, the use of the FN (cycles) parameter may not indicate the rutting resistance of some mixes reliably and effectively. Appendix E has additional FN test results along with some statistical analysis.

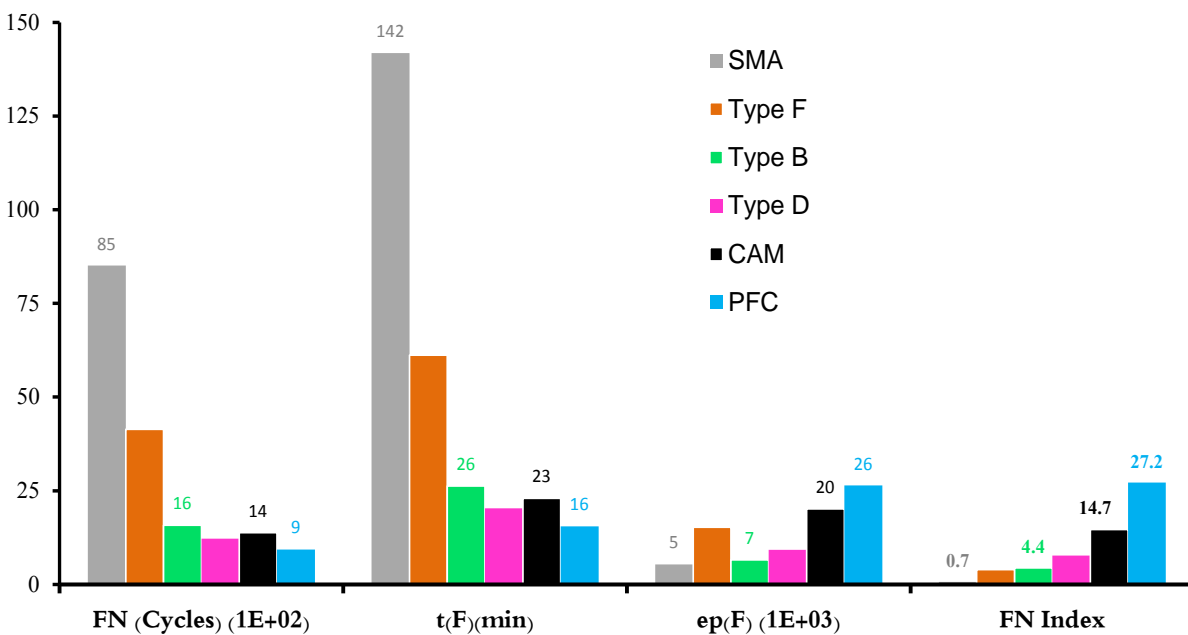


Figure 5-1. Graphical Comparison of the FN Parameters.

**Table 5-2. Summary of FN Test Results.**

#	HMA Mix (Field Hwy)	HMA Samples after Testing	Sample ID#	FN (cycles)	$\epsilon_p(F)$	FN Index
1	CAM (SH 121)		Sample #1	1,374	18,025	13.12
			Sample #2	1,258	20,374	16.20
			Sample #3	1,501	22,078	14.71
			Mean	1,378	20,159	14.67
			Stdev	122	2,035	1.54
			COV (%)	8.8	10.1	10.5
			2	Type B (IH 35)		Sample #1
Sample #2	1,550	5,074				3.27
Sample #3	1,945	6,595				3.39
Mean	1,578	6,576				4.39
Stdev	354	1,492				1.83
COV (%)	22.4	22.7				41.7
3	Type D (US 59)					Sample #1
			Sample #2	960	8,787	9.15
			Sample #3	1,205	6,962	5.78
			Mean	1,217	9,261	7.68
			Stdev	263	2,569	1.73
			COV (%)	21.6	27.7	22.5
			4	Type F (US 271)		Sample #1
Sample #2	4,583	13,138				2.87
Sample #3	2,760	17,440				6.32
Mean	4,139	15,289				3.98
Stdev	1,219	3,042				2.44
COV (%)	29.5	19.9				61.3
5	PFC (SH 121)					Sample #1
			Sample #2	1,055	24,158	22.9
			Sample #3	806	17,239	21.4
			Mean	931	26,386	27.2
			Stdev	176	10,441	8.3
			COV (%)	18.9	39.6	30.6
			6	SMA (IH 35)		Sample #1
Sample #2		No failure to 10,000 cycles				
Sample #3		No failure to 10,000 cycles				
Mean		N/A				
Stdev		N/A				
COV		N/A				

Legend: FN=flow number,  $\epsilon_p(F)$ =accumulated permanent strain at the onset of tertiary flow, Stdev=standard deviation, COV=coefficient of variation.

While the Texas specification (TxDOT, 2004) calls for use of PG 76-22 for all the CAM mix-designs, the contractor mistakenly used a lower soft-grade PG 64-22 asphalt-binder on this particular project (i.e., SH 121 highway). This could have partly contributed to this CAM mix's poor laboratory rutting resistance performance.

In addition, the results shown in Figure 5-1 suggest that the PFC mix has the highest susceptibility to rutting. This is partly due to its high total air void content (20 percent  $\pm$  2 percent) and unconfined FN testing condition. That is, the true PD performance of the PFC mix is not captured under the unconfined loading test configuration. Therefore, the FN test results of PFC mix were not used to compare with other mixes. Likewise, the PFC mix was also excluded from the comparative analysis of the subsequent DM and RLPD tests data.

If an FN Index value of 10 (i.e., FN Index  $\leq$  10) is tentatively assumed as the HMA pass-fail screening criterion, the CAM and PFC mixes would be considered unsatisfactory. That is the lower the FN Index value in magnitude, the better the HMA mix in terms of resistance to PD, and vice versa. Nonetheless, this proposed FN Index criterion still needs further verification with more HMA mix testing and correlation with field performance data.

Compared to the FN Index parameter and as evident in Appendix E, the traditional parameters computed based on the FN test (i.e., —FN (cycles),  $t(F)$ , and  $\varepsilon_p(F)$ ) as individual parameters did not provide an effective, nor statistically significant, differentiation and screening potential of resistance to PD for the HMA mixes that were evaluated in this study. Therefore, application of these parameters for routine HMA mix-design and screening of PD resistance should be approached with caution.

### **The DM Test Results and Analysis**

Figure 5-2 presents the  $|E^*|$  master curves for all the HMA mixes evaluated using the DM test. In general, high stiffness mixes (i.e., higher values of  $|E^*|$ ) are expected to be more resistant to rutting than low stiffness mixes (Hu et al., 2011; Goh et al., 2011; Witczak et al., 2002). In addition,  $|E^*|$  values at higher temperatures are generally used to estimate PD performance, since the HMA mixes are more prone to PD at these high temperatures.

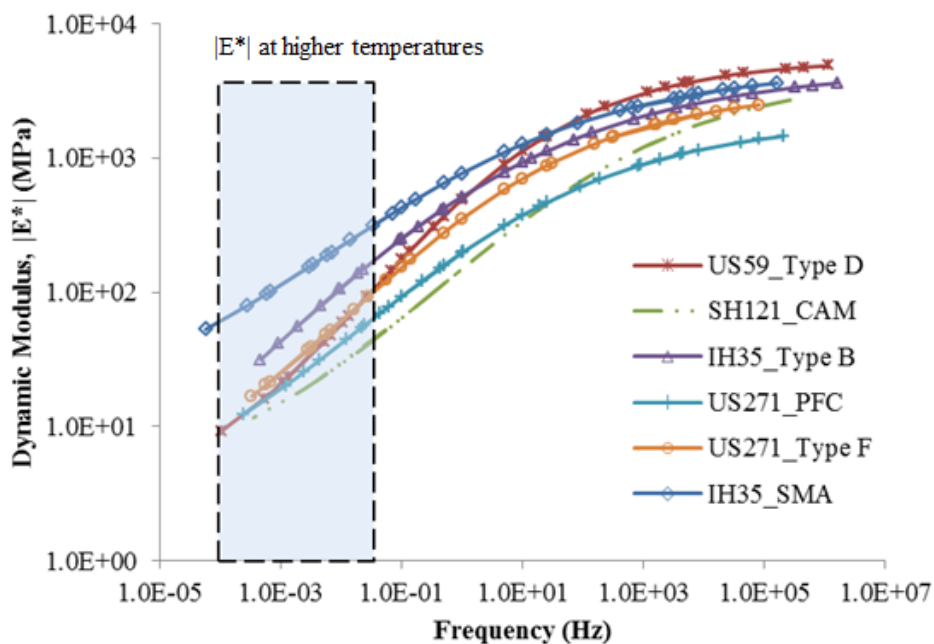


**Figure 5-2. HMA  $|E^*|$  Master-Curves at 70°F.**

Previous studies (Witczak et al., 2002; Apeyeyi, 2011) proved that the  $|E^*|$  values at 54.4°C and 37.8°C correlated well with the FN test results. In this study, values of  $|E^*|_{37.8^\circ\text{C}, 0.1\text{Hz}}$ ,  $|E^*|_{54.4^\circ\text{C}, 0.1\text{Hz}}$ ,  $|E^*|_{54.4^\circ\text{C}, 5\text{Hz}}$ , and  $|E^*|_{54.4^\circ\text{C}, 10\text{Hz}}$  were used to establish a relationship with the FN test results. These DM-FN correlations are presented and discussed in the subsequent sections of this chapter.

Based on  $|E^*|$  values at higher temperatures, the SMA exhibits higher modulus values than the rest of other mixes. The higher modulus of the SMA mix may result from a heavy-duty stone mix with a gap-graded aggregate structure that generates stone-on-stone contact in the coarse aggregate filled with high viscosity bituminous mastic. The mix with the lowest  $|E^*|$  value is the CAM, which is consistent with the preceding FN Index results.

### The RLPD Test Results and Analysis

Figure 5-3 shows the accumulated permanent strains,  $\epsilon_p$ , for the HMA mixes evaluated using the RLPD test. Higher accumulated permanent strains values theoretically indicate that HMA mixes have lower PD and rutting resistance potential. As expected, the CAM (poorest) and SMA (best) mixes have the highest and lowest accumulated permanent strain values, respectively, which is consistent with the results obtained from FN and DM tests.

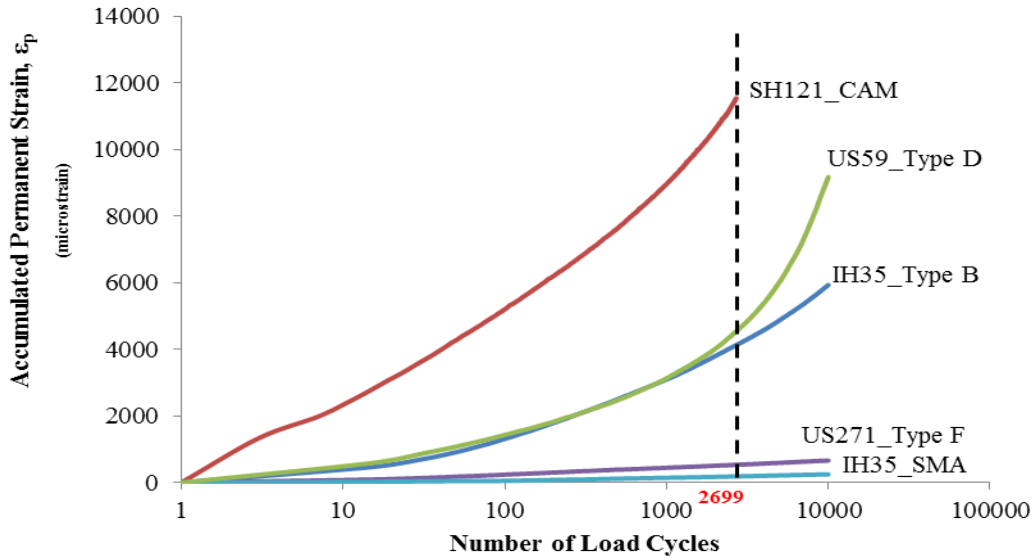


**Figure 5-3. RLPD Accumulated Permanent Strain,  $\epsilon_p$ , at 50°C.**

### Comparison of the Test Results and Ranking of the HMA Mixes

Based on the data presented in the preceding Figure 5-1, Figure 5-2, and Figure 5-3, Table 5-3 provides a comparative ranking of the mixes. Both the FN Index and  $\epsilon_p$  parameters show the same ranking of the HMA mixes. As discussed before, ranking of the CAM and Type D based on the FN (cycles) parameter is not reasonable, since the other three results (FN Index,  $|E^*|$ , and  $\epsilon_p$ ) indicate that the Type D is stiffer and more PD/rut-resistant than the CAM mix. As observed in Figure 5-2, Type B has a higher modulus value than Type F, while both the FN and RLPD tests show that Type F is much more PD/rut-resistant than the Type B. Even the subsequent HWTT test results (Table 5-3 and 5-4) shows that the Type F mix is superior to the Type B mix based on its lower rut depth, i.e., 5.45 mm versus 12.90 mm. Thus, the accuracy of the DM test results to evaluate the PD/rutting-resistance of HMA mixes is a subjective matter needing further investigations.

**Table 5-3. HMA Mix Ranking Based on the FN, DM, and RLPD Test Results.**

HMA Ranking	FN Test		DM Test	RLPD Test	HWTT Test
	FN (cycles)	FN Index (microstrain/cycle)	$ E^* $ (MPa)	$\epsilon_p$ (microstrain)	Rut Depth @ 20 000 Load Passes (mm)
1	SMA	SMA	SMA	SMA	Type D
2	Type F	Type F	Type B	Type F	SMA
3	Type B	Type B	Type F	Type B	Type F
4	CAM	Type D	Type D	Type D	Type B
5	Type D	CAM	CAM	CAM	CAM

In terms of field performance, experience has shown that various factors including material characteristics (i.e., mix-design), pavement structure, traffic, and climate (i.e., temperature) influence the rutting performance of HMA mixes. However, mixes with coarse aggregate gradation, high stone-on-stone contact in the gradation matrix (e.g., gap-graded), high asphalt-binder PG grades (e.g., PG 76-22), etc., are generally associated with good field rutting resistance.

Although the FN Index and RLPD  $\epsilon_p$  results in [Table 5-4](#) indicate a reasonable ranking trend, this is very subjective as there is a need to correlate these findings to actual field rutting data. As indicated in [Table 5-1](#), most of these HMA mixes have already been placed on in-service highways. Therefore, the ongoing performing monitoring study will readily serve as a validation platform for these results, including the PD predictive potential of the laboratory tests ([Walubita et al., 2012](#)).

### Graphical Correlations for the Laboratory Test Results

[Table 5-4](#) provides a summary of FN, DM, and RLPD test results. Graphical correlations among the FN, DM, and RLPD test results are illustrated in [Figure 5-4](#) thru [Figure 5-6](#).

**Table 5-4. Summary of FN, DM, and RLPD Laboratory Test Results.**

Mix	FN (cycles) (1E+02)	FN Index (microstrain/cycle)	E*  (MPa)				$\epsilon_p$ (RLPD) (microstrain)	HWTT Rut Depth @ 20 000 Load Passes
			E*  <sub>37.8° C, 0.1 Hz</sub>	E*  <sub>54.4° C, 0.1 Hz</sub>	E*  <sub>54.4° C, 5 Hz</sub>	E*  <sub>54.4° C, 10 Hz</sub>		
SMA	55.27	0.94	705	366	1059	1297	185	4.61
Type F	41.39	3.98	140	70	272	358	535	5.45
Type B	15.78	4.39	383	113	554	727	4131	12.90
Type D	12.17	7.68	191	71	365	412	4546	4.36
CAM	13.78	14.67	150	81	243	308	11549	18.00

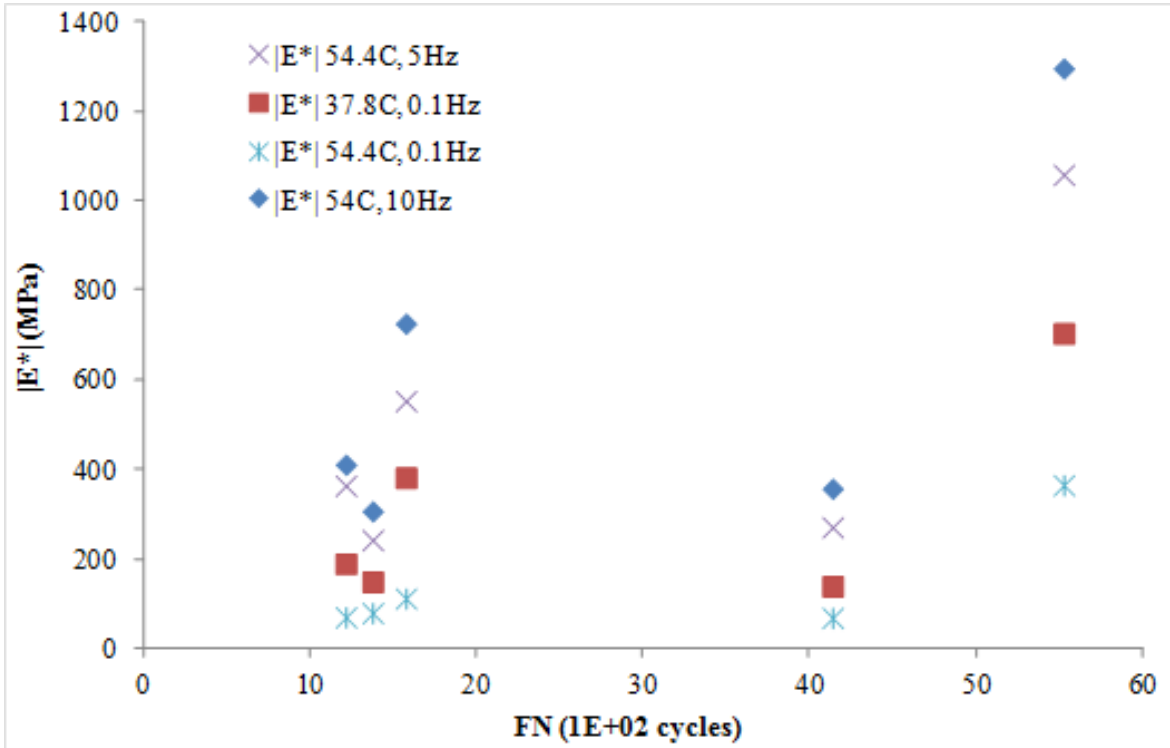


Figure 5-4. Correlations between FN Cycles and |E\*|.

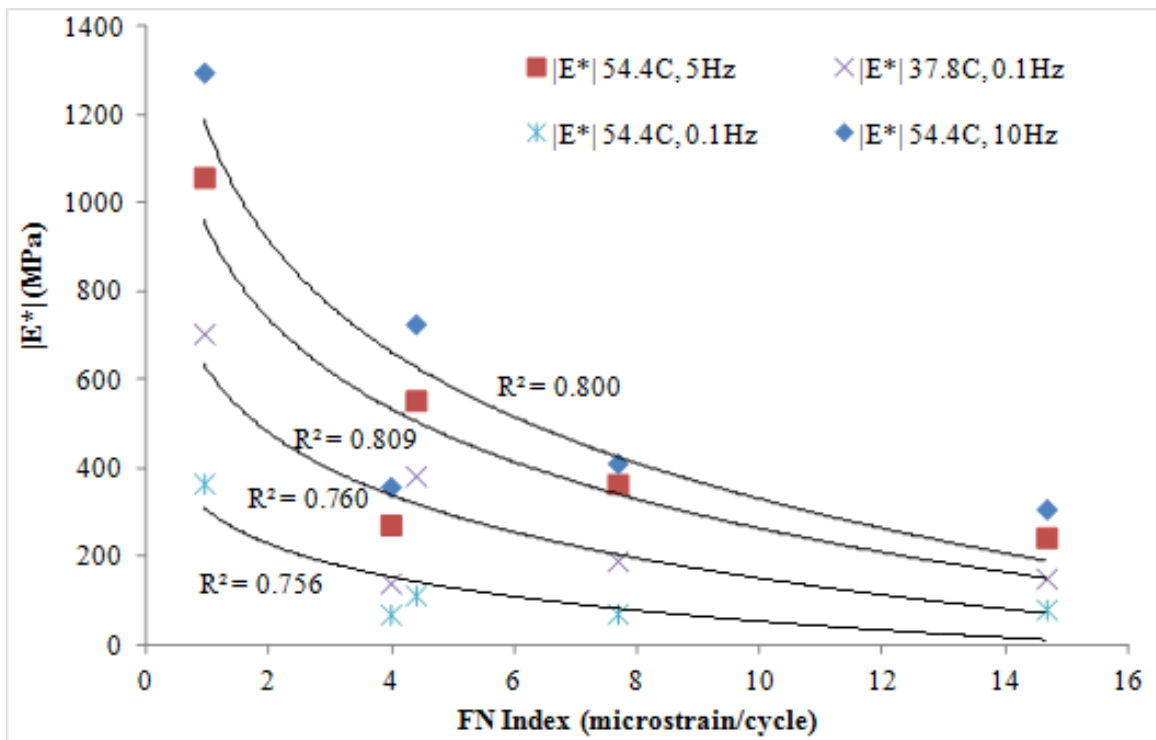
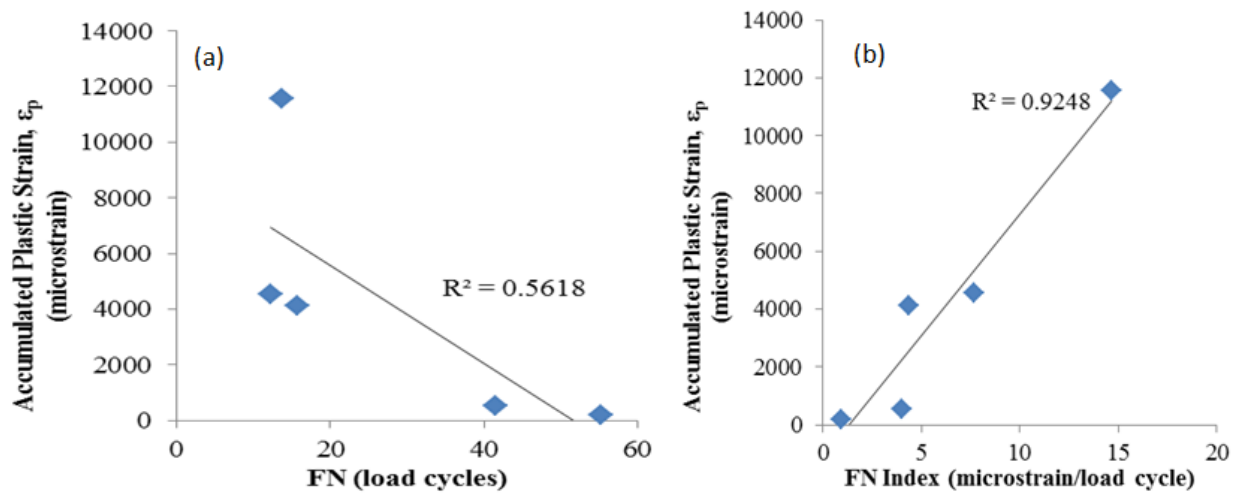


Figure 5-5. Correlations between FN Index and |E\*|.



**Figure 5-6. Correlations between FN and  $\epsilon_p$ , and FN Index and  $\epsilon_p$ .**

It is observed that there are no strong correlations between FN (cycles) and  $|E^*|$  values as shown in Figure 5-4 and between FN and  $\epsilon_p$  values as indicated in Figure 5-6(a). However, some correlations were found between the FN Index and  $|E^*|$  values shown in Figure 5-5 and between the FN Index and  $\epsilon_p$  values as shown in Figure 5-6(b). Especially, the FN Index and  $\epsilon_p$  values exhibited a strong correlation with 92.48 percent of a correlation coefficient,  $R^2$  (Figure 5-6[b]). This strong FN Index-  $\epsilon_p$  correlation suggests that the FN (FN Index) and RLPD ( $\epsilon_p$ ) tests could possibly be used in lieu of each other.

An important observation in Figure 5-5 is that the  $|E^*|$  values at 54.4°C and 5 Hz have the best correlation ( $R^2=81.0$  percent) with the FN Index compared to the other temperatures and/or frequencies. Witczak et al. (2002) also reported that both the  $|E^*|$  (54.4°C, 5 Hz) values and FN values had good correlation with field rutting performance. Thus, the  $|E^*|$  at 54.4°C and 5 Hz might be a proper DM test condition for estimating the PD/rutting-resistance potential of HMA mixes in the field.

### Comparison with the HWTT Test Results

The average HWTT results based on three replicate test sets per mix type are shown in Figure 5-7 and rank the resistance to PD of the HMA mixes as follows: Type D (4.36 mm) → SMA (4.61 mm) → Type F (5.45 mm) → PFC (7.60 mm) → Type B (12.90 mm) → CAM (18.00 mm; poorest). Clearly, the rut depths of the Type D and SMA are hardly different

and would basically rank the same top position in terms of rutting performance superiority. Using the Tex-242-F pass-fail screen criteria ( $\leq 12.5$  mm at 10 000 HWTT load passes), the CAM would be considered unsatisfactory; which is also consistent with the preceding FN Index results.

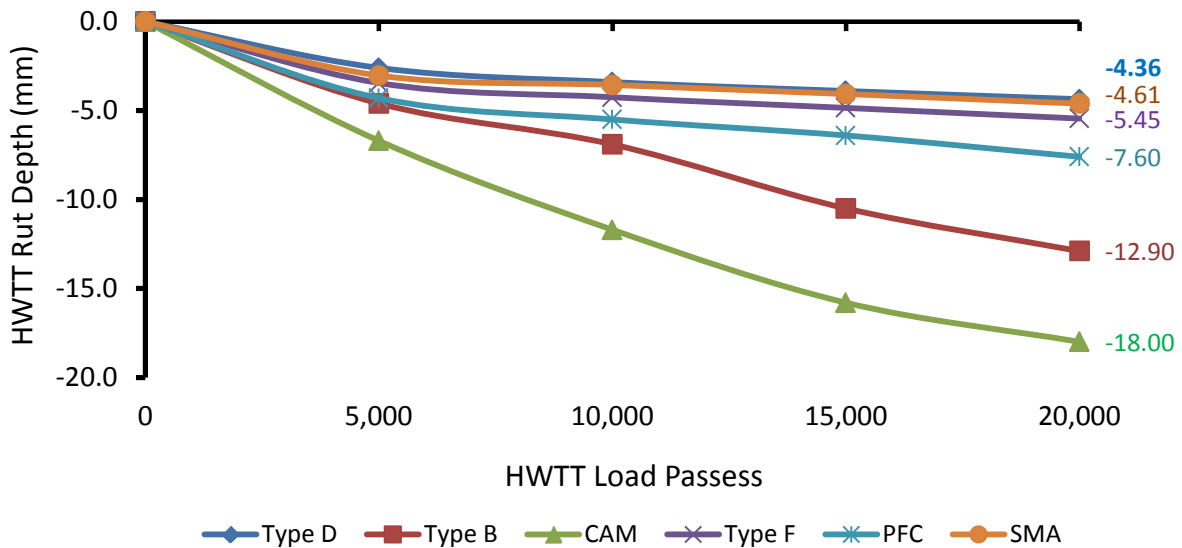


**Figure 5-7. HWTT Graphical Rutting Results.**

While the Type D, Type F, and SMA rut depths are statistically indifferent, the general difference in the ranking compared to the other test results shown previously in [Tables 5-3](#) and [5-4](#) is partially attributed to the differences in the loading configuration and high sample confinement in the HWTT setup; unlike in the unconfined FN, RLPD, and DM tests. The extreme HWTT sample confinement may be over-scoring the true PD performance of some of these mixes. As evident in [Figure 5-7](#), even the high AV content PFC mix outperformed the Type B mix in the HWTT; which is not the case with the unconfined FN, RLPD, and DM tests. The possibility of moisture damage (i.e., stripping of the Type B mix) could have been another factor; with the inflexion point seemingly occurring after 10,000 HWTT load passes in [Figure 5-7](#). By contrast, the current setup of the FN, RLPD, and DM test methods at TTI do not provide for moisture damage assessment in HMA mixes.

In all the test methods, however, the CAM mix still remains at the bottom of the ranking; see [Table 5-3](#). Lower asphalt-binder PG grade, high asphalt-binder content, and fine aggregate gradation ([Table 5-1](#)) could be some of the contributing factors for this particular result.

Although using a similar PG asphalt-binder grade and 3/8" NMAAS as the CAM mix, the other mixes such as the Type D and F out-performed the CAM partly due to the use of superior aggregates and RAP (in case of Type D). Overall, only the FN Index and the  $\epsilon_p$ (RLPD) provided a similar ranking of the HMA mixes evaluated; see [Table 5-3](#). Thus, based on these data, only the FN and RLPD tests can be used in lieu of each other.

## COMPARISON OF LABORATORY TESTS AND SYNTHESIS

This section provides a comparative summation of the test methods, namely: (1) variability and repeatability, and (2) a comparison in terms of their advantages, applications, and challenges.

### Variability and Repeatability of the Test Methods

In general, the HWTT was found to be the most repeatable test with the least variability in the test results, i.e., COV < 5 percent. Compared to the RLPD test, it is interesting to note that higher repeatability was achieved in the DM test even at temperatures of over 40°C (104°F). For these tests, variability ranged from a COV of 2 percent to as high as 40 percent depending on the test temperature. [Table 5-5](#) and [Figure 5-8](#) show some examples of variability in the test results based on the Type D Atlanta mix for the HWTT and RLPD test methods.

**Table 5-5. Comparisons of HWTT and RLPD Variability in the Test Results.**

Type D Mix (Atlanta)	Rut Depth @ 20,000 HWTT Load Passes @ 50°C ( mm)	RLPD @ 40°C		RLPD @ 50°C	
		$\alpha$	$\mu$	$\alpha$	$\mu$
Sample# 1	4.60	0.6436	0.58	0.5912	0.31
Sample# 2	4.19	0.6218	0.51	0.6872	0.49
Sample# 3	4.29	0.6145	0.50	0.7073	0.65
Avg	4.36	0.6266	0.53	0.6619	0.48
Stdev	0.2138	0.0151	0.04	0.0620	0.17
COV	4.85	2.4%	8.0%	9.4%	35.2%

Statistical results (i.e., avg, Stdev, COV) for the FN test at 50°C were listed in the preceding [Table 5-2](#). As evident in [Table 5-2](#), some of the HMA mixes (Type B, Type F, and PFC) have FN parameters and statistics with COV values that are unacceptably on the higher side (i.e., greater than 30 percent in the case of the FN Index). Although HMA, due to its visco-elastic nature, is generally associated with high variability at high test temperatures such as 50°C

(particularly for unconfined tests like the FN), this high variability in [Table 5-2](#) is primarily due to some outliers that may warrant exclusion from the overall analysis of the test results. Based on the FN Index parameter in [Table 5-2](#), Sample #1 (Type B), Sample #3 (Type D), Sample #3 (Type F), and Sample #1 (PFC) would be considered as outliers. If these outliers are discarded from the analysis, the statistics would be as shown in [Table 5-6](#), which is considered to be reasonably acceptable and comparable to the HWTT.

**Table 5-6. Statistics of the FN Index Results without the Outliers.**

	<b>Type B (IH 35)</b>	<b>Type D (US 59)</b>	<b>CAM (SH 121)</b>	<b>Type F (US 271)</b>	<b>PFC (SH 121)</b>	<b>SMA (IH 35)</b>
Avg (without outliers)	3.33	8.63	14.67	2.81	22.15	< 0.67
Stdev (without outliers)	0.08	0.74	1.54	0.08	1.06	N/A
COV (without outliers)	2.49%	8.61%	10.49%	3.02%	4.79%	N/A
Ranking (without outliers)	3	4	5	2	6	1
Avg (all samples)	4.39	7.68	14.67	3.98	27.20	< 0.67
COV (all samples)	<b>41.70%</b>	22.50%	10.49%	<b>61.30%</b>	<b>30.61%</b>	N/A
Ranking (all samples)	3	4	5	2	6	1

Statistically, [Table 5-6](#) suggests that outliers should be excluded from the final analysis and interpretation of the FN Index results. Furthermore, excluding the outliers, while having a significant impact on the statistical variability (COV), did not seem to significantly affect the HMA mix ranking and/or screening potential of the FN Index parameter. Both [Tables 5-3](#) and [5-6](#) show a similar ranking of the HMA mixes; but significantly different COV values for the Type B, Type D, Type F, and PFC mixes.

In general, variability was observed to increase with an increase in the test temperature and vice versa; see [Figure 5-7](#) for the DM test results for the Type D mix (Atlanta). This is partly attributed to the visco-elastic nature of the asphalt-binder within the HMA, whose behavior tends to be more viscous at elevated temperature and therefore, exhibits very variable response. With the exception of 0.1 Hz, variability seems to be lowest at 21.1°C. This may speculatively be due to the fact that the 21.1°C temperature, being close to the ambient or room temperature, is much easier to attain and maintain compared to all the other test temperatures; and hence, under the

current testing protocol, better temperature uniformity in the test specimen is achieved. For the mixes studied, there appeared to be no definitive trend in the relationship between variability and loading frequency. Nonetheless, all the COV values shown in [Figure 5-7](#) are within the 30 percent threshold for this Type D mix.

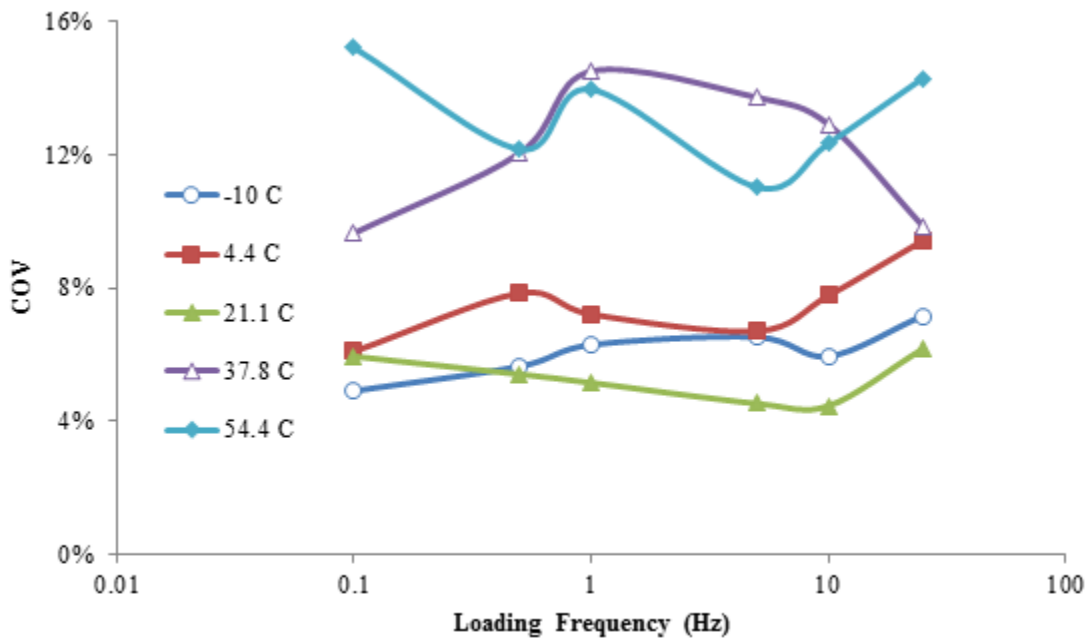


**Figure 5-8. Example of Variability in the DM Test Results (Type D Mix, Atlanta).**

### Comparison of the Test Methods

[Table 5-7](#) provides a subjective comparison of the test methods based solely on the HMA mixes evaluated in this study and on the researchers’ experience with these test methods.

**Table 5-7. Comparison of the FN, DM, RLPD, and HWTT Test Methods.**

<b>Test</b>	<b>Advantages and Applications</b>	<b>Limitations and Challenges</b>
FN	<ul style="list-style-type: none"> <li>- Reasonable test time (<math>\leq 3</math> hrs).</li> <li>- Multiple output data, including FN, <math>\varepsilon_p(F)</math>, and <math>t(F)</math>, and FN Index.</li> <li>- Reliable FN Index to evaluate rutting-resistance response of mixes.</li> <li>- Can differentiate and screen mixes based on the FN Index parameter.</li> <li>- Applicable for routine HMA mix-designs to supplement the HWTT</li> </ul>	<ul style="list-style-type: none"> <li>- Sample fabrication process is both laborious and long.</li> <li>- Cannot readily test field cores.</li> <li>- High variability at high test temperatures.</li> <li>- Problematic maintaining LVDT studs at high temperatures.</li> <li>- Requires experienced operator.</li> <li>- Requires UTM equipment.</li> </ul>
DM	<ul style="list-style-type: none"> <li>- Characterization of dynamic complex modulus, <math> E^* </math>, and visco-elastic properties (<math>E'</math>, <math>E''</math>, <math>\delta</math>).</li> <li>- Rutting performance prediction, especially based on <math> E^* </math> values at 37.8°C and 54.4°C.</li> <li>- Generation of HMA material properties for pavement structural design, Mechanistic-Empirical (M-E) models, and performance prediction.</li> </ul>	<ul style="list-style-type: none"> <li>- Specimen fabrication process is laborious and long.</li> <li>- Cannot readily test field cores.</li> <li>- Lengthy test time (minimum 3 days).</li> <li>- High variability at high test temperatures.</li> <li>- Problematic getting the temperature to below 0°C (i.e., -10°C).</li> <li>- Problematic maintaining LVDT studs at high temperatures.</li> <li>- Requires experienced operator.</li> <li>- Requires UTM or MTS equipment.</li> <li>- Not ideal for daily routine mix-design and screening.</li> <li>- Needs to be conducted at multiple temperatures.</li> </ul>
RLPD	<ul style="list-style-type: none"> <li>- Reasonable test time (<math>\leq 12</math> hrs).</li> <li>- HMA permanent deformation and visco-elastic properties.</li> <li>- HMA rutting performance prediction based <math>\varepsilon_p</math> at 122°F (50°C).</li> <li>- Can generate input data for M-E modeling</li> </ul>	<ul style="list-style-type: none"> <li>- Sample fabrication process is both laborious and long.</li> <li>- Cannot readily test field cores.</li> <li>- High variability at high test temperatures.</li> <li>- Problematic maintaining LVDT studs at high temperatures.</li> <li>- Requires experienced operator.</li> <li>- Requires UTM or MTS equipment.</li> <li>- Needs to be conducted at multiple temperatures.</li> </ul>
HWTT	<ul style="list-style-type: none"> <li>- Simplicity and practicality.</li> <li>- Can readily test both laboratory made samples and field cores.</li> <li>- Reasonable test time (<math>\leq 8</math> hours).</li> <li>- Repeatability and low variability in results (<math>COV \leq 10\%</math>)</li> <li>- Rutting and moisture damage (stripping) assessment.</li> <li>- Applicable for daily routine mix-designs.</li> <li>- Applicable for HMA mix screening and acceptance.</li> </ul>	<ul style="list-style-type: none"> <li>- Cannot readily generate HMA material properties such as modulus for structural design and mechanistic-empirical analyses.</li> <li>- High sample confinement in molds during testing that may at times negatively impact the test results and rutting performance of the HMA mix.</li> <li>- Inability to sufficiently capture the shear resistance characteristics of the HMA mix.</li> <li>- Test is run at a single temperature (50°C), so there is need to explore multiple temperatures that are reflective of field temperatures.</li> </ul>

Overall, while the HWTT is the simplest, most practical, and readily applicable for routine daily mix-design and screening, its major challenges include the adaptability to generate multiple HMA material properties (e.g., modulus) and high specimen confinement that tends to over-score the PD resistance performance of the mixes. As indicated in [Table 5-7](#), characterization of the HMA shear resistance properties such as shear strength/modulus is also one of the key challenges associated with the current HWTT test. However, all these aspects are

currently under investigation in this ongoing study. The results/findings will be documented in future report publications.

As noted in [Table 5-7](#), both the DM and RLPD exhibit potential to generate comprehensive HMA material properties for structural design, pavement modeling, and M-E analyses. However, the lengthy test implies that the tests methods cannot be readily applied for routine HMA mix-design screening without modifying the loading parameters and test conditions such as reducing the number of test temperatures and loading frequencies.

The FN shorter test time, as compared to that of the HWTT, means that the test is both cost-effective and applicable for daily routine use, particularly with the FN Index parameter that exhibited potential to sufficiently discriminate and screen mixes. Inability to readily test thin field cores and the need for field validation are some of the challenges currently being investigated in this ongoing study. Findings and results will be documented in future report publications.

### **Key Findings and Recommendations**

Based on the preceding results along with a synthesis of [Table 5-7](#), the following are the key findings and recommendations derived from the comparative evaluation of the FN, DM, and RLPD tests relative to the HWTT test:

- The FN (cycles) is a parameter traditionally used to evaluate and quantify the HMA rutting-resistance potential based on the FN test results. However, the FN Index—a parametric function of both FN (cycle) and the corresponding  $\epsilon_p(F)$ —exhibited superior potential as parameter to use for differentiating and screening in the laboratory the resistance to PD of different HMA mixes during the HMA mix-design stage. Compared to the FN (cycles), the FN Index also exhibited stronger correlations with the  $\epsilon_p$  and  $|E^*|$  values obtained, respectively, from the RLPD and DM tests. Thus, FN test with the use the FN Index offers promise for routine HMA mix-design applications in the laboratory as a supplementary PD test to the HWTT. The tentatively proposed FN Index pass-fail screening criterion for HMA mixes is 10, i.e., FN Index  $\leq 10$  for satisfactory mixes. However, more HMA mix testing in the

laboratory and correlation with field performance data is imperative to further validate these findings.

- The FN Index and the  $\epsilon_p$  (RLPD) provided a similar ranking of the HMA mixes evaluated. Thus, based on these data, the FN and RLPD tests can be used in lieu of each other to supplement the HWTT test.
- The best correlations between the FN Index and  $\epsilon_p$  (RLPD) with the  $|E^*|$  values was obtained when relating the  $|E^*|$  values measured at high temperatures (i.e., 37.8°C and 54.4°C). Based on these observations, the  $|E^*|$  values at 54.4°C and 5 Hz would thus appear to be reasonable to use for predicting and quantifying the rutting susceptibility of HMA mixes in the laboratory tests.
- Since a good correlation was observed between the FN index and  $\epsilon_p$  with over 90 percent of  $R^2$ , the FN test can be suggested as a test method, in lieu of the RLPD test, to screen and/or predict the rutting performance of HMA mixes in the laboratory to supplement the HWTT test. In addition, the FN test provides a shorter and cost-effective test procedure, since it is conducted at a single test temperature while the RLPD is conducted at multiple temperatures.
- The laboratory results suggest that the ranking order of laboratory test methods to evaluate HMA mix designs and predict rutting performance is as follows: 1) FN test, 2) RLPD test, and 3) DM test. The DM test is fairly a lengthy test and not very ideal for routine HMA mix-designs.
- The FN, DM, and RLPD test results of PFC mixes provided a piece of evidence that under unconfined test conditions, it is inappropriate to measure the true resistance to permanent deformation response of HMA mixes having high total air void content (i.e., 20 percent) and open-graded structure. These high air void content mixes should be tested in a confined test loading configuration.

In terms of test application and as noted in [Table 5-7](#), one has to be very cautious as to which PD/rutting test to use, depending on the specific needs; each test has its own merits and demerits. In general, the following are some of the key challenges associated with selecting the appropriate laboratory rutting test: sample fabrication, simplicity, and practicality of the test,

cost-effectiveness, reasonable test time, applicability for routine HMA mix-design and screening, ability to generate multiple data, and correlation with field performance.

Overall, the FN test offers promising potential as a routine PD test for HMA mix-design and screening to supplement the HWTT. Consideration should be given to adapting this test method as an integral test protocol in routine HMA mix-design activities. The RLPD and DM tests, on the other hand, are better suited for comprehensive HMA material property characterization and generation of multiple input data for M-E modeling. However, streamlining these tests to the following test conditions may render them applicable for routine use:

- RLPD at 50°C (122°F).
- DM at 54.4°C (130°F) or 50°C (122°F) at 5 and 10 Hz loading frequencies.

## **SUMMARY AND CURRENTLY ONGOING WORKS**

In this chapter, the FN, RLPD, and DM tests were comparatively evaluated for their potential to serve as surrogate and/or supplementary PD tests to the traditional HWTT tests. Based on the mixes evaluated, the results and corresponding findings indicated that the FN test has potential to supplement the HWTT as a PD test for routine HMA mix-design and screening. Consideration to adapt the FN as a standard test method, along with FN Index  $\leq 10$  as the tentative HMA pass-fail screening criterion, is recommended. However, additional laboratory testing with more mixes and correlation with field data are imperative for further validation of these findings and recommendations.

For comprehensive HMA material property characterization and generation of multiple data inputs for M-E modeling and PVMNT structural design, the following test methods are recommended:

- DM at three test temperatures, namely 70, 100, and 130°F at the low loading frequency range, i.e., 0.05, 0.1, 1.0, 5.0, and 10 Hz.
- RLPD at two test temperatures, namely 104 and 122°F (40 and 50°C, respectively).

If it is desired to use these test methods just for the purpose of HMA mix differentiation and screening, the test loading parameters should be streamlined as follows: (a) RLPD at 50°C (122°F), and (b) DM at 54.4°C (130°F) or 50°C (122°F) at 5 and 10 Hz loading frequencies.

However, there is still the need to develop and validate the HMA pass-fail screening criteria for both of these test methods through additional laboratory testing with more mixes and correlations with field data.

In view of the findings and recommendations drawn from this chapter, some of the currently ongoing works that will be documented in future Tech Memos and report publications include the following:

- 1) Correlation and validation of the results and findings with field data. This aspect will be executed in collaboration with Study 0-6658.
- 2) Development of mathematical correlations and generation/computation of HMA shear properties (i.e., shear strength, shear deformation, shear modulus, etc.) from the existing FN, RLPD, and DM test data.
- 3) Evaluation and recommendations for possible modifications of the FN, RLPD, and DM test methods to directly or indirectly measure the HMA shear properties such as shear strength, shear deformation, shear modulus, etc.
- 4) Formulation and drafting of preliminary test procedures and specifications for the FN, RLPD, and DM test methods for Texas mixes.
- 5) Comprehensive review, evaluation, and possible modification of the HWTT test method and the Tex-242-F specification. Detailed work plans and preliminary HWTT test results are listed in [Appendix F](#).



## CHAPTER 6 SUMMARY, RECOMMENDATIONS, AND FUTURE WORK

This chapter provides a summation of this Year 1 interim report and includes the key findings, recommendations, ongoing works, and future work plans.

### KEY FINDINGS AND RECOMMENDATIONS

The key findings, conclusions, and recommendations derived from the work presented in [Chapter 2](#) through [Chapter 5](#) of this interim report include the following:

- Computation modeling based on 2-D FE elastic analysis has shown that intersections are more susceptible to surface shear failure and permanent deformation compared to other sections of the road, particularly under high traffic loading and low summer HMA moduli values. The results also suggested that the top 0.5 inches should be considered as the potential critical shear and PD failure zone. Therefore, pavement designs should be cautious to ensure that HMA materials used in these special locations have sufficient resistance to shear related failures.
- FE modeling based on the ABAQUS 3-D visco-elastic analyses indicated that the PVMNT shear stress-strain responses are a function of modulus, temperature, and tire inclination angle. The results also indicated that 20° is the critical angle of tire inclination. Therefore, material design and PVMNT modeling at intersections should consider taking this tire inclination angle into account.
- The AMPT and UTM systems can be confidently used concurrently or in lieu of the other to generate similar quality and reliable results of a comparable statistical degree of accuracy with acceptable variability. The choice is basically dependent on the user as each system has its own merit and demerit. However, the use of trained operators/technicians and well-calibrated equipment is one critical factor that must not be ignored.
- The FN and RLPD tests exhibited strong correlations and can be used in lieu of the other to differentiate and screen HMA mixes in the lab. For routine HMA mix-design applications and mix screening as a supplement to the HWTT, the FN test which has a shorter test time is recommended with FN Index  $\leq 10$  as the tentative HMA pass-fail screening criterion.

- Unless the test loading parameters are streamlined as discussed in [Chapter 5](#), the RLPD and DM test methods were found to be better suited for comprehensive HMA material property characterization and generation of multiple data inputs for M-E modeling and PVMNT structural design; and not as routine HMA mix-design tests.

## **ONGOING AND FUTURE WORK PLANS**

In line with the study objectives and the findings of the work presented in the preceding chapters, some of the currently ongoing and planned future works include the following:

- 3-D FE visco-elastic modeling with Abaqus.
- Comprehensive evaluation and modification of the HWTT test method along with some revisions/modifications to the Tex-242-F test specification. [Appendix F](#) has details of the work plans for evaluating the HWTT test method and the Tex-242-F specification along with some preliminary laboratory test results.
- Evaluation and possible modifications of the test methods and the associated output data (FN, RLPD, DM, and HWTT) to generate HMA shear properties (i.e., shear strength, shear deformation, shear modulus, etc.).
- Sensitivity analysis and statistical comparison of the laboratory test methods (RLPD, FN, DM, and HWTT).
- Development and experimentation with the Simple Punching Shear Test (SPST). The detailed work plans along with some preliminary SPST test results are listed in [Appendix G](#).
- Development of the shear test procedures and specifications for the SPST along with some proposed modifications to the FN, DM, and RLPD test procedures.
- Field correlations (i.e., lab test data, field performance data, and M-E modeling).
- Development and drafting of preliminary test specifications for Texas mixes (i.e., the FN, SPST tests, etc.)

## REFERENCES

- AASHTO (2001). Standard Specifications for Transportation Materials and Methods of Sampling and Testing. Standard TP 62-03, Standard Method of Test for Determining Dynamic Modulus of Hot Mix Asphalt Concrete Mixtures, Washington, D.C., 2001.
- AASHTO (2012). AASHTO TP 79-12: Standard Method of Test for Determining the Dynamic Modulus and Flow Number for Hot Mix Asphalt (HMA) Using the Asphalt Mixture Performance Tester (AMPT). Washington, D.C., 2012.
- AASHTO (2003). AASHTO T320-03 Standard Method of Test for Determining the Permanent Shear Strain and Stiffness of Asphalt Mixtures Using the Superpave Shear Tester; Procedure C Repeated Shear Test at Constant Height. Washington, D.C., 2003.
- Archilla, A.R., L. G. Diaz, and S. H. Carpenter (2007). Proposed Method to Determine the Flow Number in Bituminous Mixtures from Repeated Axial Load Tests. *ASCE–Journal of Transportation Engineering*, Vol. 133, No. 11, November 1, 2007; pp. 610–617.
- Apeageyi, A.K. (2011). Rutting as a Function of Dynamic Modulus and Gradation. *Journal of Materials in Civil Engineering* 2011; 23(9): pp. 1302–1310.
- Bhasin, A., J. W. Button, and A. Chowdhury (2003). *Evaluation of Simple Performance Tests of HMA Mixtures from the South Central USA*, Research Report FHWA/TX-03/9-558-1, Texas Transportation Institute, College Station, TX.
- Chen, X., H. Huang, and Z. Xu. (2006). Uniaxial Penetration Testing for Shear Resistance of Hot-Mix Asphalt Mixtures, *Transportation Research Record* 1970, Washington, D.C.
- Chowdhury, A. and J. Button. (2002):  
<http://d2dtl5nmlpfr0r.cloudfront.net/tti.tamu.edu/documents/1819-1.pdf>.
- Georgia Department of Transportation (2012).  
<http://www.dot.ga.gov/doingbusiness/TheSource/gdt/gdt115.pdf>.
- Goh, S.W., Z. You, R.C. Williams, and X. Li. (2011). Preliminary Dynamic Modulus Criteria of HMA for Field Rutting of Asphalt Pavements: Michigan’s Experience. *Journal of Transportation Engineering*, ASCE 2011; 137(1): pp. 37–45.

- Hu, S., F. Zhou, and T. Scullion. (2011). Development, Calibration, and Validation of a New M-E Rutting Model for HMA Overlay Design and Analysis. *Journal of Materials in Civil Engineering* 2011; 23(2): pp. 89–99.
- Jimenez, R.A. (1974). Testing for Debonding of Asphalt from Aggregate, In *Transportation Research Record: Journal of the Transportation Research Board, No. 517*, Transportation Research Board of the National Academies, Washington, D.C., 1974.
- Pellinen, T. K., and M. W. Witczak (2002). Stress-Dependent Master Curve Construction for Dynamic (Complex) Modulus. *Journal of the Association of Asphalt Paving Technologists*, Vol. 71, 2002.
- Pavement Technology, Inc. 2012: Pocket Facts and Online Publications, Accessed in 2012.  
<http://www.pavementtechnology.com/products/pavementanalyzer.asp>.
- Skok, E., E. Johnson, and A. Turk. (2002). *Asphalt Pavement Analyzer (APA) Evaluation*, Research Report MN/RC 2003-02, Department of Civil Engineering, University of Minnesota, Minneapolis, MN.
- Sousa et.al. 1994. Online Publication. <http://onlinepubs.trb.org/onlinepubs/shrp/SHRP-A-698.pdf>
- Sulukcu, S. and R. Ulusay. (2001). Evaluation of the Block Punch Index Test with Particular Reference to the Size Effect, Failure Mechanism and Its Effectiveness in Predicting Rock Strength, *International Journal of Rock Mechanics & Mining Science*, Vol. 38, pp. 1091–1111.
- R. Dongré, J. D'Angelo, and A. Copeland (2009). Refinement of Flow Number as Determined by Asphalt Mixture Performance Tester: Use in Routine Quality Control–Quality Assurance Practice. *Journal of the Transportation Research Board*, Vol. 2127, pp. 127–136.
- Tukey, J.W. The Problem of Multiple Comparisons. Draft Manuscript. Princeton, New Jersey, Princeton University, 1953.
- Texas Department of Transportation (2009). *Test Procedure for Hamburg Wheel-Tracking Test*, TxDOT Designation: Tex-242-F, Texas Department of Transportation, Austin, TX.

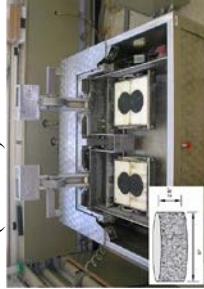
- Van de Ven, M.F.C. and L.F. Walubita. (2000). Test Result of the Micropave ZM12 Mix, Draft ITT Report 4/2000, Institute for Transport Technology, University of Stellenbosch, Stellenbosch, South Africa.
- Walubita, L. F., W. Liu, and T. Scullion (2010). *The Texas Perpetual Pavements: Experience Overview and the Way Forward*. Technical Report: 0-4822-3, Texas Transportation Institute, Texas A&M University, College Station, TX.  
<http://tti.tamu.edu/documents/0-4822-3.pdf>.
- Walubita LF, Gautam Das, Elida Espinoza, Jeongho Oh, Tom Scullion, Soheil Nazarian, Imad Abdallah, and Jose L. Garibay. (2011). *Texas Flexible Pavements and Overlays: Data Analysis Plans and Reporting Format*. Technical Report 0-6658-P3. Texas Transportation Institute, Texas A&M University, College Station, TX.  
<http://tti.tamu.edu/documents/0-6658-P3.pdf>.
- Walubita, L. F., E.M. Espinoza, G. Das, J.H. Oh, T. Scullion, J.L. Garibay, S. Nazarian, I. Abdallah, and S. Lee. (2012). *Texas Flexible Pavements and Overlays: Year 1 Report—Test Sections, Data Collection, Analyses, and Data Storage System*. Technical Report: 0-6658-1, Texas Transportation Institute, Texas A&M University, College Station, TX.
- Wen, H., S. Bhusal, and X. Li. (2013). Double Punch Test: A Simple Performance Test to Evaluate the Fatigue and Rutting Potential of Asphalt Concrete, *Journal of Material in Civil Engineering*, Vol. 25, Issue 5, ASCE.
- Witczak, M.W., K. Kaloush, T. Pellinen, M. El-Basyouny, and H.V. Quintus. (2002). *Simple Performance Test for Superpave Mix Design*. NCHRP Report 465. National Cooperative Highway Research Program; 2002.
- Zhou, F. and T. Scullion. (2004). *Input Parameters of Enhanced VESYS5*, Implementation Report 9-1502-01-4, Texas Transportation Institute, College Station, TX.
- Zhou, F., and T. Scullion (2001). *Laboratory Results from Heavy Duty Asphalt Mixes*. Technical Memorandum to TxDOT, Texas Transportation Institute, College Station, TX.

Zhou, F., E.G. Fernando, and T. Scullion, T. (2009), *Laboratory and Field Procedures Used to Characterize Materials*, FHWA/TX-09/0-5798-P1, Texas Transportation Institute, College Station, TX.

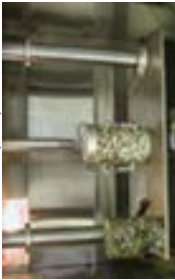
Zhou, F., E.G. Fernando, and T. Scullion (2010). Development, Calibration, and Validation of Performance Prediction Models for the Texas M-E Flexible Pavement Design System. Technical Report: 0-5798-2, Texas Transportation Institute, Texas A&M University, College Station, TX. <http://tti.tamu.edu/documents/0-5798-2.pdf>.

# APPENDIX A. LIST OF LABORATORY TESTS REVIEWED

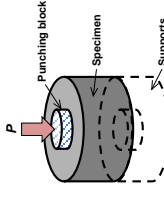
**Table A-1. Review Results of Laboratory HMA Shear, PD, and Rutting Tests**

#	Test Type & Schematic	References	Test Conditions/Parameters	Output Data	Advantages	Limitations & Challenges	Proposed Modification	Does Test Have Potential for Texas Application & Will It be Evaluated in this Study?
1	Hamburg Wheel Tracking Test (HWTT) 	Tex-242-F Walubita et al. (2012)	Load: 158 lb Temp.: 122°F (in a water bath) Rate: 52 pass/min Sample: 6" φ by 2.5" thick	-No. of passes to failure -Rut depth	-Simplicity and practicality -Lab and field-cores -Reasonable test time -Good repeatability -Daily routine design -Good correlation with field performance	-HMA material property for structure design and M-E analysis -High sample confinement -Low AV -HMA shear properties	-Multiple temperature -Wheel speed -Confinement conditions -Load & speed -Failure criteria -Multiple AVs -Analysis parameters	YES
2	Repeated Loading Permanent Deformation (RLPD) 	Report 0-5798-P1 (new)	20psi & 10,000 cycles at 104°F 10psi & 10000 cycles at 122°F Sample: 4" φ by 6" high	- Visco-elastic properties (α,μ)	-Reasonable test time HMA PD and visco-elastic properties -Design & ME models -HMA rutting performance prediction	-Specimen fabrication -Field cores -High variability at high temperature -Problems testing field cores	-Temperature -Loading -Specimen geometry -Analysis parameters	YES
3	Flow Number (FN) 	Reports 0-6658-P3, 0-6658-1	30 psi & 10,000 cycles at 50°C Sample: 4" φ by 6" high	-Flow number -Load cycles - Deformation	-Reasonable test time -Good correlation to field performance	-Specimen fabrication -Not reliable to represent field performance in some cases -Problems testing field cores	-Temperature -Loading -Specimen geometry -Analysis parameter	YES

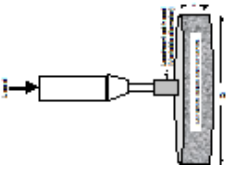
**Table A-1 (Continued). Review Results of Laboratory HMA Shear, PD, and Rutting Tests.**

#	Test Type & Schematic	References	Test Conditions/Parameters	Output Data	Advantages	Limitations & Challenges	Proposed Modification	Does Test Have Potential for Texas Application & Will It be Evaluated in this Study?
4	Flow Time (FT) 	Bhasin et al. (2003)	Load: 30 psi (static) Temp: 30, 60°C Sample: 4" φ by 6" high	-Flow time -Load cycles - Deformation	-Reasonable test time -Good correlation to field rutting for confined condition	-Specimen fabrication -Confined test may require for open-graded mixes -May not simulate field dynamic phenomena -Problems testing field cores	-Temperature -Loading -Specimen geometry -Analysis parameters	YES
5	Dynamic Modulus (DM) 	AASHTO TP 62-03	Load: 0.5–250 psi (sinusoidal) Freq: 0.1, 0.5, 1.0, 5, 10, 25 Hz Temp: -10°C, 4.4°C, 21.1°C, 37.8°C, 54.4°C Sample: 4" φ by 6" high	-Dynamic modulus (E*) -Phase angle (φ)	-HMA modulus & visco-elastic properties -Design & M-E Models -HMA stiffness/rutting performance prediction	-Specimen fabrication -Field cores -High variability at high test temperature -Problematic getting test temperature to -10°C -Problems testing field cores, particularly for thin PVMNT structures. -Lengthy test time	-Temperature -Loading -Frequency -Specimen geometry	YES
6	Asphalt Pavement Analyzer (APA) 	Skok et al. (2002)	Load: 100 psi (wheel pass) Temp: controlled (in dry) Specimen cylinder or beam	-No. of pass to failure -Rut depth	-Temperature controlled -Reliable & repeatable -Simulate field traffic & temp. -Can evaluate moisture damage	-High sample confinement -Sensitive to AV change	-Conduct parallel testing with the HWTT & other tests -Multiple temperature -Wheel speed -Confinement conditions -Load & speed -Failure criteria -Multiple AVs -Analysis parameters	YES

**Table A-1 (Continued). Review Results of Laboratory HMA Shear, PD, and Rutting Tests.**

#	Test Type & Schematic	References	Test Conditions/Parameters	Output Data	Advantages	Limitations & Challenges	Proposed Modification	Does Test Have Potential for Texas Application & Will It be Evaluated in this Study?
7	Indirect Tensile Test (IDT) 	Tex-226-F	Load: compressive until failure (2 in/ min.) Temp: 25°C	Indirect tensile strength	-Simple & rapid test -Easy to fabricate specimens -Can easily test both lab & field core specimens	-May not simulate field dynamic phenomena	-Temperature -Loading rate	NO
8	Double Punching Test 	Jimenez (1974) Wen et al. (2012)	Load: compressive until failure Punch head size: 1.5"φ Temp: controlled	Shear strength	-Simple & rapid test -Easy to fabricate specimen -Good correlation with field performance and flow number -Good repeatability	-May not simulate field dynamic phenomena	-Temperature -Loading (type & rate/frequency) -Load head size -Specimen geometry	YES
9	Simple Punch Test (Proposed) 	Chen et al. (2006) Sulukcu et al. (2001)	Load: static or cyclic load until failure Punch head size: 1.5"φ Temp: controlled	Shear strength	-Simple & rapid test -Easy to fabricate specimen -Good repeatability	-Need to be verified with the UTM/MTS	-Temperature -Loading (type & rate/frequency) -Load head size -Specimen geometry	YES

**Table A-1 (Continued). Review Results of Laboratory HMA Shear, PD, and Rutting Tests.**

#	Test Type & Schematic	References	Test Conditions/Parameters	Output Data	Advantages	Limitations & Challenges	Proposed Modification	Has Test got Potential for Texas Application & Will it be Evaluated in this Study??
10	Indentation Test 	Van de Ven et al. (2000)	Load: 0.5 & 1 MPa until failure Load head size: 0.4" & 0.8" Temp: 50°C Specimen: cylinder type (4" dia. x 1" ht.)	-Total deformation (mm) -Time elapsed at failure (sec.)	-Simple & rapid test -Easy to fabricate specimens	-Needs to be verified with the UTM/MTS	-Conduct parallel testing with other tests (HWTT, RLPD, etc.) -Temperature -Loading (type & rate/frequency) -Load head size -Specimen geometry	YES
11	The AMPT System 					System needs verification with the UTM system	Conduct parallel RLPD, FN, & DM tests with the UTM system	YES
12	The UTM system 	Traditional system setup used for RLPD, DM, FN, & FT testing.			Traditional system setup used for RLPD, DM, FN, & FT testing.	System takes long time to cool to lower temperatures, particularly below 0°C	Will be used as a reference benchmark for comparatively evaluating & validating the AMPT system	YES

## APPENDIX B. THE PLAXIS SOFTWARE (2-D FE LINEAR ELASTIC ANALYSIS) AND RESULTS

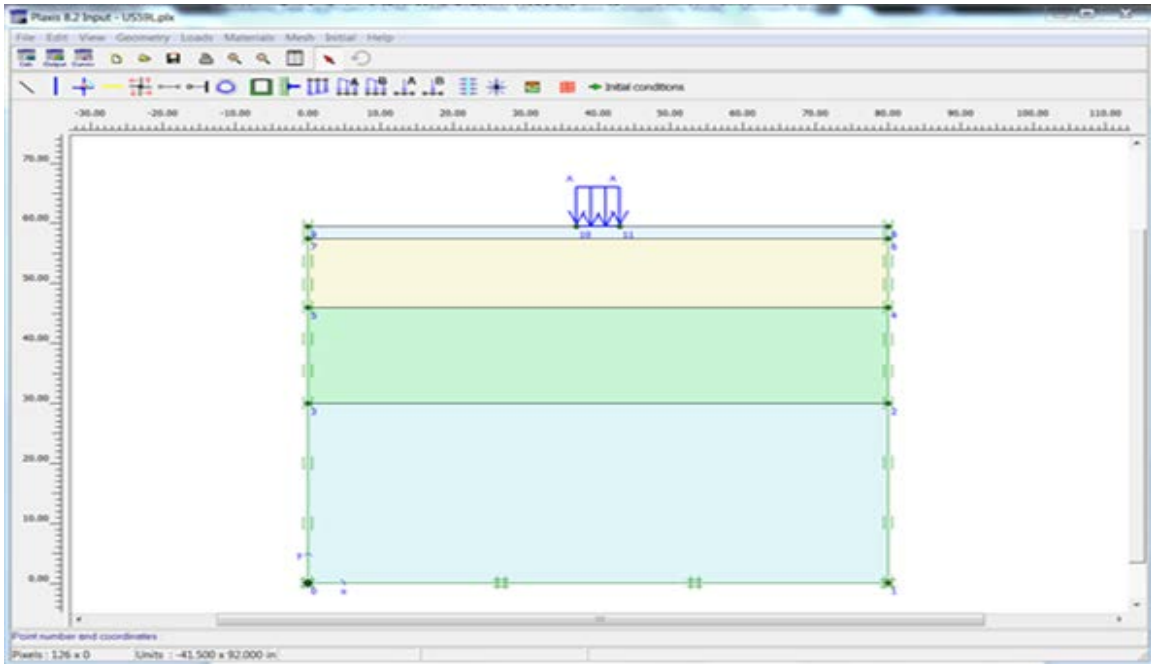


**Figure B-1. PLAXIS Software Main Input Screen Module.**

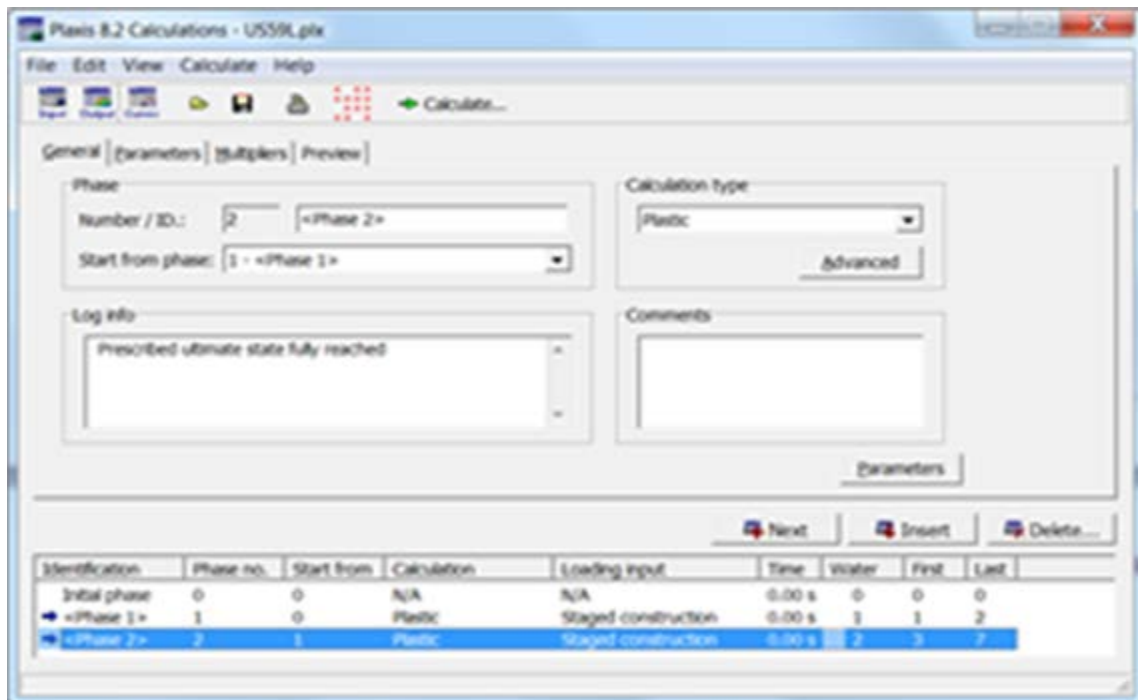


**Figure B-2. PLAXIS Software Calculation Screen Module.**

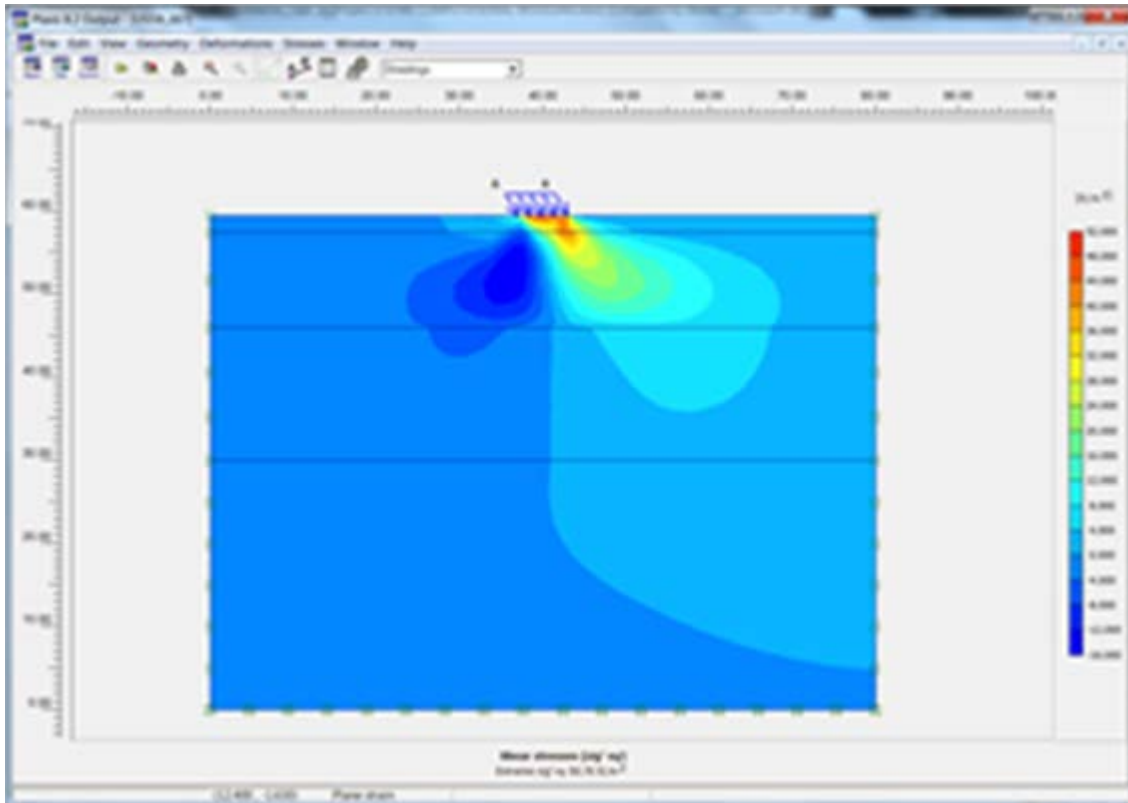


**Figure B-3. PLAXIS Software Output Screen Module.**

Contour Distribution of Shear Effect Zone by Tire Inclination  
 (2-inch Overlay with 256.7 ksi Modulus)

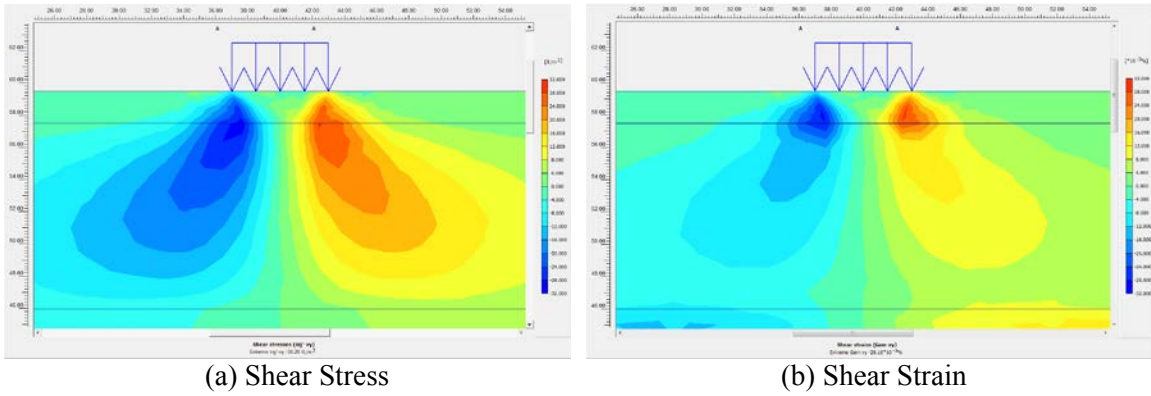


Figure B-4. Distribution of Shear Effect Zone (Vertical Tire Loading = 0° Inclination).

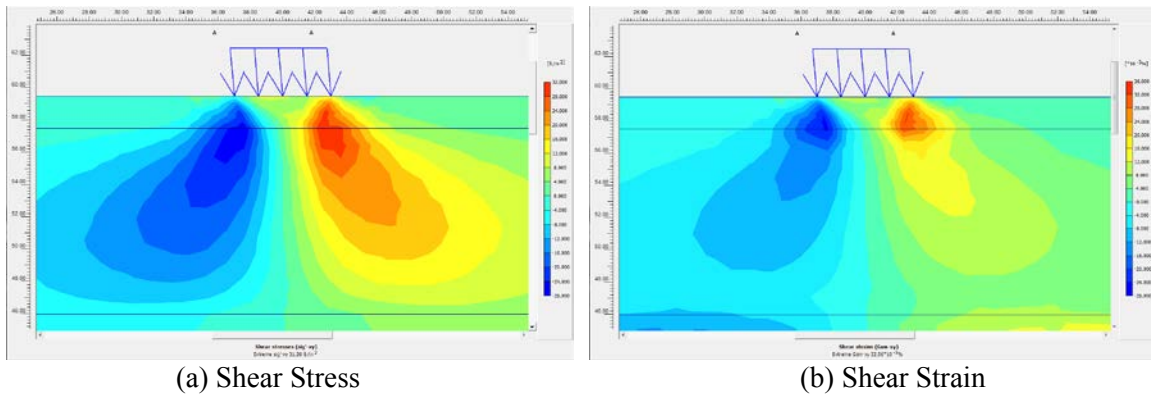


Figure B-5. Distribution of Shear Effect Zone (Vertical Tire Loading = 5° Inclination).

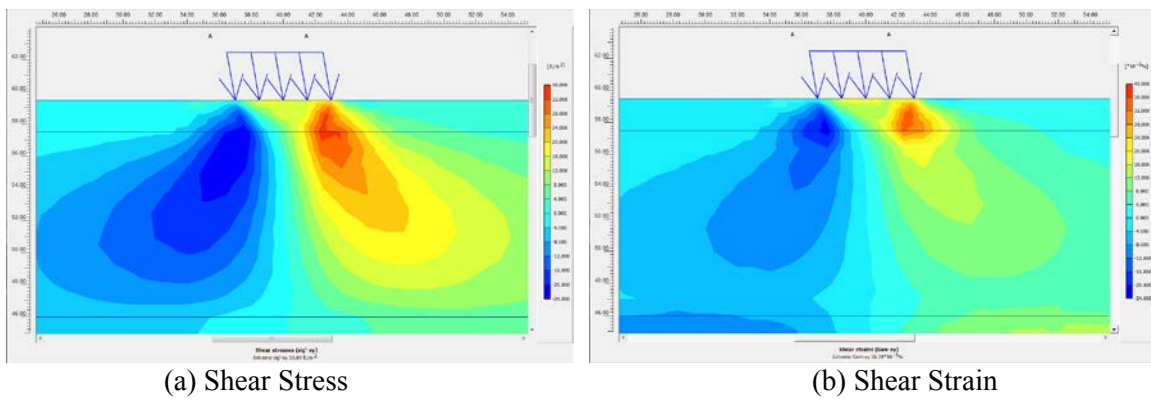
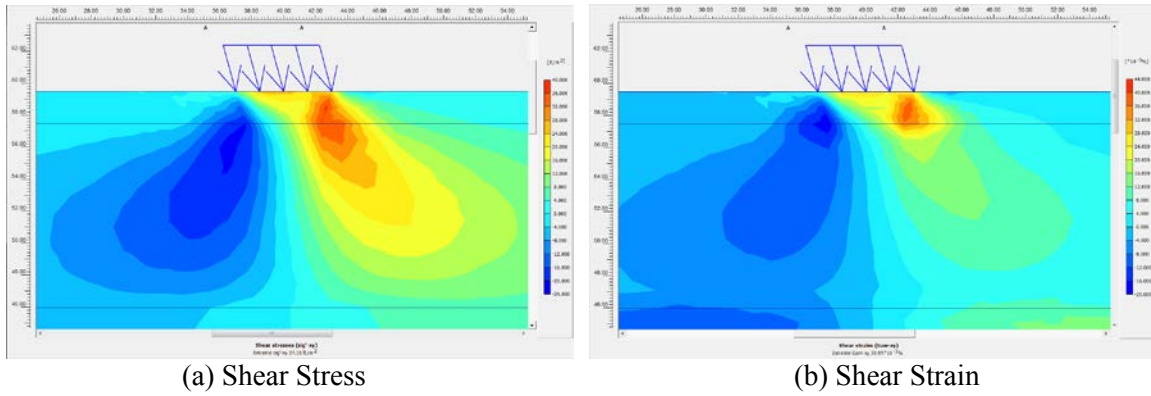
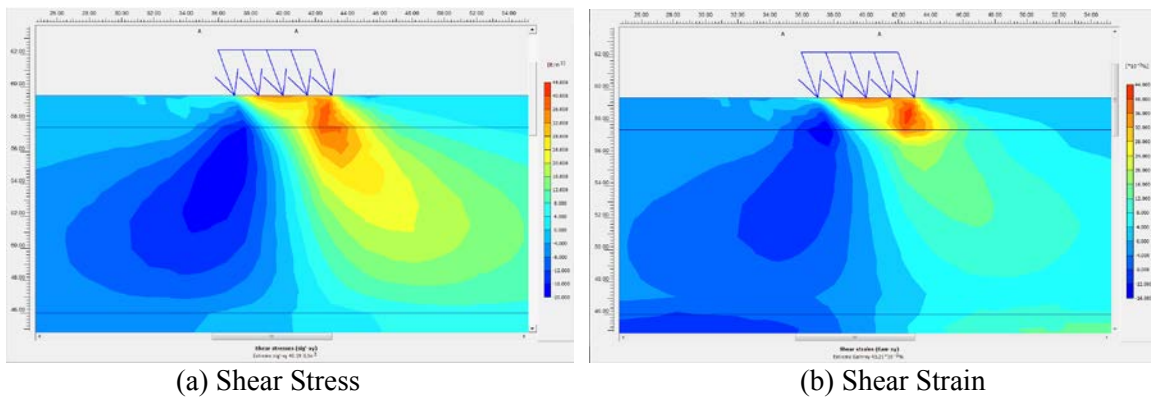


Figure B-6. Distribution of Shear Effect Zone (Vertical Tire Loading = 10° Inclination).



**Figure B-7. Distribution of Shear Effect Zone (Vertical Tire Loading = 15° Inclination).**



**Figure B-8. Distribution of Shear Effect Zone (Vertical Tire Loading = 20° Inclination).**

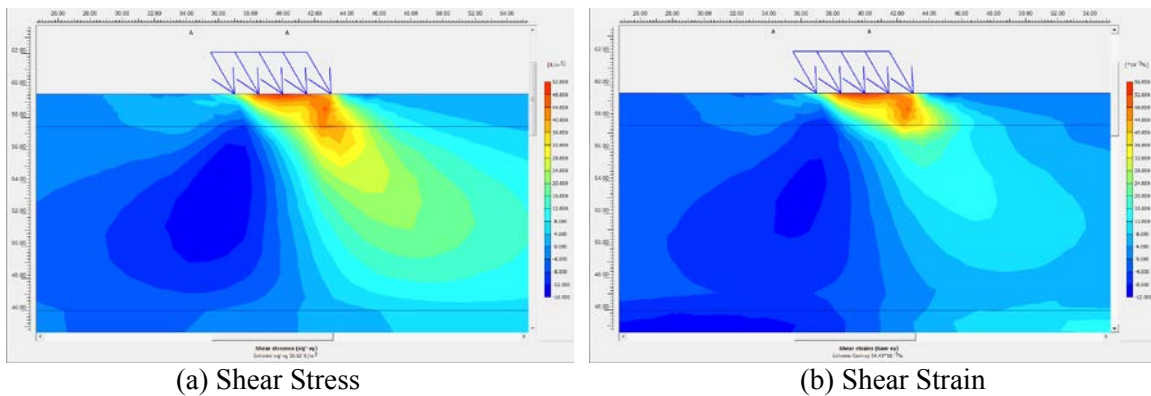


**Figure B-9. Distribution of Shear Effect Zone (Vertical Tire Loading = 30° Inclination).**

Comparison of Location of Maximum Shear Stress and Strain by Tire Loading.

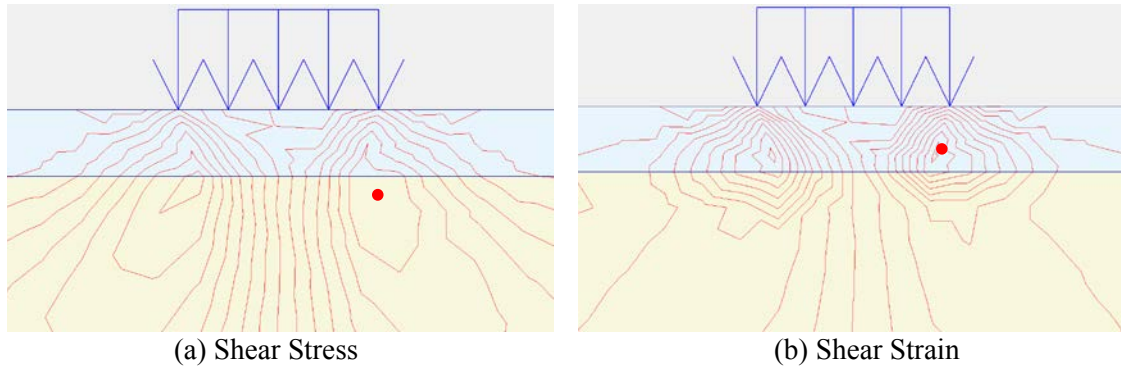


**Figure B-10. Location of Max Shear Stress and Strain (Vertical Tire = 0° Inclination).**

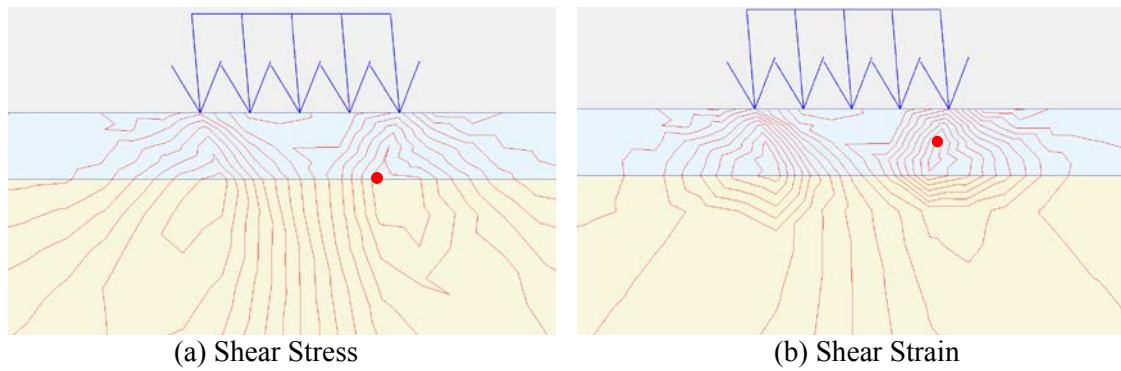


**Figure B-11. Location of Max Shear Stress and Strain (Vertical Tire = 5° Inclination).**

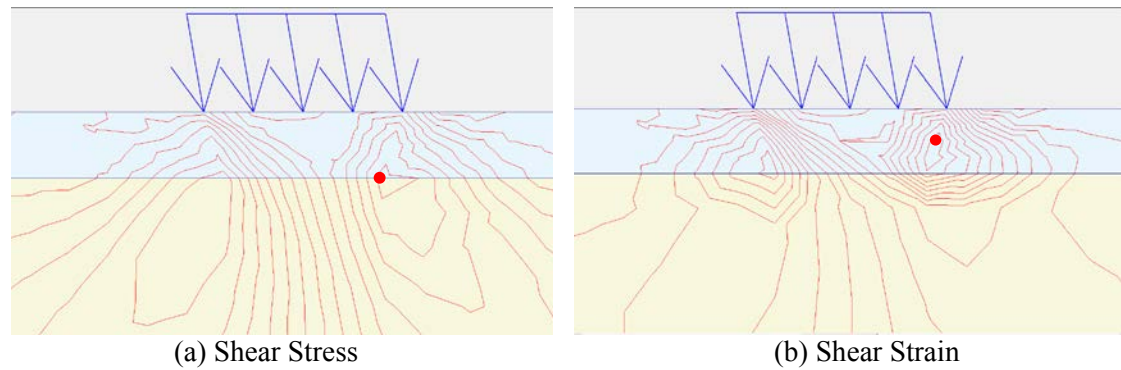


**Figure B-12. Location of Max Shear Stress and Strain (Vertical Tire = 10° Inclination).**

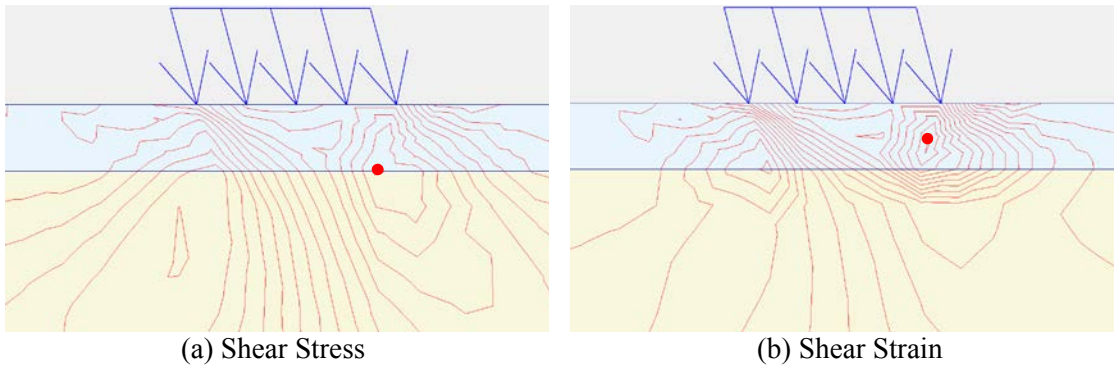


**Figure B-13. Location of Max Shear Stress and Strain (Vertical Tire = 15° Inclination).**

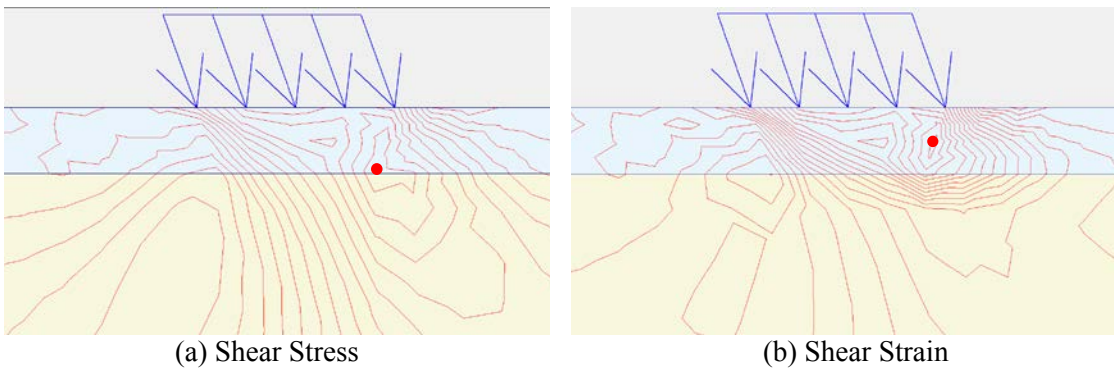


**Figure B-14. Location of Max Shear Stress and Strain (Vertical Tire = 20° Inclination).**

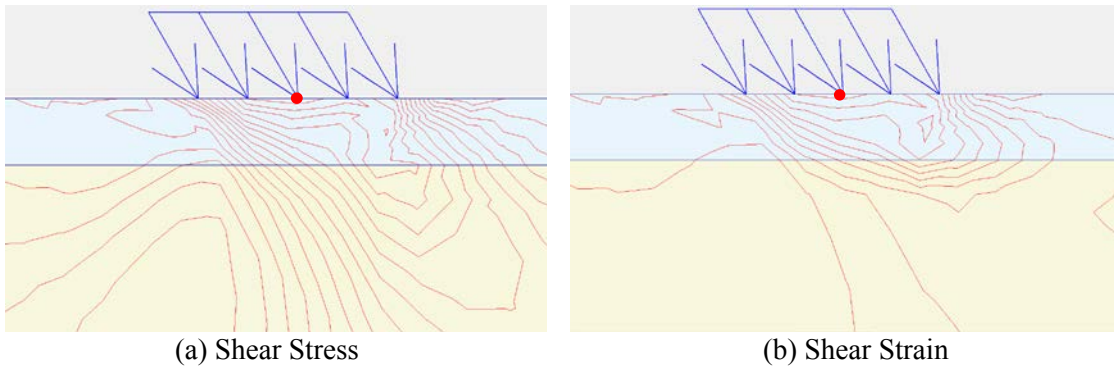


**Figure B-15. Location of Max Shear Stress and Strain (Vertical Tire = 30° Inclination).**

Comparisons of Shear Stress and Strain by HMA Modulus Variation.

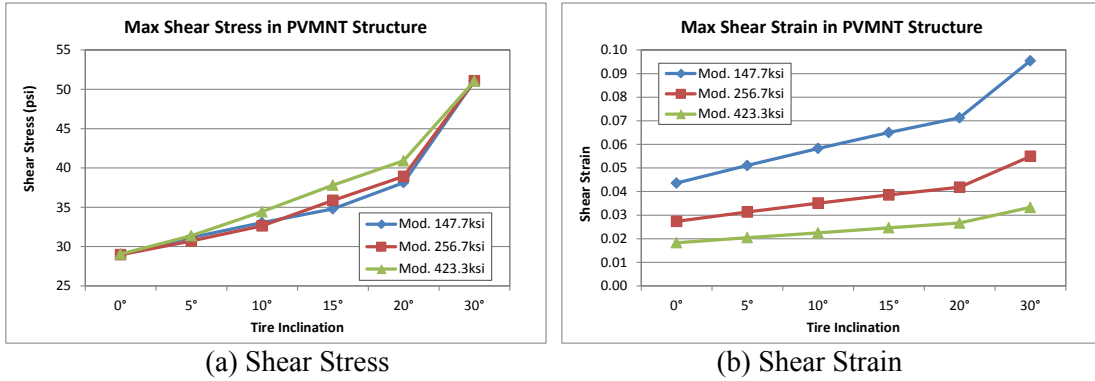


**Figure B-16. Maximum Shear Stress and Strain by Modulus (1.5-Inch HMA Overlay).**

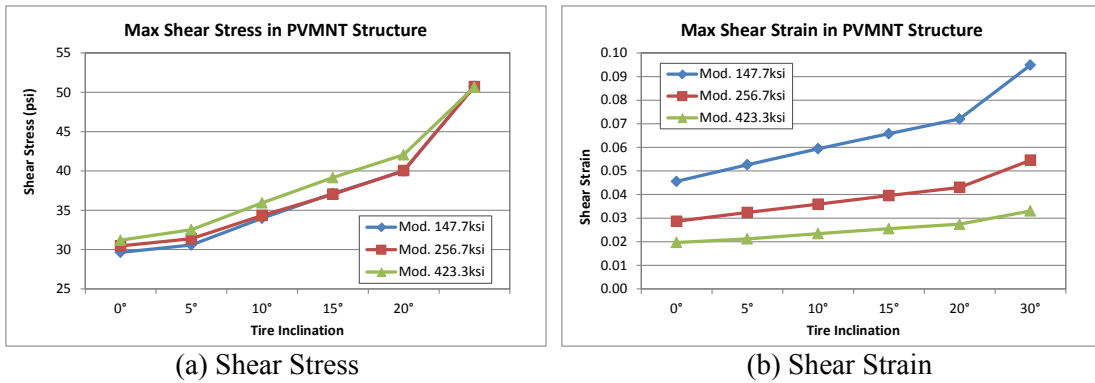


**Figure B-17. Maximum Shear Stress and Strain by Modulus (1.75-Inch HMA Overlay).**

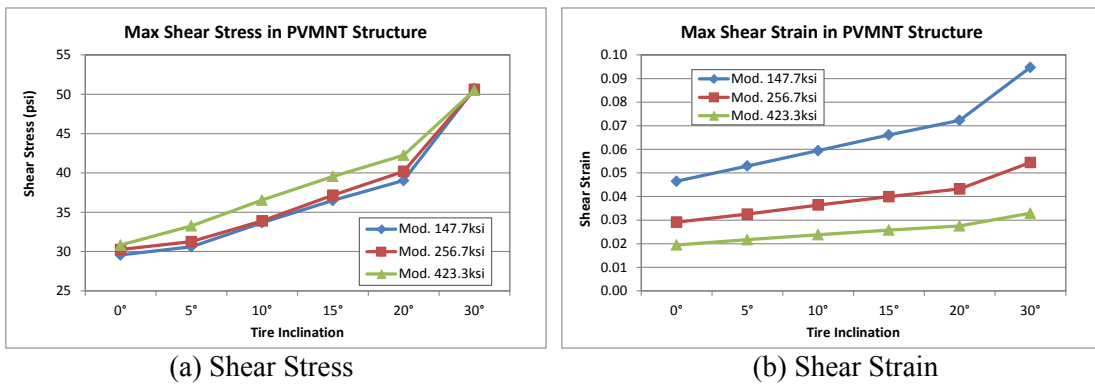
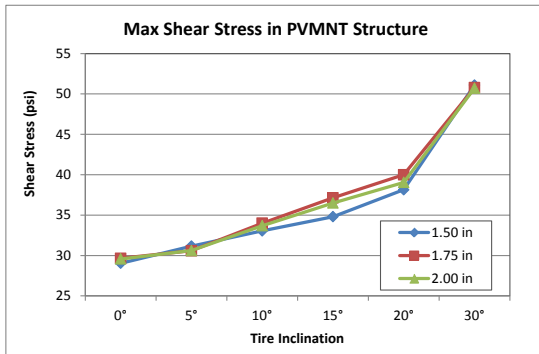
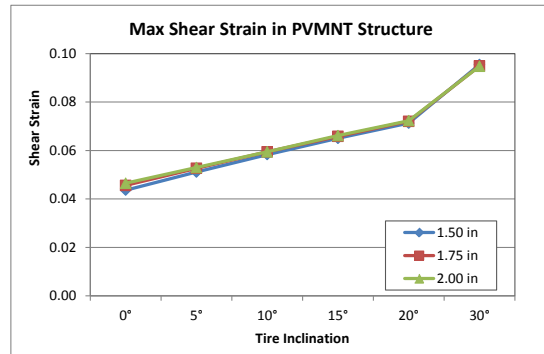


**Figure B-18. Maximum Shear Stress and Strain by Modulus (2.0-Inch HMA Overlay).**

Comparisons of Shear Stress and Strain by HMA (Overlay) Layer Thickness.

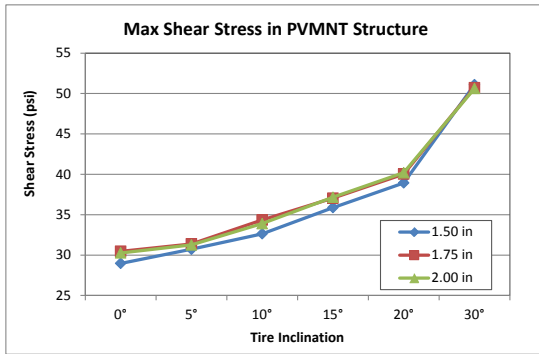


(a) Shear Stress

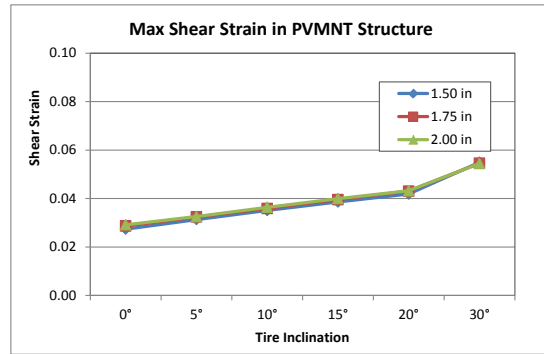


(b) Shear Strain

**Figure B-19. Maximum Shear Stress and Strain by Thickness (147.7 ksi HMA Modulus).**

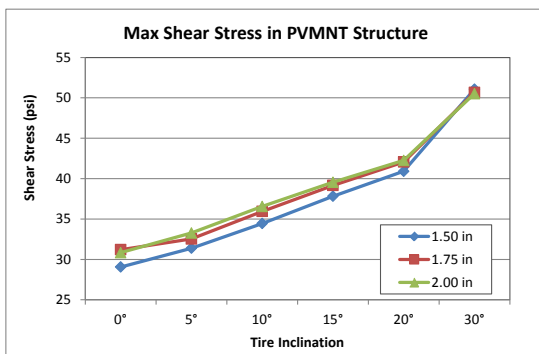


(a) Shear Stress

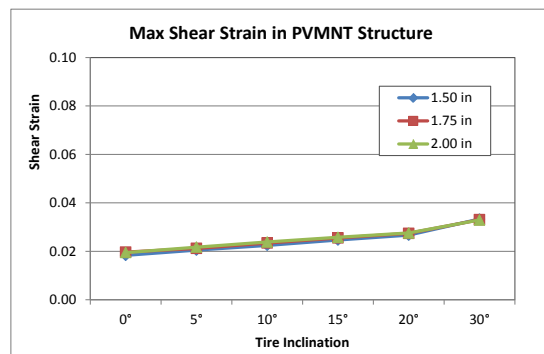


(b) Shear Strain

**Figure B-20. Maximum Shear Stress and Strain by Thickness (256.7 ksi HMA Modulus).**



(a) Shear Stress



(b) Shear Strain

**Figure B-21. Maximum Shear Stress and Strain by Thickness (423.3 ksi HMA Modulus).**

## APPENDIX C. THE ABAQUS SOFTWARE (3-D FE VISCO-ELASTIC ANALYSIS) AND RESULTS

**Figure C-1. ABAQUS Stress Computations.**

**Max Shear Stress (psi) in PVMNT**

Temp. (°F)	Loading Condition			
	0°	10°	20°	30°
112	98.82	-	113.19	111.04
92	158.38	-	-	-
77	202.62	-	219.01	209.58

**Max Transverse Stress (psi) in PVMNT**

Temp. (°F)	Loading Condition			
	0°	10°	20°	30°
112	362.31	-	626.43	599.74
92	752.61	-	-	-
77	1257.50	-	1579.49	1492.46

**Max Longitudinal Stress (psi) in PVMNT**

Temp. (°F)	Loading Condition			
	0°	10°	20°	30°
112	375.07	-	673.42	644.12
92	781.19	-	-	-
77	1294.92	-	1653.46	1560.63

**Max Vertical Stress (psi) in PVMNT**

Temp. (°F)	Loading Condition			
	0°	10°	20°	30°
112	267.16	-	311.69	304.58
92	263.39	-	-	-
77	260.64	-	303.42	296.46

**Max Shear Strain in PVMNT**

Temp. (°F)	Loading Condition			
	0°	10°	20°	30°
112	2.12E-04	-	2.49E-04	2.35E-04
92	1.20E-04	-	-	-
77	5.90E-05	-	5.92E-05	5.49E-05

**Vertical Strain on PVMNT Surface**

Temp. (°F)	Loading Condition			
	0°	10°	20°	30°
112	3.31E-05	-	9.44E-05	8.81E-05
92	3.37E-05	-	-	-
77	1.78E-05	-	2.28E-05	2.13E-05

**Figure C-2. ABAQUS Stress-Strain Computations.**

Y	0° Vertical s'_xy [in] [lb/in^2]	Y	5° 5 degree s'_xy [in] [lb/in^2]	Y	10° 10 degree s'_xy [in] [lb/in^2]	Y	15° 15 degree s'_xy [in] [lb/in^2]	Y	20° 20 degree s'_xy [in] [lb/in^2]	Y	30° 30 degree s'_xy [in] [lb/in^2]
0	0	0	0	0	0	0	0	0	0	0	0
0	7.257858	0	8.067095	0	15.82692	0	22.88311	0	29.7627	0	42.81476
1.752752	23.76074	1.962854	25.65371	1.995882	30.04525	1.995882	32.64942	1.995882	35.00526	1.991803	38.79487
1.752752	26.71501	1.962854	21.09458	1.995882	25.18472	1.995882	28.06084	1.995882	30.72322	1.991803	35.25232
2	29.58713	2	21.82762	2	25.26877	2	28.14178	2	30.80043	2	35.38608
2	29.89722	2	28.93296	2	22.99413	2	35.42899	2	37.59452	2	30.91954
3.855695	26.74092	3.978874	24.20494	4.016849	26.03121	4.016849	26.703	4.016849	27.17207	4.012159	27.3801
5.71139	21.87435	5.957748	17.0203	6.033698	17.30743	6.033698	17.01458	6.033698	16.59242	6.024318	15.32599
5.71139	21.66287	5.957748	17.14738	6.033698	17.44515	6.033698	17.1193	6.033698	16.66309	6.024318	15.32145
6.374769	19.899	6.325412	16.3714	6.270666	16.8677	6.270666	16.48826	6.270666	15.98318	6.277427	14.5097
6.374769	19.2608	6.325412	15.63758	6.270666	16.03298	6.270666	15.69445	6.270666	15.23587	6.277427	13.88981
8.549858	14.69458	8.096024	12.28242	8.075446	12.31341	8.075446	11.75591	8.075446	11.10737	8.077987	9.49113
10.72495	10.31402	9.866636	9.1295	9.880226	8.868007	9.880226	8.241599	9.880226	7.549324	9.878548	5.949691
12.90004	5.325973	11.63725	6.034159	11.68501	5.659556	11.68501	5.128857	11.68501	4.556467	11.67911	3.281601
12.90004	5.052388	13.40786	2.929126	13.48979	2.732263	13.48979	2.472531	13.48979	2.194304	13.47967	1.558023
13.5	2.812536	13.40786	2.698234	13.48979	2.534697	13.48979	2.338247	13.48979	2.126029	13.47967	1.621333
13.5	2.703398	13.5	2.568488	13.5	2.522551	13.5	2.329252	13.5	2.120216	13.5	1.622699
16.42817	2.036406	13.5	1.91834	13.5	1.837819	13.5	1.672153	13.5	1.500903	13.5	1.099352
16.42817	2.052232	16.07692	1.484223	16.12637	1.42267	16.12637	1.29589	16.12637	1.161385	16.12027	0.850972
16.47683	2.040995	16.07692	1.471811	16.12637	1.409588	16.12637	1.283255	16.12637	1.148983	16.12027	0.839652
16.47683	2.050378	17.08958	1.381513	17.01067	1.337454	17.01067	1.221363	17.01067	1.097025	17.02041	0.81052
16.62815	2.019489	17.08958	1.372586	17.01067	1.327466	17.01067	1.21143	17.01067	1.087016	17.02041	0.800896
16.62815	1.994545	18.82893	1.16997	18.79379	1.132256	18.79379	1.034777	18.79379	0.927858	18.79813	0.684276
18.63484	1.686059	20.56828	1.006023	20.57691	0.972548	20.57691	0.890552	20.57691	0.798868	20.57584	0.591292
20.64154	1.420703	20.56828	1.013046	20.57691	0.979771	20.57691	0.897679	20.57691	0.806059	20.57584	0.598436
20.64154	1.428112	22.30109	0.908134	22.23802	0.883657	22.23802	0.809904	22.23802	0.727264	22.24581	0.540446
22.88879	1.238327	24.0339	0.81648	23.89914	0.798135	23.89914	0.730676	23.89914	0.655862	23.91579	0.487538
22.88879	1.236759	24.0339	0.815237	23.89914	0.797065	23.89914	0.729822	23.89914	0.655337	23.91579	0.487146
24.57135	1.098892	24.42084	0.790645	24.43856	0.764281	24.43856	0.69924	24.43856	0.627243	24.43637	0.46568
24.57135	1.095422	24.42084	0.792689	24.43856	0.765675	24.43856	0.700499	24.43856	0.628287	24.43637	0.46701
26.73375	0.970466	26.17367	0.711754	26.88207	0.661632	26.88207	0.604259	26.88207	0.541492	26.79457	0.40331
28.89615	0.867243	27.92649	0.647519	29.32558	0.574978	29.32558	0.524178	29.32558	0.469645	29.15278	0.350779
28.89615	0.866574	27.92649	0.647537	29.32558	0.584253	29.32558	0.53369	29.32558	0.479234	29.15278	0.357868
29.5	0.834397	29.42412	0.601195	29.49159	0.58013	29.49159	0.530029	29.49159	0.476137	29.48326	0.353552
29.5	0.8322603	29.42412	0.602107	29.49159	0.580496	29.49159	0.529774	29.49159	0.475254	29.48326	0.351622
31.84443	0.611277	29.5	0.600528	29.5	0.580332	29.5	0.529632	29.5	0.475139	29.5	0.3515
31.84443	0.612771	29.5	0.594716	29.5	0.573426	29.5	0.52328	29.5	0.469362	29.5	0.347201
32.52615	0.542969	32.27492	0.422892	29.81839	0.55753	29.81839	0.510191	29.81839	0.45916	30.13382	0.336747
32.52615	0.544085	32.27492	0.417553	29.81839	0.552069	29.81839	0.504776	29.81839	0.45385	30.13382	0.328781
34.36197	0.422571	32.2786	0.41742	32.2277	0.402645	32.2277	0.372886	32.2277	0.340191	32.23401	0.265205
36.19778	0.332208	32.2786	0.40652	32.2277	0.408766	32.2277	0.378424	32.2277	0.345132	32.23401	0.268944
36.19778	0.331774	32.39118	0.401776	32.30527	0.402647	32.30527	0.372752	32.30527	0.339941	32.30163	0.265378
37.22174	0.284113	32.39118	0.411491	32.30527	0.407722	32.30527	0.378524	32.30527	0.346317	32.30163	0.273052
37.22174	0.284331	34.54511	0.301123	34.47266	0.296431	34.47266	0.272991	34.47266	0.247301	34.47448	0.190703
39.21443	0.228029	36.69904	0.213048	36.64005	0.20504	36.64005	0.181321	36.64005	0.155995	36.64733	0.103315
41.20713	0.187635	36.69904	0.217464	36.64005	0.208514	36.64005	0.184598	36.64005	0.159041	36.64733	0.105823
41.20713	0.186714	36.847	0.211216	36.8911	0.197124	36.8911	0.172712	36.8911	0.146765	36.88565	0.093892
42.60787	0.159925	36.847	0.212427	36.8911	0.198368	36.8911	0.174217	36.8911	0.148484	36.88565	0.096046
42.60787	0.16051	39.2386	0.146115	39.23575	0.123922	39.23575	0.092056	39.23575	0.059379	39.23611	-0.00376
44.25618	0.13992	41.6302	0.096621	41.58041	0.063134	41.58041	0.02047	41.58041	-0.02213	41.58656	-0.10212
45.9045	0.123196	41.6302	0.096384	41.58041	0.062699	41.58041	0.020001	41.58041	-0.02262	41.58656	-0.10262
45.9045	0.122919	42.35157	0.080994	42.38173	0.040924	42.38173	-0.00603	42.38173	-0.05255	42.37801	-0.13868
46.57509	0.117745	42.35157	0.082015	42.38173	0.041843	42.38173	-0.00511	42.38173	-0.05164	42.37801	-0.13781
46.57509	0.117288	44.04933	0.05426	44.26765	-0.00059	44.26765	-0.05854	44.26765	-0.11511	44.24068	-0.21779
47.00182	0.114639	44.04933	0.054039	44.26765	-0.00087	44.26765	-0.05882	44.26765	-0.11539	44.24068	-0.21803
47.00182	0.114646	46.57802	0.019127	46.57768	-0.04834	46.57768	-0.12076	46.57768	-0.19039	46.57772	-0.31743
48.6017	0.104441	46.57802	0.019378	46.57768	-0.04816	46.57768	-0.1206	46.57768	-0.19025	46.57772	-0.31733
50.20157	0.097706	48.18713	2.4E-05	48.04764	-0.07696	48.04764	-0.15941	48.04764	-0.23795	48.06486	-0.38214
50.20157	0.097689	48.18713	-1.7E-05	48.04764	-0.07701	48.04764	-0.15947	48.04764	-0.23802	48.06486	-0.38221
51.98563	0.094989	50.18127	-0.02387	50.18365	-0.11984	50.18365	-0.21748	50.18365	-0.30945	50.18336	-0.47822
53.76969	0.097044	50.18127	-0.02394	50.18365	-0.1199	50.18365	-0.21755	50.18365	-0.30952	50.18336	-0.47825
53.76969	0.09749	53.05718	-0.05505	51.72392	-0.15059	51.72392	-0.25985	51.72392	-0.36216	51.71099	-0.55097
54.14773	0.098495	53.05718	-0.05524	53.26418	-0.18108	53.26418	-0.30219	53.26418	-0.4155	53.23861	-0.62662
54.14773	0.09797	54.0579	-0.06605	53.26418	-0.18116	53.26418	-0.30224	53.26418	-0.41554	53.23861	-0.62668
54.37085	0.098863	54.0579	-0.06555	54.08534	-0.19767	54.08534	-0.32503	54.08534	-0.4445	54.08196	-0.6699

Figure C-3. ABAQUS Shear Stress-Strain Tabulation.





**HMACP MIXTURE DESIGN : SUMMARY SHEET**

File Version: 11/03/11 09:08:32

SAMPLE ID:	SAMPLE DATE: 7/23/12
LOT NUMBER: DESIGN	LETING DATE:
SAMPLE STATUS:	CONTROLLING CSJ:
COUNTY:	SPEC YEAR: 2004
SAMPLED BY: Jerry Groves	SPEC ITEM: 3224
SAMPLE LOCATION: PLANT	SPECIAL PROVISION:
MATERIAL CODE:	MIX TYPE: SS3224_C_Coarse_Surface
MATERIAL NAME: DENSE GRADED C MIX	
PRODUCER: KNIFE RIVER-BRYAN, TX	
AREA ENGINEER:	PROJECT MANAGER:

COURSE/LIFT: Surface	STATION:	DIST. FROM CL:	CONTRACTOR DESIGN # : KRC-189-RAS
----------------------	----------	----------------	-----------------------------------

Target Density, %:	97.0
Number of Gyration:	

Note: This mix design requires an asphalt content of at least **4.0%** to meet the Maximum Ratio of Recycled to Total Binder requirement.

Asphalt Content (%)	Binder Ratio (%)	Specific Gravity Of Specimen (Ga)	Maximum Specific Gravity (Gr)	Effective Gravity (Ge)	Theo. Max. Specific Gravity (Gt)	Density from Gt (Percent)	VMA (Percent)	Mixture Evaluation @ Optimum Asphalt Content		
								Indirect Tensile Strength (psi)	Hamburg Wheel Tracking Test	Overlay Tester Min. Number of Cycles
4.0	35.0	2.345	2.500	2.658	2.460	95.3	13.8			
4.5	31.1	2.350	2.459	2.631	2.443	96.2	14.1			
5.0	26.0	2.365	2.400	2.581	2.425	97.5	14.0			
5.5	25.5	2.357	2.398	2.599	2.408	97.9	14.7			
6.0	23.3	2.358	2.373	2.589	2.391	98.6	15.1			

Effective Specific Gravity:	2.612
Optimum Asphalt Content:	4.8
Binder Ratio @ OAC:	29.2
VMA @ Optimum AC:	14.0
<b>Interpolated Values</b>	
Specific Gravity (Ga):	2.359
Max. Specific Gravity (Gr):	2.423
Theo. Max. Specific Gravity (Gt):	2.432

Estimated Percent of Stripping, %: 0

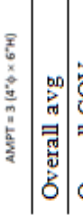

Mixing Temp., F:

**Figure D-2. Type C HMA Volumetrics.**

Table D-1-1. RLPD HMA Sample Dimensions.

The AMPT System			The UTM System				
Picture	Sample ID#	H (Inches)	$\phi$ (Inches)	Picture	Sample ID#	H (Inches)	$\phi$ (Inches)
	1 (40 °C)	6.04	3.97		1 (40 °C)	6.05	3.98
	2 (40 °C)	6.07	3.96		2 (40 °C)	6.07	3.95
AMPT = 3 (4" $\phi$ x 6"H)			3.95	UTM = 3 (4" $\phi$ x 6"H)			3.97
	4 (50 °C)	6.05	3.96		4 (50 °C)	6.04	3.96
	5 (50 °C)	6.06	3.98		5 (50 °C)	6.07	3.97
AMPT = 3 (4" $\phi$ x 6"H)			3.97	UTM = 3 (4" $\phi$ x 6"H)			3.96
Overall avg		6.06	3.97	Overall avg		6.06	3.97
Overall COV		0.23%	0.26%	Overall COV		0.23%	0.26%

Table D-2. RLPD HMA Sample AV Measurements.

The AMPT System		The UTM System	
Picture	Sample ID#	Sample ID#	AV (7 $\pm$ 1%)
	1 (40 °C)	1 (40 °C)	6.59%
	2 (40 °C)	2 (40 °C)	7.25%
AMPT = 3 (4" $\phi$ x 6"H)		3 (40 °C)	6.85%
	4 (50 °C)	4 (50 °C)	7.50%
	5 (50 °C)	5 (50 °C)	7.72%
AMPT = 3 (4" $\phi$ x 6"H)		6 (50 °C)	6.84%
Overall avg		Overall avg	7.13%
Overall COV		Overall COV	5.60%
Overall AV range		Overall AV range	6.59% - 7.72%

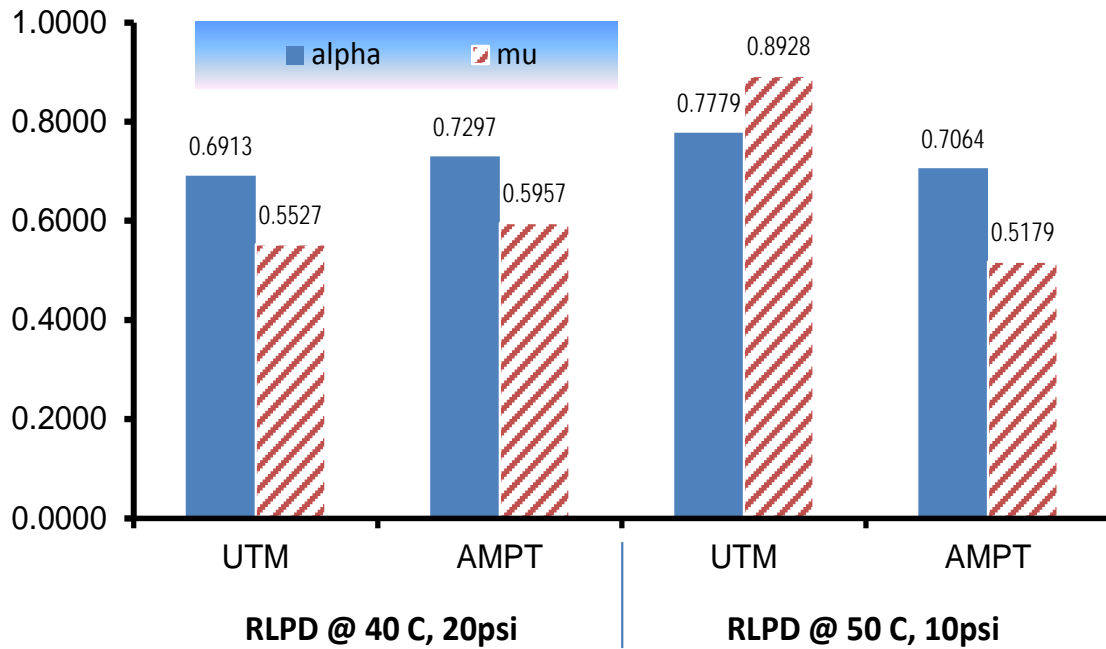


Figure D-3. Comparison of Alpha and Mu from RLDP Testing.

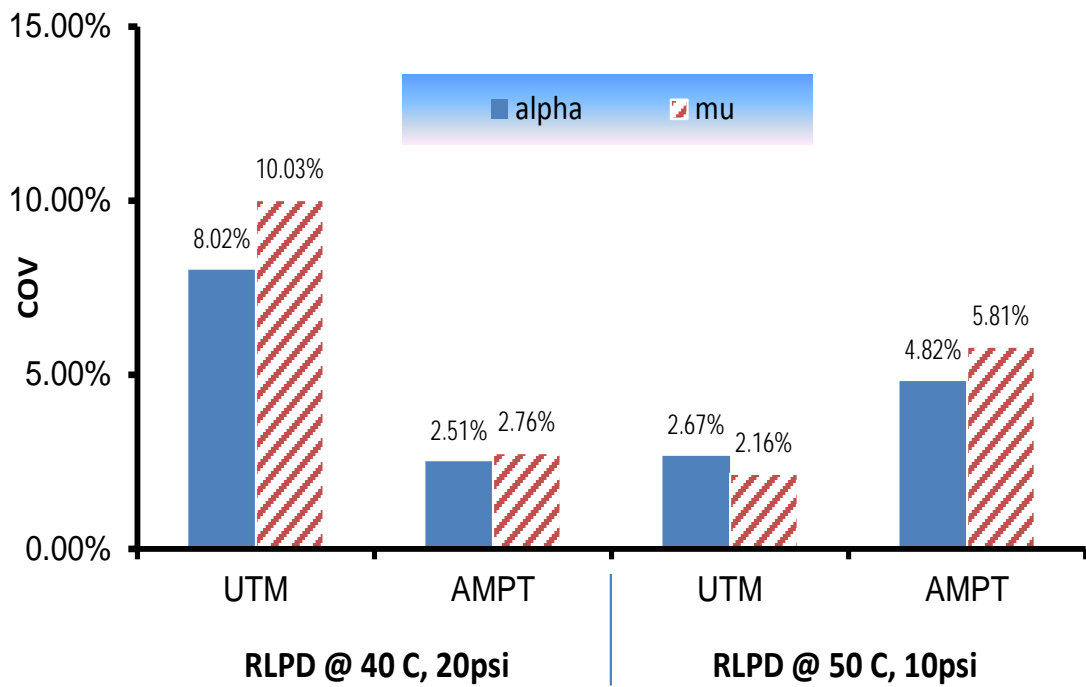


Figure D-4. COV Comparison from RLDP Testing.

**Table D-3. Tukey's HSD Analysis at 95% Confidence Level – RLPD Test Data.**

Alpha (a)							mu (μ)						
ANOVA							ANOVA						
Source of Variation	SS	df	MS	F	P-value	F crit	Source of Variation	SS	df	MS	F	P-value	F crit
Between Groups	0.0129	3	0.00430	3.43719	0.07220	4.06618	Between Groups	0.2651	3	0.08838	2.85096	0.10495	4.06618
Within Groups	0.0100	8	0.00125				Within Groups	0.2480	8	0.03100			
Total	0.0229	11					Total	0.5132	11				
<b>Tukey's HSD</b>							<b>Tukey's HSD</b>						
Q <sub>cr</sub> (for k=4 and df <sub>wg</sub> =8)							Q <sub>cr</sub> (for k=4 and df <sub>wg</sub> =8)						
MS <sub>wg</sub>							MS <sub>wg</sub>						
Number of samples per group (n)							Number of samples per group (n)						
Critical mean difference (Q <sub>cr</sub> *sqrt[MS <sub>wg</sub> /n])							Critical mean difference (Q <sub>cr</sub> *sqrt[MS <sub>wg</sub> /n])						
			4.53000							4.53			
			0.00125							0.031001			
			3							3			
			<b>0.092</b>							<b>0.460</b>			

**Table D-4. HMA Sample Dimensions.**

FN Samples				DM Samples			
Picture	Sample ID#	H (Inches)	$\phi$ (Inches)	Picture	Sample ID#	H (Inches)	$\phi$ (Inches)
	1	6.04	3.97		1	6.05	3.98
	2	6.08	3.96		2	6.07	3.96
	3	6.07	3.98		3	6.08	3.95
	1	6.05	3.97		1	6.04	3.97
	2	6.07	3.98		2	6.07	3.96
	3	6.06	3.95		3	6.06	3.95
Overall avg		6.06	3.97	Overall avg		6.06	3.96
Overall COV		0.24%	0.29%	Overall COV		0.24%	0.30%

**Table D-5. HMA Sample AV Measurements.**

FN Samples		DM Samples	
Picture	Samp le ID#	AV (7±1%)	Sampl e ID#
	1	7.59	1
	2	6.80	2
	3	7.24	3
	1	7.26	1
	2	7.66	2
	3	7.15	3
Overall avg		7.28	Overall avg
Overall COV		4.30%	Overall COV
Overall AV range		6.80-7.66	Overall AV range
			7.26
			7.46
			3.01%
			7.26-7.80



## APPENDIX E. ADDITIONAL DATA AND RESULTS FOR THE FN, DM, AND RLPD TESTS

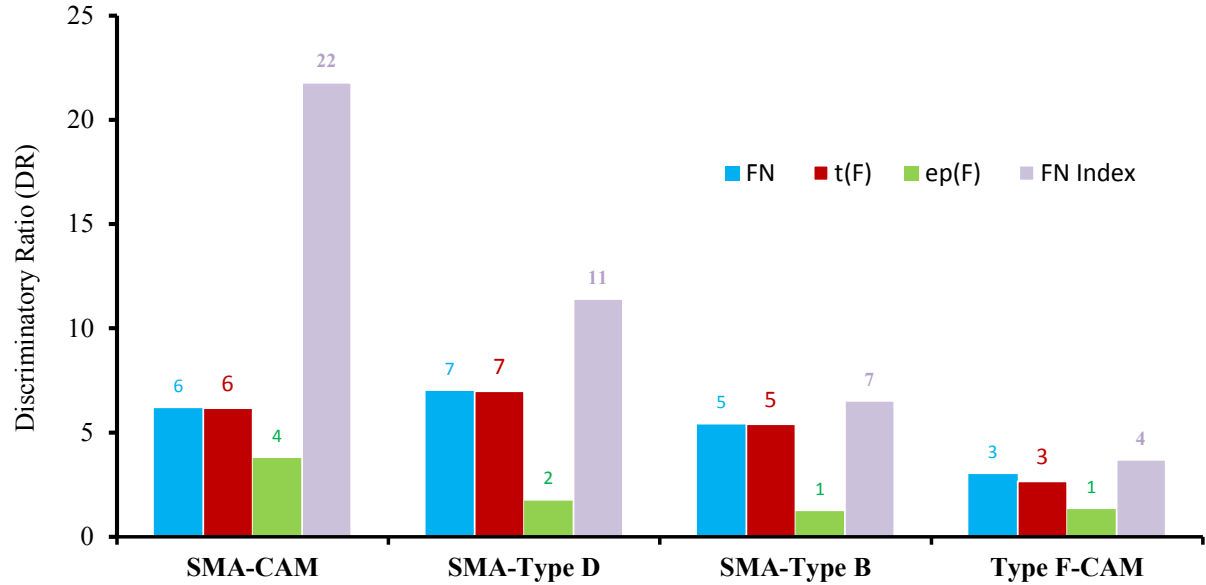


Figure E-1. Discriminatory Ratios (DR) Computed for the FN Test Parameters.

Table E-1. ANOVA and Tukey's HSD Test Analyses for the FN Test Methods.

HMA Mix	FN (cycles)	$t(F)$	$\epsilon_P(F)$	FN Index
Type F	B	B	B	B
Type B	B	B	C	B
Type D	B	B	C	B
CAM	B	B	A	A
SMA	A	A	C	C

Table E-2. Statistics of the FN Index Results after Discarding the Outliers.

	Type B (IH 35)	Type D (US 59)	CAM (SH 121)	Type F (US 271)	PFC (SH 121)	SMA (IH 35)
Avg	3.33	8.63	14.67	2.81	22.15	< 0.67
Stdev	0.08	0.74	1.54	0.08	1.06	N/A
COV	2.49%	8.61%	10.49%	3.02%	4.79%	N/A

**Table E-3. Ranking of the HMA Mix Based on the FN Index Parameter.**

	<b>SMA (IH 35)</b>	<b>Type F (US 271)</b>	<b>Type B (IH 35)</b>	<b>Type D (US 59)</b>	<b>CAM (SH 121)</b>	<b>PFC (SH 121)</b>
FN Index ranking	1	2	3	4	5	6
Table 3 FN Index	< 0.67	3.98	4.39	7.68	14.67	27.20
<b>(All results)</b>						
Table 8 FN Index	< 0.67	2.81	3.33	8.63	14.67	22.15
<b>(Excluding outliers)</b>						
Table 3 FN Index (COV – All replicates)	N/A	61.30%	41.70%	22.50%	10.49%	30.61%
Table 8 FN Index (COV – Excluding outliers)	N/A	3.02%	2.49%	8.61%	10.49%	4.79%

# **APPENDIX F. WORKPLANS FOR EVALUATING THE HWTT TEST METHOD, TEX-242-F SPECIFICATION, AND PRELIMINARY RESULTS**

## **Target HMA Mixes Being Evaluated**

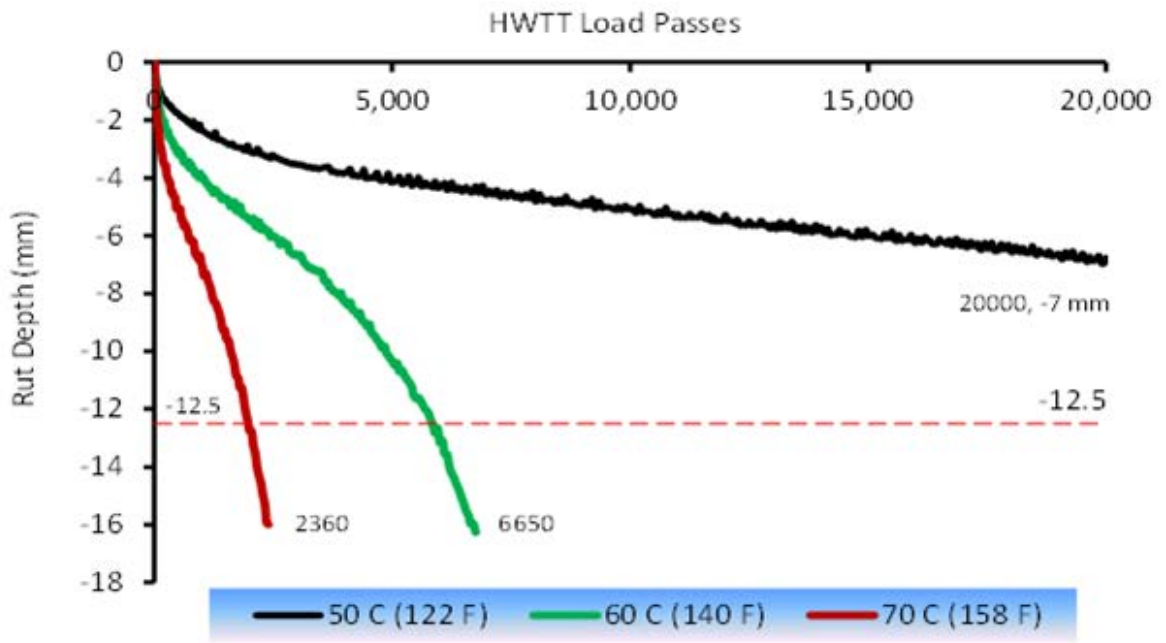
- 1) Minimum 5 (at least one poor, one good/middle, and one excellent rut/shear resistant)
- 2) Include in matrix at least two fine-graded mixes and one dense-graded mix
- 3) Include minimum 3 surfacing mixes and one intermediate mix
- 4) At least one mix must have RAP and RAS
- 5) At least one mix must have PG 64-22 & one PG 76-22
- 6) One mix must consist of raw materials for asphalt-binder and aggregate variations
- 7) Target mixes from hotter areas of Texas
- 8) Target mixes from heavily trafficked highways with slow-moving and/or turning traffic.

## **Target Test Variables and Loading Configuration Being Evaluated**

- 1) AV variation = minimum 3 levels (2 to 10%) with 7% included.
- 2) Temperature variation = minimum 3 levels (i.e., 50, 60, 70°C) – include 80°C if the asphalt-binder is PG 76-XX or PG 82-XX
- 3) Speed variation = minimum 3 levels (i.e., 42, 47, & 52 passes per minute)
- 4) Load variation = minimum 3 levels if possible (i.e., 158, 60, & 162 lb)
- 5) Explore the possibility to try pneumatic tires in comparison with the current steel wheels
- 6) Sample mold and specimen configuration variations = target minimum 3 options (current one + plus two others). Argument is that current mold induces too much confinement.
- 7) Asphalt-binder variation = OAC-0.5%, OAC, & OAC+0.5%
- 8) Aggregate variation = minimum 3 types (limestone should be included).
- 9) Mechanical modifications to measure HMA shear properties.
- 10) Software review and recommendations for modifications to capture additional data.
- 11) Any other test variables that can be modified.

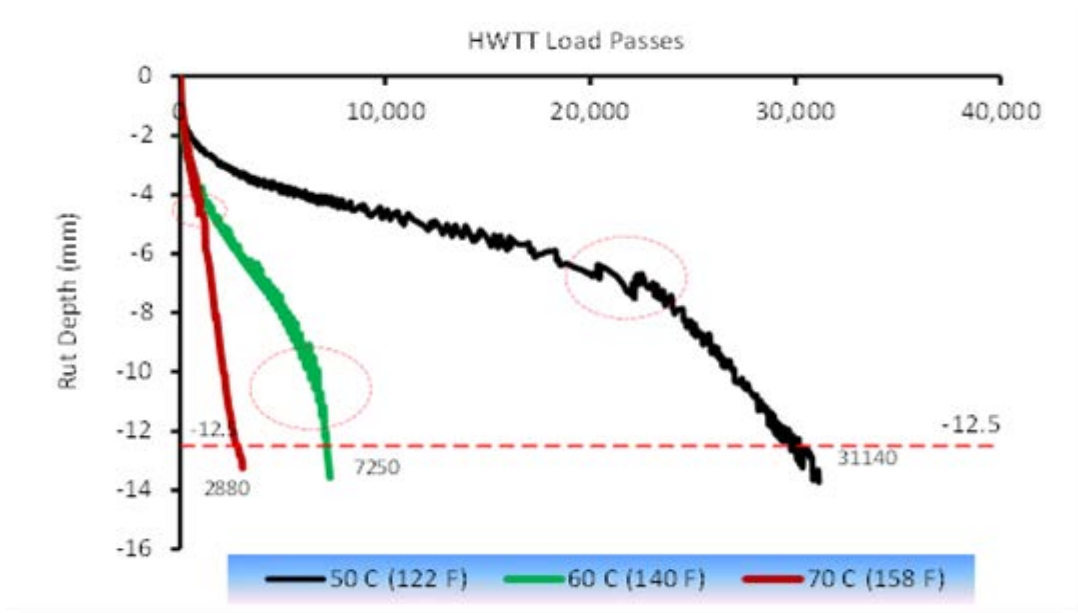
## **Target Data Analysis Variables Being Investigated**

- 1) Review and/or modify HWTT pass-fail criterion to cater for intersections, high temperature areas, slow moving traffic, etc.
- 2) Explore and/or devise other alternative HWTT data analysis parameters other than the rut depth and number of HWTT passes.
- 3) Explore the concept of HWTT PD Energy, i.e., area under the graphical plot of rut depth versus load passes.  
 $\Rightarrow \text{HWTT PD Energy} = \Sigma (\text{rut depth} \times \text{corresponding number of load passes}) \text{ (mm.passes)}$
- 4) Explore the concept of HWTT Rut Index, i.e., ratio of rut depth to corresponding number of passes.  
 $\Rightarrow \text{HWTT Rut Index} = 1 \times 10^4 \times (\text{rut depth [mm]} \div \text{corresponding number of load passes})$
- 5) Convert and relate the generated HWTT data to HMA shear properties (i.e., shear strength, shear modulus, shear deformation, etc.)
- 6) Relate the SGC compaction parameters (i.e., shear stress, number of gyrations, slope of thickness-gyrations curve, slope of AV-gyrations curve etc.) to HMA shear properties and rutting.
- 7) Review, revise, and modify the Tex-242-F specification as necessary.
- 8) If applicable, develop a preliminary HWTT shear test specification
- 9) Sensitivity evaluation and statistical analysis
- 10) Correlations with other lab tests and field data including APT
- 11) Any other ideas as deemed feasible!



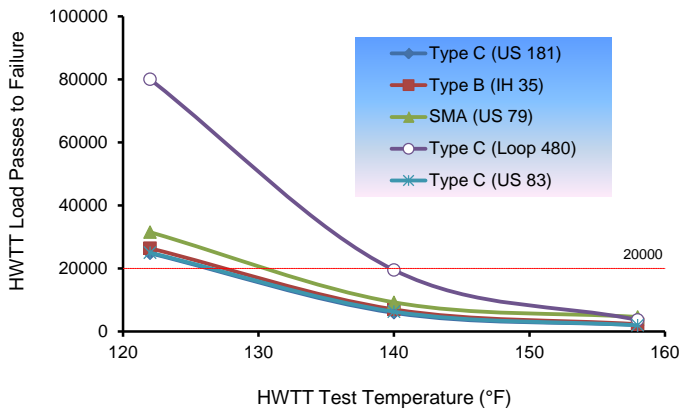
Type C Plant-Mix = 5.1% PG 64-22 + 20% RAP, US 181 (Corpus Christi)  
 Actual measured PVMNT surface temperature in Summer2012 = 143.1 °F (62 °C)

**Figure F-1. HWTT Rutting as a Function of Test Temperature - Type C (US 181).**



Type B Plant-Mix = 4.6% PG 64-22 + Limestone + 30% RAP, IH 35 (Waco)  
 Actual measured PVMNT surface temperature in Summer 2012 = 131.3 °F (55 °C)

Figure F-2. HWTT Rutting as a Function of Test Temperature - Type B (IH 35).



Item	HWTT Load Passes to 1/2-Inch Rut Failure			
	Temperature (°F)	122 (50 °C)	140 (60 °C)	158 (70 °C)
Type C (US 181)		24800	5900	2000
Type B (IH 35)		26400	7000	2300
SMA (US 79)		31500	9250	4600
Type C (Loop 480)		80000	19500	3640
Type C (US 83)		25000	6280	1960

Figure F-3. HWTT Load Passes to 1/2-Inch (12.5 mm) Rut Failure versus Temperature.

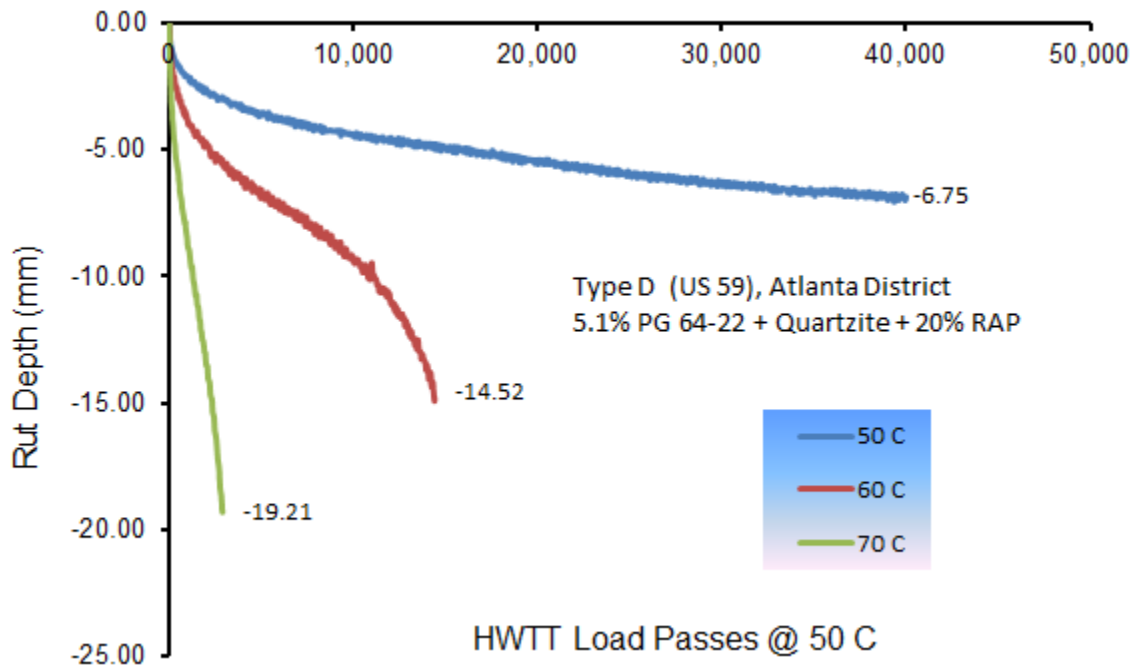


Figure F-4. HWTT Rutting as a Function of Test Temperature - Type D (US 59).

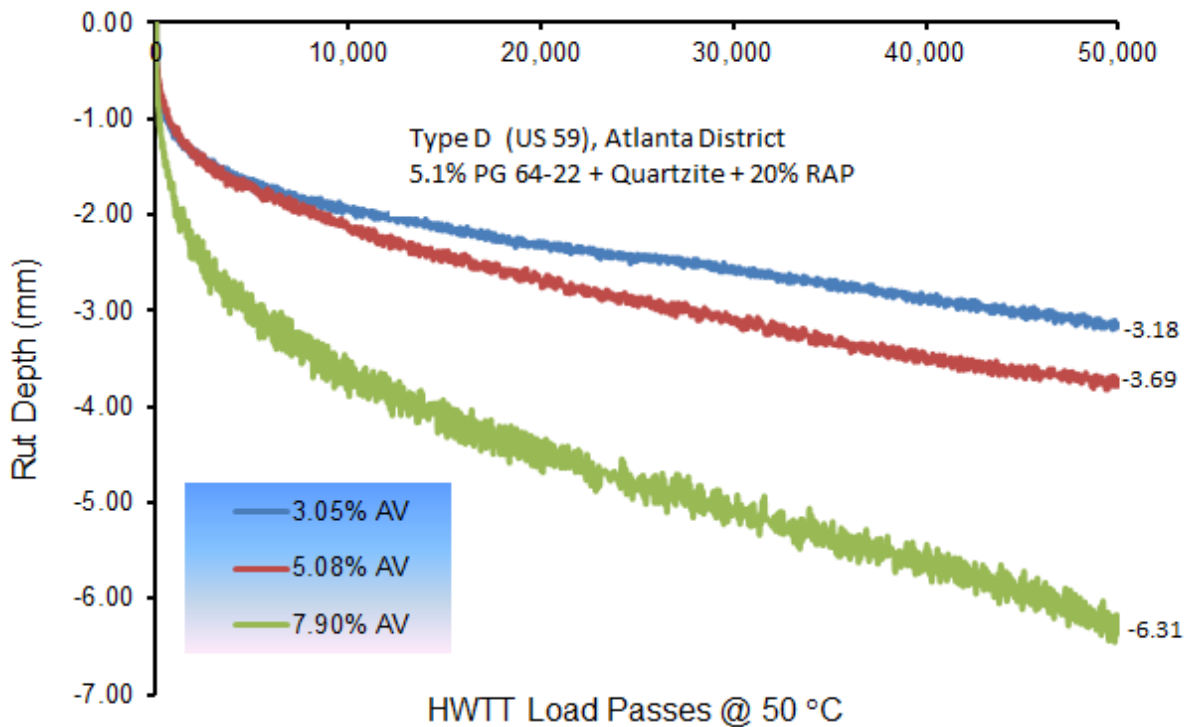
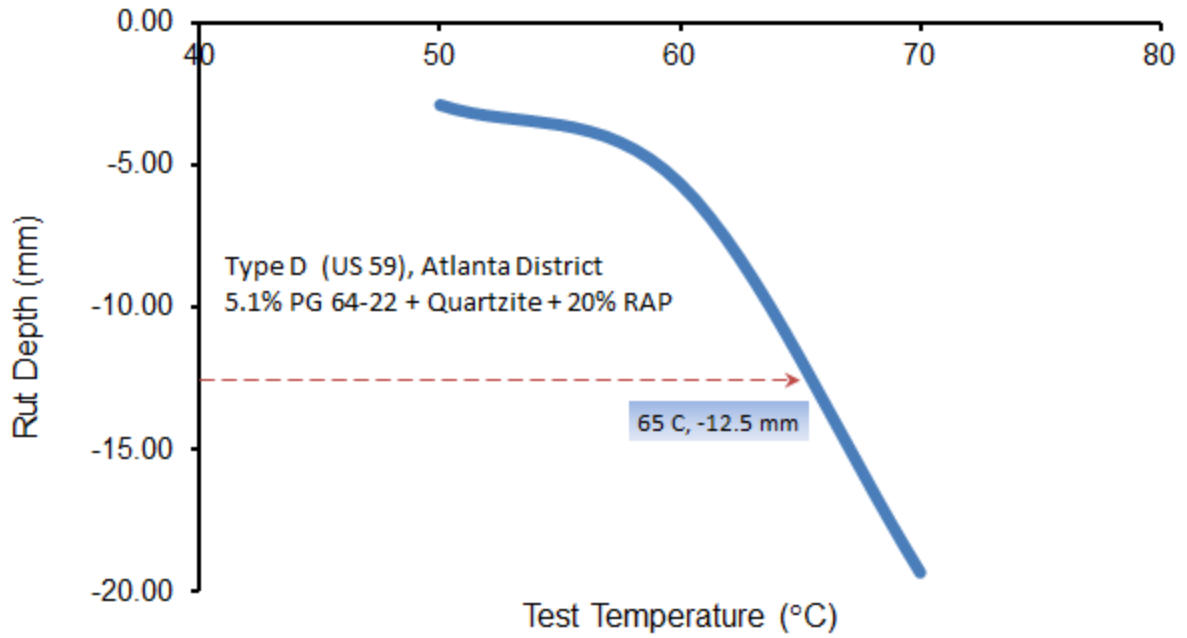


Figure F-5. HWTT Rutting as a Function of Density (Air Voids) - Type D (US 59).



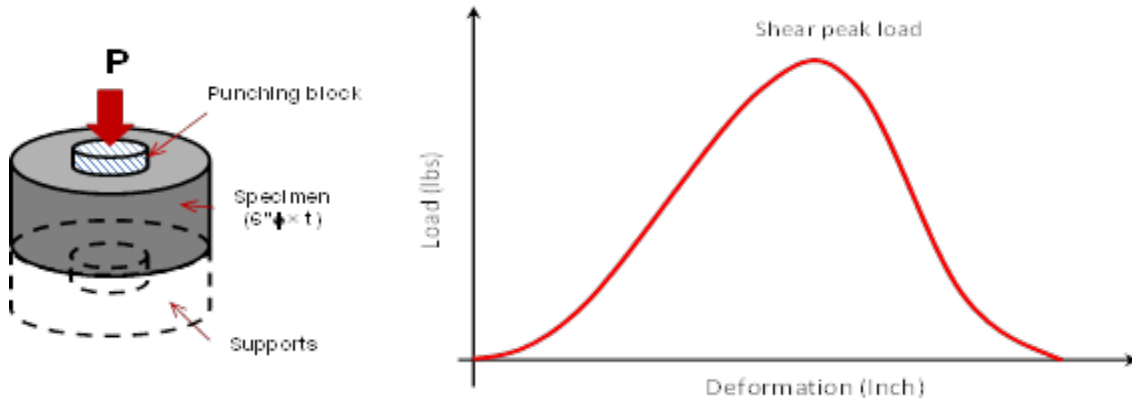
**Figure F-6. Example Determination of the Critical Failure HWTT Test Temperature for a Type D Mix (US 59).**



## APPENDIX G. WORK PLANS FOR THE DEVELOPMENT OF THE SIMPLE PUNCHING SHEAR TEST (SPST) AND PRELIMINARY RESULTS

### The Simple Punching Shear Test (SPST) – Monotonic (Static) Loading SETUP (SPST-ML)

---



- Test objective: Characterization of HMA shear resistance properties
- Load: Monotonic axial compressive loading
- Load mode/control: Load (actuator)
- Shape: Axial continuously increasing load
- **Test** sitting loads: a) 5.0 lb or b) 10.0 lb
- **Input** loads: Try = a) 0.50 inch/min, b) 1.0 inch/min, & c) 1.5 inch/min
- **Punching** loading heads: Try = a) 1.0"  $\phi$ , b), 1.5"  $\phi$ , & c) 2.0"  $\phi$
- Test temperatures: Try = a) 40 $\pm$ 2 $^{\circ}$ C (77 $^{\circ}$ F), b) 40 $\pm$ 2 $^{\circ}$ C (104 $^{\circ}$ F), c) 50 $\pm$ 2 $^{\circ}$ C (122 $^{\circ}$ F), & d) 60 $\pm$ 2 $^{\circ}$ C (140 $^{\circ}$ F)
- Specimen conditioning: Minimum 2 hrs
- Sample confinement: Without & with
- Monitor temperature: Via thermocouple inside a dummy specimen
- Data capturing: Every 0.10 seconds (except temperature; at least every 5 seconds)
- Measurements: Temp, time, load, & deformations (actuator [RAM] – No LVDTs)
- **Test termination:** a) 2.49" RAM vertical movement for 2.5" thick specimens  
b) 4.99" RAM vertical movement for 5.0" thickness specimen
- Test duration:  $\leq$  10 minutes ???
- Specimen: b) 6"  $\phi$   $\times$  2.5"  $t$ , & c) 6"  $\phi$   $\times$  5.0"  $t$
- AV: 7 $\pm$ 1%
- Replicates:  $\geq$  3 per mix per test variable
- Target mixes: Surfacing or intermediate layer mixes, fine- or dense-graded
- Parameters of interest: Shear peak failure load (lb), Shear failure deformation @

peak load (inches), HMA shear strength (psi), HMA shear modulus (ksi), Shear failure strain @ peak load (in/in), Shear Strain Energy (SSE) (J/m<sup>2</sup>), & Shear Strain Energy Index (SSE Index)

## Derivation of Shear Data Analysis Models – SPST Monotonic (Static) SETUP (SPST-ML)

---

1) Shear peak failure load (lb)  $= P_{\max} (lbs)$

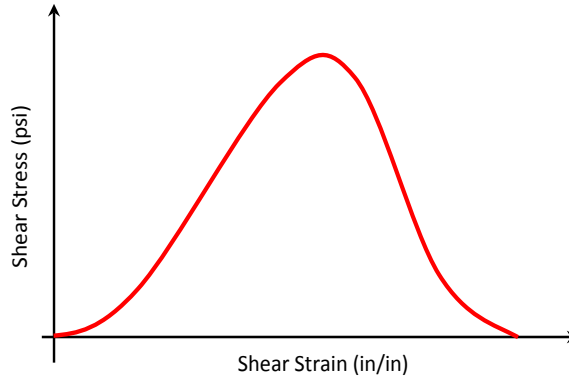
2) Shear failure deformation @ peak load (inches)  $= Deformation @ P_{\max} = d_{P_{\max}} (inch)$

3) HMA shear strength (psi)  $= \tau_s = \frac{P_{\max}}{A} = \frac{P_{\max}}{\pi D t} (psi)$

4) Shear failure strain @ peak load (in/in)  $= \gamma_s = \frac{d_{P_{\max}}}{t}$

5) HMA shear modulus (ksi)  $= G_s = \frac{\tau_s}{\gamma_s} = \frac{P_{\max}}{\pi D (d_{P_{\max}})}$

6) Shear strain energy (SSE) (J/m<sup>2</sup>)  $= SSE = \frac{1}{A} \int_0^{\infty} f(x) dx = \frac{1}{\pi D t} \int_0^{\infty} f(x) dx$



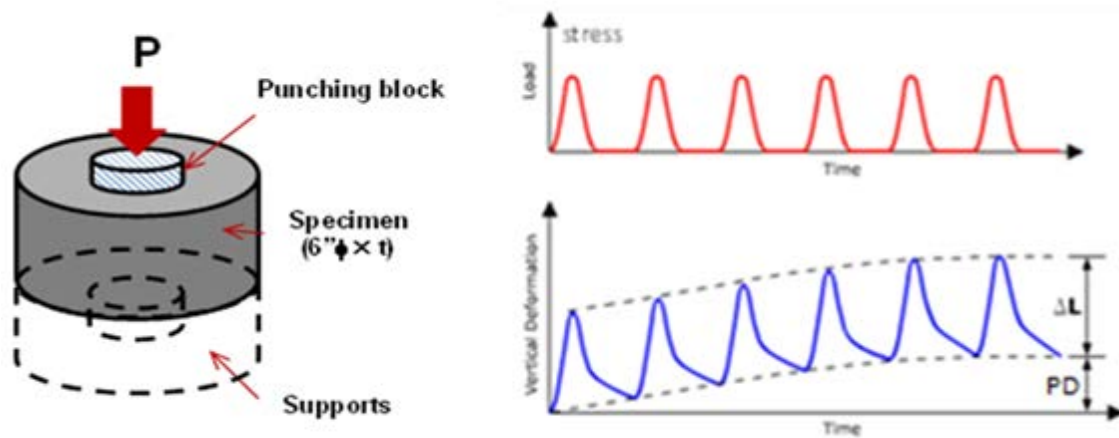
7) SSE Index  $= 10^3 \times SSE \frac{\gamma_s}{t \tau_s}$

Definition of Equation Parameters:

- $f(x)$  = Integral area under the shear stress-strain response curve
- $D$  = Diameter of the punching (loading) head (inches)
- $t$  = Thickness of the sample (inches)

## The Simple Punching Shear Test (SPST) – Dynamic (Repeated) Loading SETUP (SPST-DL)

---



- Test objective: Characterization of HMA visco-elastic shear resistance properties
- Load: Dynamic (repeated) axial compressive loading
- Load mode/control: Stress (actuator)
- Shape: Haversine (repeated)
- **Trial** sitting loads: a) 5.0 lbs or b) 10.0 lbs
- **Input** stress levels: For M-E analysis
- Loading frequency: 1 Hz (0.1 sec loading & 0.9 sec loading)
- **Punching** loading heads: Use selection from SPST-ML
- Test temperatures: Use selection from SPST-ML
- Specimen conditioning: Minimum 2 hrs
- Sample confinement: Without & with
- Monitor temperature: Via thermocouple inside a dummy specimen
- Data capturing: Every 0.10 seconds (except temperature; at least every 5 seconds)
- Measurements: Temp, time, load, & deformations (actuator [RAM] – No LVDTs)
- **Test termination:**
  - a) 2.49" RAM vertical movement for 2.5" thick specimens
  - b) 4.99" RAM vertical movement for 5.0" thickness specimen
- Test duration:  $\leq 3$  hrs???
- Specimen: a) 6"  $\phi \times 2.5$ " t, & b) 6"  $\phi \times 5.0$ " t
- AV:  $7 \pm 1\%$
- Replicates:  $\geq 3$  per mix per test variable
- Target mixes: Surfacing or intermediate layer mixes, fine- or dense-graded
- Parameters of Interest: Shear modulus, shear deformation, shear strain, etc.

## **SPST Sensitivity Evaluation**

---

### **HMA Mixes**

- 1) Use same mixes as the other tests, i.e., the HWTT
- 2) Minimum 5 (at least one poor, one good/middle, and one excellent rut/shear resistant)
- 3) Include in matrix at least two fine-graded mixes & one dense-graded mix
- 4) Include minimum 3 surfacing mixes and one intermediate mix
- 5) At least one mix must have RAP & RAS
- 6) At least one mix must have PG 64-22 & one PG 76-22
- 7) One mix must consist of raw materials for asphalt-binder and aggregate variations
- 8) Target mixes from hotter areas of Texas
- 9) Target mixes from heavily trafficked highways with slow-moving and/or turning traffic.
- 10) Three replicates per mix per test condition

### **SPST Test Variables**

- 1) Two loading modes = Monotonic and dynamic, but with focus on Monotonic
- 2) AV variation = minimum 3 levels (2 to 10%) with 7% included.
- 3) Temperature variation = minimum 3 levels (i.e., 20, 50, 60, 70°C) – include 80°C if the asphalt-binder is PG 76-XX or PG 82-XX
- 4) Speed variation = minimum 3 levels (Monotonic)
- 5) Load (stress) variation = minimum 3 levels (Dynamic)
- 6) Sample confinement = with & without
- 7) Asphalt-binder variation = OAC-0.5%, OAC, and OAC+0.5%
- 8) Aggregate variation = minimum 3 types (at least limestone should be included)
- 9) Any other test variables that can be modified!!
- 10) Establish preliminary SPST pass-fail screening criteria.

### **Data Analysis to Include, but NOT limited to the Following:**

- 1) Use the newly derived SPST models
- 2) Compare and relate to the SGC compaction parameters
- 3) Compare and relate to the HWTT and other tests
- 4) Statistics = Avg, CoV, t-tests, ANOVA, Tukey's HSD, etc.
- 5) Sensitivity to mix-design variables
- 6) Repeatability
- 7) Potential to screen and differentiate mixes
- 8) Correlation to field conditions and performance data including APT
- 9) Practicality of implementation
- 10) Develop a preliminary SPST test specification

**Preliminary SPST (Monotonic) Test Results on a Type C Mix (US 83, Laredo) at 50°C (122°F) at a Load Rate of 0.5 Inch/Min**

**Table G-1. Preliminary Test Results from SPST Monotonic Testing at 50°C.**

Sample #	Shear Peak Failure Load (lbs)	Shear Deformation @ Peak Load (in)	HMA Shear Strength (psi)	Shear Strain (in/in)	HMA Shear Modulus (psi)	SSE (J/m <sup>2</sup> )	SSE Index
Confined #1	2,054	0.263	43.58	0.105	415	5,527	30.441
Confined #2	2,444	0.204	51.87	0.082	634	6,115	22.025
Confined #4	2,380	0.215	50.50	0.086	589	5,702	22.132
<b>Avg</b>	<b>2,293</b>	<b>0.227</b>	<b>48.65</b>	<b>0.091</b>	<b>546</b>	<b>5,781</b>	<b>24.866</b>
<b>COV (%)</b>	<b>9.13%</b>	<b>13.70%</b>	<b>9.13%</b>	<b>13.70%</b>	<b>21.22%</b>	<b>5.23%</b>	<b>19.42%</b>
Unconfined #1	1,405	0.065	29.82	0.026	1140	820	1.643
Unconfined #2	1,434	0.064	30.42	0.026	1184	867	1.673
Unconfined #3	1,412	0.073	29.95	0.029	1023	801	1.789
<b>Avg</b>	<b>1,417</b>	<b>0.068</b>	<b>30.07</b>	<b>0.027</b>	<b>1115</b>	<b>829</b>	<b>1.701</b>
<b>COV (%)</b>	<b>1.05%</b>	<b>7.23%</b>	<b>1.05%</b>	<b>7.23%</b>	<b>7.47%</b>	<b>4.09%</b>	<b>4.53%</b>

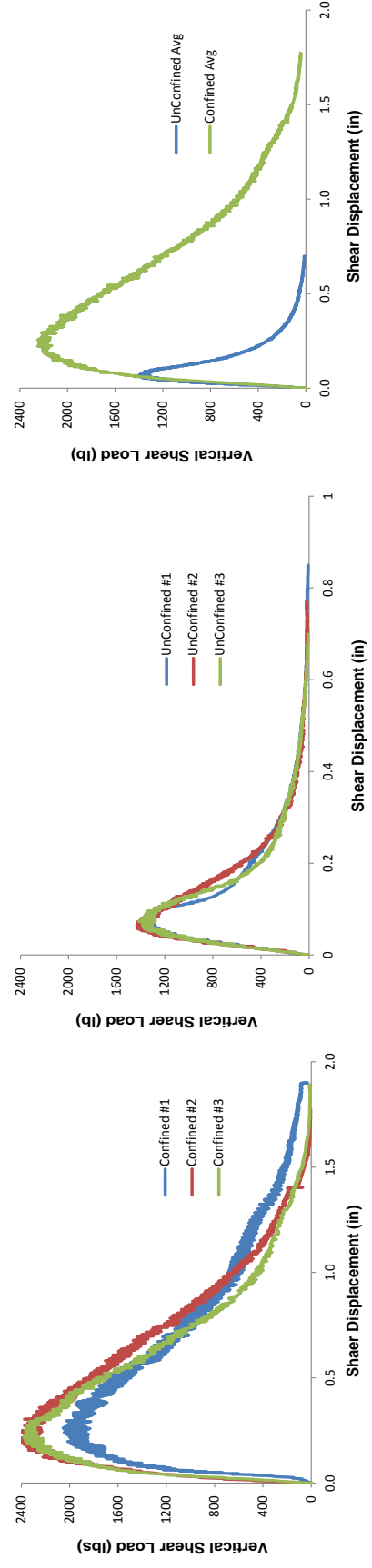


**Figure G-1. Preliminary SPST Monotonic Test Results – Graphical Response Curves.**

